Materials Development for the Fabrication of Metal Supported-Solid Oxide Fuel Cells by Co-sintering

Pradnyesh Satardekar

Advisor: Prof. Vincenzo M. Sglavo
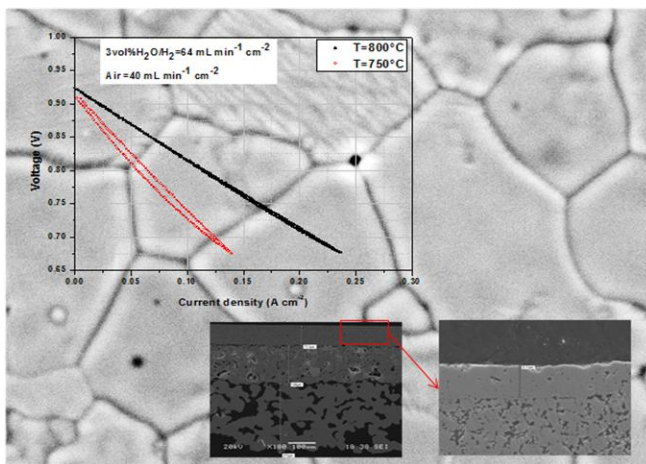
September 2014

Materials Development for the Fabrication of Metal Supported-Solid Oxide Fuel Cells by Co-sintering

Pradnyesh Satardekar
E-mail: pradnyesh.satardekar@unitn.it

Approved by:

Ph.D. Commission:

Prof. Vincenzo Maria Sglavo,
Advisor
Department of Industrial
Engineering
University of Trento, Italy.

Prof. Flavio Deflorian
Department of Industrial
Engineering
University of Trento, Italy.

Prof. Peter Leisner
Jönköping University-
School of Engineering,
Gjuterigatan 5, Sweden.

Dr. Stefano Pandini
Department of Mechanical
and Industrial Engineering
University of Brescia, Italy.

University of Trento,
Department of Materials Science and Engineering

September 2014

To my family

Abstract

Solid Oxide Fuel Cell (SOFC) is an upcoming technology seen with great expectations for the production of electrical energy with good efficiency and minimal environmental impact. Successful commercialization of SOFCs has however been hindered despite the optimistic promises made by some developers. This slackened commercialization of SOFCs technology is mainly due to the high cost associated with SOFC production and its limited long term stability. The long term stability of conventional Anode Supported-Solid Oxide Fuel Cell (AS-SOFC) with Ni based anode is tested by its limited tolerance towards redox cycling and rapid thermal cycling.

The introduction of new generation SOFC, the so called Metal Supported- Solid Oxide Fuel Cell (MS-SOFC) has shown to overcome the drawbacks associated with the conventional AS-SOFC. Thus, MS-SOFC is looked upon as the potential candidate for the rapid commercialization of SOFC technology. In MS-SOFC design, the cell is supported on a porous metal substrate instead of expensive and non-reliable anode as in AS-SOFC. In this design the thickness of the functional layers (anode, cathode and electrolyte) is kept thin as possible (in the order of 10-50μm) just necessary for electrochemical activities while the support being provided by the metal substrate.

Although MS-SOFC can be fabricated by different routes, co-sintering of metal/anode/electrolyte multilayers in non-oxidizing atmosphere at high temperatures (1300 to 1400°C) is the most promising as far cost efficiency and industrial scale up is concerned. The cathode is usually applied after high temperature processes and sintered in situ during operation in this route. This fabrication approach however has some drawbacks associated with it. This work is basically on the development of materials and optimization of the multilayer design for the production of MS-SOFC by cost-effective co-sintering approach. YSZ (Y_2O_3 stabilized ZrO_2), Ni-YSZ cermet, and ferritic stainless steel are considered for the electrolyte, anode and the support respectively. The anode and electrolyte were modified with the help of suitable dopants and the multilayer design was also altered in order to facilitate the co-sintering, preventing or reducing the generally encountered issues in this fabrication route.

Coarsening of Ni in Ni-YSZ anode cermet and over-sintering of anode during high temperature co-sintering is a well-known issue. Ni coarsening reduces the number of triple phase boundaries (TPB) thereby affecting electrochemical performance. The electrical

conductivity of the anode also degrades due to Ni coarsening. In current work, the effect of Al doping on Ni-YSZ anode sintering in Metal Supported-Solid Oxide Fuel Cell (MS-SOFC) was studied. It was found that, the addition of Al into the anode accounts for a finer microstructure if compared to undoped Ni-YSZ anode material. The electrical conductivity of the Al-doped anode was also found to increase considerabely and such result may be attributed to the fine microstructure caused by the segragation of Al_2O_3 formed during the course of sintering on the grain boundaries of both Ni and YSZ, thus inhibiting the sintering. 5wt% Al-doped NiO used for Ni-YSZ anode material gave the finest microstucture and the highest electrical conductivity at room temperature although it showed the lowest bulk density. Overall, Al-doped Ni-YSZ anode material was found to be a suitable material for the anode in MS-SOFC produced by co-sintering.

The modification of the reduction kinetic of NiO and the interaction between the anode and steel during the fabrication of Metal Supported Solid Oxide Fuel Cells (MS-SOFC) is also studied in the present work. With the aim to limit NiO reduction under inert atmosphere at high temperature, doping elements such as Al and Ce were considered for NiO powders modification and anode production. In order to simulate the reactions at the metal/anode interface, NiO/YSZ/steel composites were prepared with pure and Al-doped NiO. A sudden volume expansion above 1000^0C followed by substantial shrinkage above 1200^0C was observed for the composites when sintered in Ar at 1400^0C. Such volume expansion can be related to the oxidation of steel due to the RedOx reaction between NiO and steel. Moreover, it was found that the volume expansion, i.e. the steel oxidation, can be minimized to a good extent when Al-doped NiO is used. Hence it is proposed that Al-doped NiO is a promising candidate material to be used for anodes in high temperature sintering of MS-SOFC.

Other problems encountered during co-sintering of multilayers for MS-SOFC include delamination, cracking, bending, and interdiffusion of Fe,Cr and Ni between anode and the substrate. In another section of work, green multilayers were produced by tape-casting for the fabrication of MS-SOFC half-cell by co-sintering. The binder loss step during co-sintering was optimized so as to prevent the cracking of the multilayers due to the binder loss events. Intermediate layers (layer between metal support and rest of the layers) composed of metal-ceramic powder composite were also investigated to prevent delamination and to inhibit interdiffusion of the elements.CeO_2-steel, YSZ-steel, and LDC(La doped Ceria)-steel powder composites were considered for investigation to use as

intermediate layer. Out of the different multilayer design considered for investigation, YSZ/(Al-NiO)-YSZ/LDC-steel/steel multilayer design was found to be a good compromise so as to give a half-cell, with good bonding between the layers, which is camber free, and with moderate interdiffusion of elements between the substrate and the anode. It was however found in all the designs that complete densification of YSZ electrolyte could not be obtained.

In order to address the issue of limited densification of YSZ electrolyte during co-sintering, Fe was considered for doping YSZ. A comparative study was done on Fe doped YSZ samples for sintering in air and argon atmosphere, with the aim to analyze the effect of Fe as sintering aid under MS-SOFC fabrication by co-sintering conditions. Samples showed enhanced densification with increasing Fe concentration in both the sintering atmospheres thus concluding that Fe can be used as a sintering aid for YSZ even in argon. The samples sintered in argon atmosphere were however characterized by larger lattice parameter, density and grain size. The increase in lattice parameter can be attributed to the oxygen vacancies generated under low $p(O_2)$ in argon atmosphere. The microstructural analysis of the samples showed the presence of small amount of secondary phase, and the concentration of such phase was seen to be higher in the argon sintered samples. Comparison of colors of argon and air sintered samples indicates the reduction and/or precipitation of Fe dopant in samples sintered in argon. Gas tight dense electrolyte could be obtained for MS-SOFC fabricated by co-sintering when Fe doped YSZ is employed for electrolyte, although the performance of the cell was quite poor.

1. Introduction

Combustion of fossil fuels has been the primary route for generation of electricity since past 100 years. This route is however associated with limitations such as intrinsically low conversion efficiency, and emission of carbon dioxide and other air pollutants affecting the environment. The increasing demand for energy, exhaustion of fossil fuel reserves, and the growing concern about the environment has implemented the need to generate electricity more efficiently, and with minimal impact on environment. The use of fuel cell to generate electricity is a very promising approach to overcome the above mentioned issues. Fuel cell is an energy conversion device to electrochemically convert directly the chemical energy of the fuel such as hydrogen, methanol, ethanol, natural gas and hydrocarbons to electricity, and hence, fuel cells offer higher conversion efficiency than conventional energy conversion technologies such as internal combustion engine (ICE).

Among the various types of fuel cells, solid oxide fuel cells (SOFCs) are considered to be most promising, as they let internal reforming, promote fast kinetics with non-precious catalyst materials, and allow the use of various fuels, all due to its high operating temperature. The compactness, modularity, and durability SOFCs find in particular applications in stationary, distributed power generation, a niche market in which conventional heat engines find it hard to compete. These unique advantages of SOFCs have retained the interest of researchers and developers worldwide for their commercialization since last few decades.

The two basic designs of SOFC are the planar and tubular design, which have been widely studied and developed. These units of SOFCs are coupled electrically to give the required power output.

1

Each design has its own advantages and disadvantages, but planar design has however gained more attention as higher power densities can be obtained. YSZ (Y_2O_3 stabilized ZrO_2) has been the preferred electrolyte material for SOFC due to its pure ionic conducting behavior and its excellent stability under SOFC operating conditions. Ni/YSZ cermet has been the most widely used anode material, and LSM (Sr doped $LaMnO_3$) and LSCF (Lanthanum strontium cobaltite ferrite) are the standard cathode materials used in SOFCs.

Commercialization of SOFC technology is however been slackened due to the two major obstacles, i.e. product cost and system reliability. High cost of materials and cell processing is still hindering the commercial deployment of SOFCs. Furthermore, the long-term stability of the conventional anode supported SOFC (AS-SOFC) with Ni base anode is challenged by its limited redox stability. One of the strategies to crack these issues is the introduction of metal support in cell's architecture.

The limited thickness of typical zirconia electrolyte (<50 μm) in AS-SOFC allows to operate at temperature as low as $700^{\circ}C$, sensibly lower than the first generation electrolyte-supported SOFC, which operated in the range 850°-$1000^{\circ}C$. The lower operating temperature has opened the possibility to use less expensive metal/alloys not only for interconnects and BoP, but also for the SOFC support. This has led to the advent of a new generation of cells, the so called Metal Supported-SOFC (MS-SOFC) where the cell is supported by a porous relatively thick metal substrate while the ceramic layers, i.e. anode, electrolyte and cathode are in the order of 10-50 μm. MS-SOFC has several advantages over the conventional AS-SOFC such as lower material cost, mechanical ruggedness, higher tolerance towards rapid thermal cycling and redox cycling and good manufacturability. Ferritic stainless steel represents the preferred choice for the support in MS-SOFC not only because it is

relatively cheap but also because of its high temperature oxidation resistance and thermal expansion coefficient (TEC) which closely matches that of interconnects.

For SOFC to be commercially competitive it is necessary to reduce raw materials and the fabrication costs; therefore, the fabrication of MS-SOFC by cost efficient way can serve both purposes. Co-sintering of metal/anode/electrolyte multilayer in non-oxidizing atmosphere is a simple, inexpensive and industrially viable route for the fabrication of MS-SOFC. The cathode is usually applied after high temperature processing and sintered in situ during operation. The temperature required to achieve gas tight dense zirconia electrolyte is normally between 1300°C to 1400°C. Such high temperatures along with non-oxidizing atmosphere cause Ni coarsening in anode and adverse interaction between steel and anode substrate like Fe, Cr and Ni interdiffusion and RedOx reaction between NiO and steel. Coarsening of Ni in the anode reduces the number of triple phase boundaries (TPB) which are the active sites for the electrochemical reactions, and it can also reduce the electrical conductivity of the anode. Diffusion of Ni in the substrate can lead to austinisation of the ferritic stainless steel which has comparatively higher TEC, and can cause the cell to crack, whereas, diffusion of Fe and Cr in the anode can lead to formation of unwanted oxides in the anode degrading its performance. RedOx reaction between NiO and steel leads to intolerable volume expansion. Besides these, there are always these problems of delamination of layers and, bending and cracking of the cell during co-sintering. Limited densification of YSZ electrolyte under the constrained multilayers geometry is also a major issue in co-sintering approach. Although a Diffusion Barrier Layer (DBL) between the steel substrate and the anode can be used to inhibit interdiffusion upon co-sintering at high temperature, it does not address to the issues of NiO reduction by the chromium present in the

3

steel and of Ni coarsening. The reason is that the oxygen partial pressure in the furnace can be controlled by the release of O_2 due to NiO reduction and, therefore, it does not need a direct interface between the two phases. Nevertheless, the high temperature effect on steel and anode can be reduced by decreasing the electrolyte sintering temperature by using low-temperature processes such as Pulsed Laser Deposition (PLD) and Vacuum Plasma Spray (VPS). Another approach is the infiltration of Ni catalyst into the porous metal/porous YSZ/dense YSZ multilayer structure after high temperature processing. In any case such low temperature processes are multistep and expensive and therefore not suitable for production on an industrial scale. Therefore, the co-sintering of multilayer still remains an attractive choice.

In this work, cost-effective co-sintering route has been considered for the fabrication of planner MS-SOFC.YSZ, Ni-YSZ cermet, and ferritic stainless steel are considered for the electrolyte, anode and the support respectively. The main aim of this work is to develop materials and to optimize the processing route in order to reduce or prevent the abovementioned problems during co-sintering for MS-SOFC.

The 'theoretical background' section of this thesis discusses about fuel cells, SOFCs, and different topics on MS-SOFC such as their evolution, materials and fabrication routes. This section also briefly puts light on topics such as tape casting, sintering and constrained sintering. The next section i.e. 'experimental procedure and results' gives the general experimental procedure and the techniques, which is followed by the 4 topics addressed in this work. In the first topic, the effects of Al dopant on Ni/YSZ anode material under MS-SOFC co-sintering conditions have been discussed. The second topic is on the study of anode-steel interface and the effect of doped anode on the interface during co-sintering. The next topic is

4

about the optimization of sintering condition, and multilayer design produced by tape casting for the fabrication of MS-SOFC. The last topic is on sintering of Fe doped YSZ electrolyte under non-oxidizing atmosphere for the MS-SOFC. The final section of this thesis is the general conclusion where the entire work is concluded in general.

Some work related to the deposition of protective coating on the porous stainless steel substrate was also done during this PhD period. This work is however not reported in this thesis as it is subjected to a patent at Italian Patent and Trademark Office (IPTO) since August, 2013.

This PhD work was co-funded by SOFCpower SpA in the frame of RAMSES project.

2. Theoretical background

2.1. Fuel Cells v/s SOFCs

Fuel cells are electrochemical devices which converts the chemical energy in the fuel directly into electrical energy with high efficiency and in environmental friendly manner. Power generation by fuel cells unlike the conventional modes of generating electricity does not involve intermediate steps of producing heat and mechanical work. Thus, fuel cells are not limited by the thermodynamic limitations of heat engines such as Carnot efficiency and therefore have inherently higher efficiency. Higher efficiency also means lower CO_2 emission per unit production of electricity when hydrocarbons are used as fuel. In a fuel cell the reaction between fuel and oxidant takes place electrochemically as a result of which there is no combustion of fuel; hence electricity is generated with minimal pollutants. In addition, fuel cells have good size flexibility i.e. they can be scaled up to systems ranging from few watts to megawatts theoretically without any loss in efficiency. Another advantage is that, quiet and vibration-free operation of fuel cells also eliminates the noise usually associated with conventional power generation systems [1] [2] [3].

Although fuel cells are promising, they are associated with major practical issues which involve materials and manufacturing cost. In addition, there these two fundamental technical issues; the slow reaction rate leading to low currents and power, and that hydrogen which is the most preferred fuel is not readily available [4]

To solve the technical problems, many different types of fuel cells have been tried. The most common classification of fuel cells depends on the type of electrolyte used in the cell, which in turn determines the operating temperature range of the cell. The different kinds of fuel cells are polymer electrolyte fuel cells (PEFC), alkaline

fuel cells (AFC), phosphoric acid fuel cell (PAFC), molten carbonate fuel cells (MCFC), and solid oxide fuel cells (SOFC).Overview of different types of fuel cells and their features are given in Table 1.

Features	PEFC	AFC	PAFC	MCFC	SOFC
Electrolyte	Polymeric membrane	Potassium hydroxide	Phosphoric acid	Carbonate salt mixture	Ceramic
Catalyst	Platinum	Platinum	Platinum	Electrode material	Electrode material
Operating T(^{o}C)	50-100	70-250	150-200	600-700	400-1000
Charge Carrier	H^+	OH^-	H^+	CO_3^{2-}	O^{2-}
External Reformer for HC fuels	Yes	Yes	Yes	No, for some fuels	No, for some fuels and cell design
External shift conversion of CO to H_2	Yes, plus removal of CO traces required	Yes, plus removal CO and CO_2 required	Yes	No	No

Table 1. Overview of different types of fuel cells [2] [5]*.*

Each of the above mentioned fuel cells have different advantages and preferential application field depending on the operating temperature and the fuel used.

As indicated by the name itself, in SOFC the electrolyte is a solid, oxygen ion conducting metal oxide, usually Y_2O_3 stabilized ZrO_2. The gas tight electrolyte is sandwiched between porous anode and cathode. Typical anode material used is Ni/ZrO_2 cermet and the

7

cathode is a perovskite such as Sr doped $LaMnO_3$. The operating temperature of SOFC is between 400-1000°C. Due to the solid electrolyte, SOFCs possess advantages over other type of fuel cells consisting of non-solid electrolyte such as, they can be fabricated in various shapes like planner, tubular and monolithic. The solid electrolyte in SOFC also allows to precisely engineer the triple phase boundaries and there is no problem of electrolyte flooding into the electrodes. Moreover, since the unit cell is constructed of solid ceramics there are no corrosion issues.

The most important advantages of SOFC over other fuel cells are associated with their higher operating temperatures typically in the range of 600-1000°C. Higher temperature means that there is no need of valuable metal catalyst. Also, SOFC can be used with variety of fuel ranging from hydrogen to CO to hydrocarbon (both in liquid and gaseous state). The higher operating temperatures efficiently activate the process of reforming and electrochemical oxidation of hydrocarbon fuel in the presence of catalyst. The reforming of hydrocarbon fuels which is highly endothermic can be achieved internally on-cell from the high quality heat generated by exothermic electrochemical oxidation of fuel, giving H_2 and CO. CO with H_2O shifts to H_2 and CO_2. Thus, CO acts as a fuel in SOFC unlike the fuel cells operating at lower temperature (such as PEM fuel cells) where it poisons the anode. The overall energy efficiency of SOFC can be further improved (85-90%) by the recovery of waste heat along with electricity generation, often known as combined heat and power (CHP). Another way of recovering the waste heat is by integrating the SOFC stack systems with micro gas turbines, thus forming a hybrid system. In order to maximize the electrical efficiency, the SOFC/micro gas turbine hybrid systems are often operated at high pressure thus improving the performance of SOFC and effectiveness of gas turbine. Furthermore, a bottom cycle steam

turbine can be added to these above mentioned hybrid systems in order to be even more efficient. Applications and integration of SOFC with other systems for power generation has been extensively reviewed in [6] [7] [8].

Unfortunately the major drawbacks of SOFCs are also associated with their higher operating temperatures. Due the high operating temperature the material selection for the core of SOFC system is limited only to those which can withstand such temperatures. Therefore organic materials and low temperature metal alloys cannot be used. The material selection remains limited to ceramics, metal/ceramic composites and high temperature alloys. Another problem is that the thermal expansion coefficients (TEC) of the components in particular anode, electrolyte, cathode, sealing and interconnect have to be carefully matched. The mismatch in TEC of these components often destroys the cell during temperature variations for production, operation, and thermal cycles from room temperature to operating temperature. Finally the fragile nature of ceramics in SOFC makes them intolerable to stresses when used in stacks under real operating conditions. These stresses arise from thermal shocks, mechanical solicitations or RedOx cycles. Moreover, the compressive sealing which requires high applied pressure cannot be used.
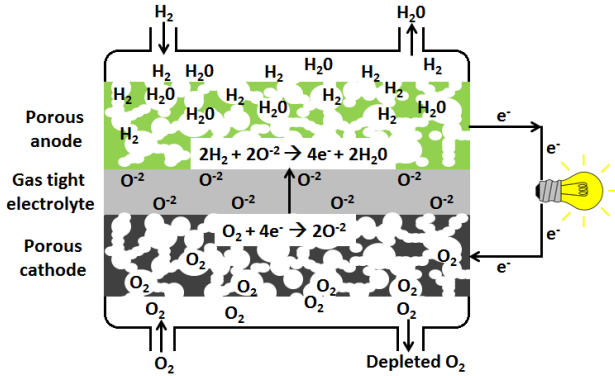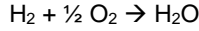
2.2. SOFCs basic principles

In a Solid Oxide Fuel Cell, the electrical power is generated by the electrochemical reaction between fuel and oxygen. The driving force is the global cell reaction free energy change; ΔG. SOFCs consists of 3 fundamental layers, a central gas tight dense electrolyte layer and the porous anode and cathode layers on either side of the electrolyte. The basic requirement of electrolyte material is that it should be good oxygen ion conductor and insulating towards electrons. The working principle of SOFC is depicted in Fig.1. Fuel such as H_2 is fed in the anode side and oxidant i.e. air or O_2 is supplied in the cathode side. Oxygen ions are formed at the cathode by reduction of oxygen. These oxygen ions, driven by the difference in oxygen chemical potential between fuel and air compartment, are transported through the electrolyte by vacancies migration mechanism to the anode side. On the anode side the fuel is oxidized by oxygen ions by mechanism which can involve series of adsorption and dissociation steps over the catalyst surface, generating electrons. Since the electrolyte is insulating towards electrons, the electrons are forced to flow through external circuit between anode and cathode to balance the internal ionic current.

The operating temperature of SOFC which is usually between $400^{o}C$ -$1000^{o}C$ is determined by the oxygen ion conductivity of the electrolyte material and also the thickness of this electrolyte layer.

When hydrogen is used as fuel, the half-cell reactions occurring at the electrodes are:

$$\text{Anode: } H_2 + O^{2-} \rightarrow H_2O + 2e^-$$
$$\text{Cathode: } \frac{1}{2} O_2 + 2e^- \rightarrow O^{2-}$$
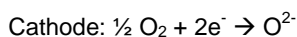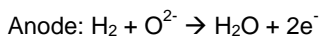
The overall cell reaction is given as:

$$H_2 + \tfrac{1}{2} O_2 \rightarrow H_2O$$

Fig.1. Operating principle in solid oxide fuel cell with H_2 as fuel and O_2 as oxidant.

For a fuel cell, the performance is evaluated as the voltage output at a given current flow. The current and the DC power output are usually normalized as current density and power density per unit surface of the electrolyte, respectively.

At equilibrium the cell voltage is given by the Nernst equation:

$$E = E^o + \frac{RT}{2F} \ln\left(\frac{p_{H_2} p_{O_2}^{1/2}}{p_{H_2O}} \right)$$

Where R is the perfect gas constant, F is the Faraday's constant, 2 is the number of electrons transferred in the half cell reaction; the terms in natural logarithmic are the partial pressure of the reactants and the products of the reaction. E^o is the standard potential difference between the two half-cell reaction and is given as:

$$E^o = -\frac{\Delta G^o}{2F} = \frac{\Delta H^o - T\Delta S^o}{2F}$$

Where ΔG^o is the standard Gibbs free energy change for the hydrogen oxidation, ΔH^o is the standard enthalpy change and ΔS^o is the standard entropy change.

The Nernst potential, E, gives the ideal open circuit cell potential. This potential sets the upper limit or the maximum performance achievable by fuel cell. For the overall cell reaction the potential increases with an increase in partial pressure (concentration) of reactants and decrease in partial pressure of products.

Under operating condition when the current is flowing through the cell, the actual cell potential is lower than its ideal potential due to several types of irreversible loses, namely, activation, ohmic, and concentration polarization. A typical voltage-current density plot is shown in Fig.2.
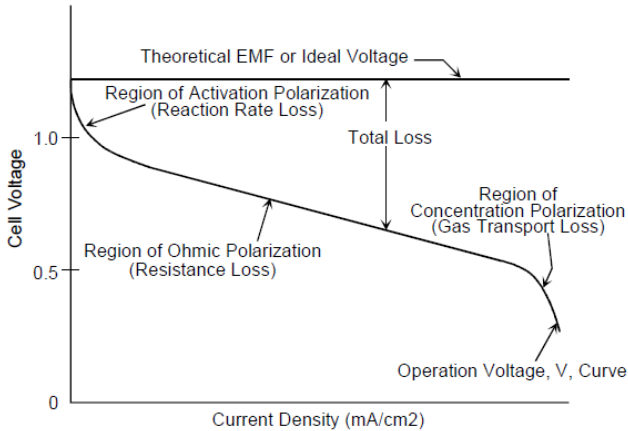
Fig.2. Typical fuel cell i-v curve [9].

12

Activation polarization (η_{act}) stem from the activation energy of the electrochemical reactions at the electrodes i.e. the charge transfer processes, and depends on the nature of electrode-electrolyte interfaces. The charge transfer reactions are thought to occur within a limited distance from the electrolyte/electrode interfaces (in the order of 10 µm) at zones known as triple phase boundaries (TPB). TPB are the regions where the three phases involved in the reaction i.e. electrolyte, electrode catalyst and the gas meet, and are the active points for the charge transfer reaction to occur. TPB length can be increased by making the electrode microstructure finer and thus the activation losses can be reduced.

The ohmic polarization (η_{ohm}) is the voltage loss due to ohmic resistances. The parameters contributing to the overall ohmic loss are ionic conductivity of electrolyte, ionic and electronic conductivity of the two electrodes, thickness of the electrolyte and the electrodes, and the ohmic resistances associated with the interfaces. The main contribution to the ohmic polarization is through the electrolyte. A high ionic conductivity and small electrolyte thicknesses are the desired characteristics of the solid electrolyte to minimize the ohmic contribution. On the other hand, ohmic contribution from the electrodes depends on the relative composition of the two phases (in composite electrodes), amount of porosity and microstructure, in particular the geometry of the particle to particle contact. Finally the contact resistance associated to electrode-current collectors interfaces must also be considered in SOFC stack.

The concentration polarization (η_{conc}) contribution to the voltage loss is associated to transport of gaseous species through the electrodes. As the reactants are consumed by electrochemical reaction at the electrode, it is often diluted by the products, when the finite mass transport rate limits the supply of fresh reactant and evacuation of products. The factors contributing to the concentration

13

polarization are electrode porosity, pore size and pore morphology (which affects the tortuosity factor) and electrode thickness (thinner the electrode, the lower is the concentration polarization). At low current density the concentration polarization is negligible, however under practical conditions (high current density and low fuel and air concentration), they contribute significantly for the loss in cell potential.

2.3. Basic SOFC designs

The electrolyte and the two electrodes in a SOFC can be configured in different geometrical configurations giving several designs. Planar and tubular are the two basic SOFC designs which have been extensively studied and developed since the last few decades. These units of SOFCs are connected electrically to obtain the desired power output. Reference [10] summarizes world-wide efforts in the field of SOFC, presenting an overview of the main SOFC design and the main developers' active in this field.
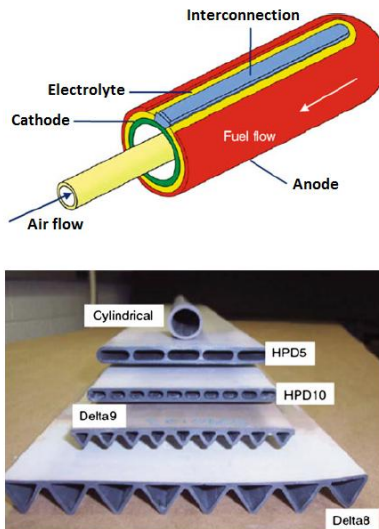
2.3.1. Tubular design

Tubular SOFCs can be of tubes with large diameter (>15mm), or of tubes with much smaller diameter (< 5mm), the so called microtubular cells. In order to increase the power density and to allow the easier deposition of the electrodes these tubes may be flat and joined together (Fig.3.). Siemens Westinghouse Power Corporation or SWPC have been the major developers of tubular SOFC since late 1970s. The design illustrated by SWPC is given in Fig.3.The porous tube composed of lanthanum doped manganite with one end closed is fabricated by extrusion and sintering. Dense YSZ electrolyte, porous Ni-YSZ anode and doped lanthanum chromite interconnects are then deposited in the form of thin layers by atmospheric plasma spraying.

The oxidant is fed inside the tube near the closed end with the help of an alumina injector tube placed co-axially. The oxidant flows through the annular space formed between the injector tube and the cell, and travels towards the open end of the cell tube. The fuel flows outside the cell from the closed end, and is electrochemically oxidized while flowing towards the open end

generating electricity. The biggest plus point associated with the tubular SOFC design is that it does not require high temperature seals to prevent the mixing of the fuel and the oxidant. This in fact is the reason why stable performance is achieved for SOFC with tubular concept over a large period of time (several years). However, as a result of long path for electrical power through each cell, and the large void within the cell structure, low power densities are obtained for tubular SOFCs which is its biggest setback.

Fig.3. Tubular solid oxide fuel cell design and alternate geometries investigated by Siemens [3]

2.3.2. Planar design

In the planar design the electrolyte and the electrodes are configured in the form of thin, flat plates to form a SOFC. The planar

SOFC can be, electrolyte-supported, electrode-supported or metal-supported. Furthermore, the flat cells can be circular in shape where the fuel is supplied through the central hole, or it can be in the square or rectangular shape fed from the sides. The variants of planar SOFC are illustrated in Fig.4. The manufacturing methods of SOFC with
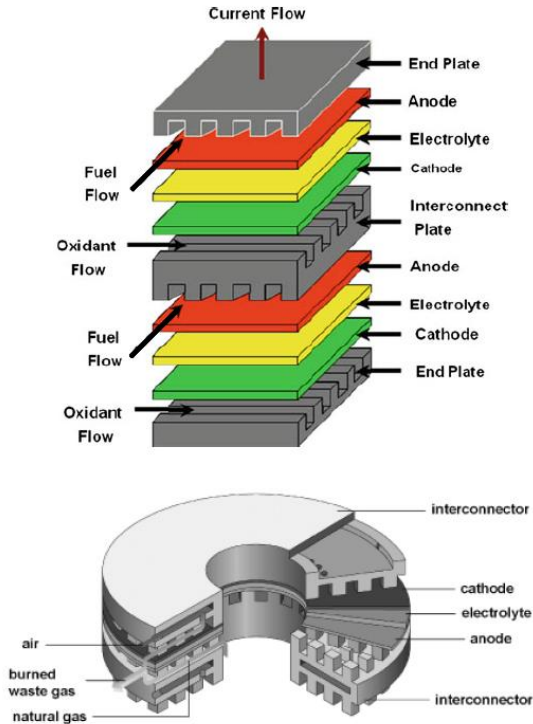
Fig.4. Planar solid oxide fuel cells with rectangular and circular shapes showing the modes of fuel and oxidant supply [3] [10]*.*

planar configuration are less complicated and less expensive as compared to that of SOFC with tubular design. The major advantage of planar SOFC design over the tubular is that higher power densities

can be obtained in the case of former. The areal power density of planar SOFC (up to 2 W/cm^2 for single cell and min 0.5 W/cm^2 for the stack) is much higher than that for tubular SOFC (about 0.2 W/cm^2).The volumetric power density of planar cell is also higher than that of the tubular cell. However, planar designs require high temperature gas-tight sealants between the cell components in order to prevent the mixing of fuel and the oxidant; such seals are not necessary in the tubular design. Development of reliable sealing is crucial for successful commercialization of SOFC with planner design. Use of sealants can be minimized by careful Configuration of gas flow, and gas flow manifold. Generally, interconnects are ribbed on both the sides of cell which provide the channels for the gas flow and also acts as the current collectors.

2.4. Advent and advantages of MS-SOFC

SOFC technology has been thoroughly investigated by companies and researchers world-wide for many decades. Two generations of planer SOFCs with significant improvement in performance have been explored; first the electrolyte-supported SOFC (ES-SOFC) and then the electrode-supported SOFC. However, successful commercialization of traditional SOFC technology is prohibited for many reasons; high cost associated with raw material, unreliable cell sealing, limited tolerance of cell to the stresses due to rapid thermal transients, mechanical shocks, or oxidation of anode and, manufacturing issues related to high-yield production of large, complex ceramic parts . The further refinement of the SOFC design has led to the advent of 3rd generation SOFC, the so called 'Metal-supported SOFC (MS-SOFC). MS-SOFC design is the recently introduced concept with the potential to overcome the above mentioned problems, thus making itself a promising candidate for commercialization [11]. The comparison of different generations of planner SOFCs is illustrated in the Fig.5.
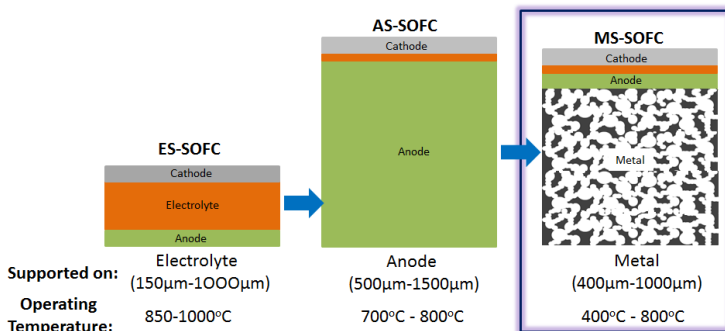
Fig.5. Comparison of different generations of SOFC.

In the case of ES-SOFC the mechanical support for the thin electrode layers (~50μm) is provided by comparatively thicker electrolyte layer (>150μm), typically Y_2O_3 stabilized ZrO_2 (YSZ) .In a SOFC, the main contribution to the ohmic polarization is through electrolyte. For ES-SOFC the ohmic contribution is large due to the high electrolyte resistivity. The electrolyte resistivity can be reduced by increasing the operating temperature as the conductivity of typical SOFC electrolyte display Arrhenius-dependence on temperature. Therefore, these cells are operated at high temperature of ~1000°C to achieve sufficiently low electrolyte resistivity (~20 Ω cm).Another way of reducing the ohmic contribution due to the electrolyte at lower temperature is by simply making it thinner. For instance, at 800°C the resistivity of YSZ is about 50 Ω cm giving the area specific resistance (electrolyte contribution) of about 0.75 Ω cm^2 when 150 μm thick YSZ electrolyte is used. This is a very high value with the result that the power density is rather low at temperatures below about 950°C. However, when the thickness of electrolyte is reduced to, say 10 μm, the area specific resistance of electrolyte is only 0.05 Ω cm^2 at 800°C. Thus, efficient operation of SOFC is made possible in principle at such a low temperature of 700°C to 800°C by reducing the electrolyte thickness. This lower operating temperature does not require the use of significant thermal insulation and expensive high-temperature materials to be used in stack and balance-of-plant (BOP).Here came in the concept of electrode supported cell where electrolyte (thickness is <20 μm) is supported on the comparatively thicker one of the two electrodes [12] [11]. Although in electrode-supported SOFC either anode or cathode can be used for mechanical support, anode-supported SOFC (AS-SOFC) are more popular than the cathode-supported SOFC (CS-SOFC). This is because of the mass transport limitations (high concentration polarization) and manufacturing

20

challenges (it is difficult to obtain fully sintered YSZ electrolyte without oversintering the Sr doped $LaMnO_3$ i.e. LSM cathode) associated with cathode-supported SOFC.

In the electrolyte-supported, and the electrode-supported SOFC the mechanical support is the expensive and brittle, ceramic or cermet material. In contrast, in the case of metal supported design the electrode and the electrolyte layers are supported on the comparatively inexpensive and robust, porous metal substrate. The ceramic layers only as thick (under processing constraints) as necessary for the electrochemical activities are applied directly to the metal substrate. The metallic support can be either on the cathode side or anode side, but mostly latter is preferred due to manufacturability and stability issues. Although most developers of MS-SOFC use planner support, tubular supports are also gaining popularity.

MS-SOFC design thus promises advantages over the conventional ceramic/cermet supported cells such as low materials cost, ruggedness and abuse tolerance, good manufacturability and operational advanteges.MS-SOFC design allows the use of conventional metal joining techniques, such as welding or brazing for sealing during assemblage of cells. Good thermal conductivity and ductility of metallic substrate, which may both improve thermal shock resistance, and lower the internal temperature gradient, allows the quicker startup. This, along with mechanical ruggedness of MS-SOFC is advantageous in APU application where the cell or stack is likely to experience shock, vibration, or mechanical loading. Another advantage is the redox cycling tolerance which allows the cells to cool down without the need of blanketing, interruption in fuel supply, and catalyst oxidation at high current density.

2.5. Materials for MS-SOFC

2.5.1. Choice of substrate

The alloy/metal substrate used in MS-SOFC should satisfy the requirements which are similar to that of alloy interconnects used in SOFC. The basic difference between substrate and the interconnect material is that later should be gas tight and, former should be porous (~ 30-35 vol% porosity) to allow the mass transport. Besides, interconnects are exposed to dual atmosphere i.e. cathode and anode atmosphere whereas, the metal substrate is exposed to one the two atmospheres depending on the side which it is attached. The requirements for alloy/metal to use as substrate are as follows. The alloy should have high electrical conductivity, high mechanical strength and low oxidation rate. The low resistivity of the protective oxide scales formed by the alloy during operation is also desired. Furthermore, thermal expansion coefficients (TEC) of the alloy should fairly match with that of other cell components from room temperature up to operating temperature. Finally, the substrate should also have chemical compatibility with components of cell in contact during operation, and cost factor should also be considered.

Properties of alloy depend on their nominal composition and the use of additives. The phase diagram evaluated by Yang et al [13] for Cr-Ni-Fe system is given in Fig.6., and their properties are summarized in Table 2.The properties of other material currently being considered for substrate are also given. Austenitic stainless steels (ASS) have good oxidation resistance, high mechanical strength, good manufacturability and low cost. However, they are not preferred for support because these alloys have higher TEC than most of the ceramic electrolyte explored for SOFC. Ferritic stainless steels (FSS) have an average TEC matching with most of the

electrolyte materials, they are cheap, have good oxidation resistance, and their forming and production technology is well established. One drawback of FSS is that they possess low mechanical strength. Ni and Ni-Fe supports are studied as potential support candidates, as their well-developed manufacturing technology relieves considerably the cell fabrication limitations. Drawbacks of these materials are
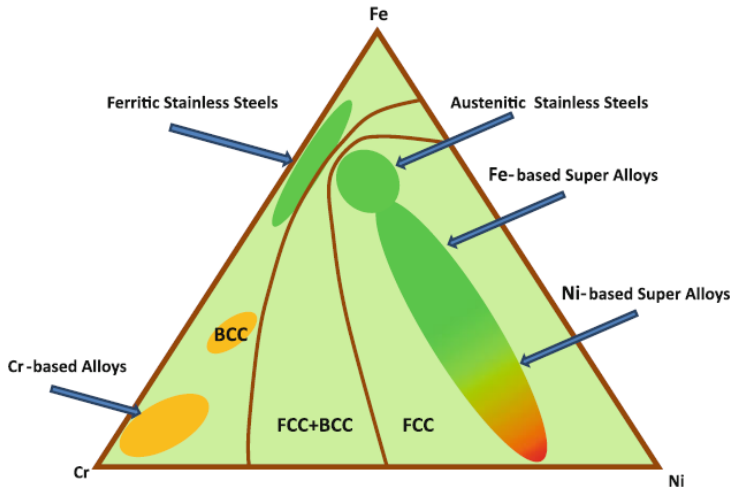
Fig.6. Schematic phase diagram for Cr-Ni-Fe system [13]

that, in addition to their poor redox resistance, low oxidation resistance, and relatively low mechanical strength, they are susceptible to coking under lower steam to CH_4 ratio and are expensive. The issues associated with Ni-Cr containing alloys are that they have TEC lager than most of the electrolyte and they are expensive.

Thus, for most of the SOFC developers, ferritic stainless is the choice of material for interconnects. FSS also appears as the prime material for substrate in MS-SOFC and is thus discussed in more detail ahead. For optimizing the performance and stability of the

23

FSS candidates, two additional parameters should be considered, namely particle size and the oxidation rate constant of the alloy.

Alloys	TEC[a](10^{-6}K^{-1})	Oxidation resistance	Mechanical strength	Manufact urability	Cost
Cr based	11.0-12.5	Good	High	Difficult	Very expensive
Ferritic SS	11.5-14.0	Good	Low	Fairly readily	Cheap
Austenitic SS	18.0-20.0	Good	Fairly high	Readily	Cheap
Fe based supper alloy	15.0-20.0	Good	High	Readily	Fairly cheap
Ni based super alloys	14.0-19.0	Good	High	Readily	Expensive
Ni	16.0-17.0	Low	Low	Readily	Expensive
NI-Fe	13.0-14.0	Low	Low	Readily	Fairly expensive

Table 2. Comparison of key properties of selected alloys [3] .
[a] *average between 25 and 900°C*
Note that TEC of electrolytes (YSZ, CGO, LSGM= 10-12 x 10^{-6}K^{-1})

(a) Effect of Alloy particle size

Particle size of the alloy plays an important role in manufacturability of the alloy substrate. For instance, if the substrate is to be manufactured by conventional powder metallurgy methods than large particles are preferred in order to form a porous interconnected network. Particle size requirements can be made less stringent to some extent by the use of pore formers during processing to give porous interconnected structure. Since other functional layers

have to be deposited on the metal substrate, alloy is desired to have smooth surface with small pores. In this case small alloy particles are preferred.

The performance and stability of ferritic alloys are also determined by their particle size. The particle size of ferritic alloy should be large enough to form the continuous protective Cr_2O_3 scale on the surface, while still retaining sufficient Cr in the bulk.

Fig.7. gives the estimate of the particle size for alloy containing 22 wt% Cr for ideal support microstructure consisting of spherical spheres. The critical thickness of Cr_2O_3 scale is considered to be around 1μ which is assumed to fully cover the sphere surface. It is assumed that the thickness of neck between metal particles should be at least between 4-5μ to avoid complete corrosion of these conducting paths. Density of the Cr_2O_3 scale is used to calculate the Cr concentration to form the scale and thus the Cr remaining in the bulk.
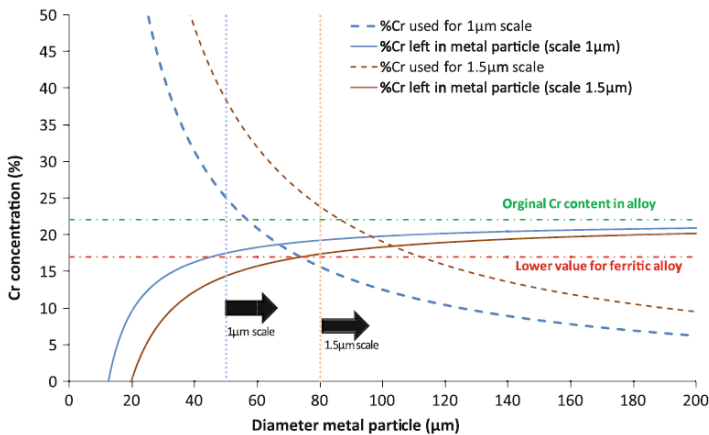

Fig.7. Evolution of Cr concentration (in wt%) in the bulk and in the oxide scale (thickness:1 and 1.5 μ) as a function of particle size for alloy with 22 wt% Cr [3].

25

It can be seen from Fig.7. that it is not possible for the alloy particles with size less than 10μ to form continuous Cr_2O_3 scale with 1μ thickness. Particle size of at least around 50μ is required to form continuous Cr_2O_3 scales of 1μ thickness and at the same time maintain the minimum Cr concentration of 17wt % in the bulk. This threshold allows to maintain the ferritic structure of the alloy and to prevent phase change, evolution of TEC, and to improve the ability of alloy to heal the cracks formed in the oxide scale.

Similar calculations can be done to obtain the Cr_2O_3 scale with 1.5 μm thickness. It should be noted that large thickness is not preferred because it can add extra resistance to the cell and also there is the risk of spallation of the scale.
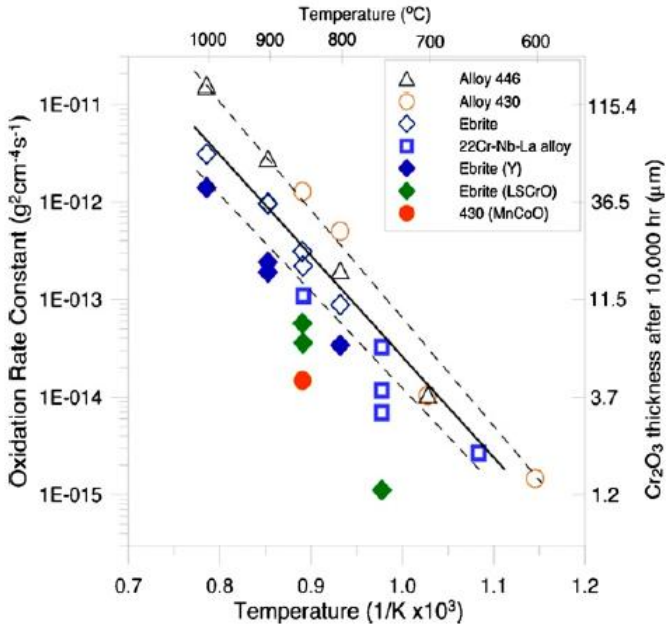
(b) Effect of oxidation rate constant

Excessive oxidation of the alloy substrate leads to spallation of the protective oxide scale after reaching a particular thickness. The spallation may lead to electrical disconnection inhibiting the current collection from the electrode and thus cannot be tolerated. Besides, metallic contacts between the metal grains should be maintained to ensure the continuous electrical and thermal trails. Moreover, excessive scale formation can also inhibit the gas transport through the support.

The observed oxidation rate is roughly the same for stainless steel contacting air or fuel [14]. The oxidation of substrate and thus the thickness of the scale is determined by the parabolic growth rate constant K_p ($g^2cm^{-4}s^{-1}$). K_p should be less than 10^{-15} $g^2cm^{-4}s^{-1}$ so that the scale thickness is not more than 1μ after 10kh operation. Below this thickness the oxide scale is not expected to spall. This calculation is based on ideal parabolic oxidation behavior

of alloy and may deviate due to Cr evaporation in air from the scale. Cr evaporation is enhanced in presence of steam.

K_p values for variety of coated and uncoated FSS measured in oxidizing atmosphere as a function of temperature is shown in Fig.8. All alloys contain more than 17wt% Cr with minor additives liike Ti, Ce, Y, Nb, Ta and Mo to improve oxide scale adherence and to reduce the oxidation rate [15] [16]. These alloys have low values of K_p between 700-850°C (1×10^{-14} - 5×10^{-14} $g^2 cm^{-4} s^{-1}$). It can be seen that oxidation rate is reduced significantly for the alloys coated with protective layers and is also reported in [16] [17] [18].

Thus, for 10^3 h operation with 1µ as critical oxide scale thickness for an alloy with K_p around 1×10^{-15} $g^2 cm^{-4} s^{-1}$ requires coated alloys for temperature above 750°C. It is anticipated that continuous development in material design will lead to improved tolerance of the alloys towards oxidation.

27

Excessive oxidation of the porous substrate can lead to rapid and significant decrease in open porosity of the substrate as shown by [20].This can cause severe problem for gas permeation. Fig.9. shows the open porosities for porous 430L FSS substrate as a function of time when oxidized at 800°C in air. The test was performed on the substrates with different initial open porosities. The samples with high initial porosities expose larger area for oxidation reaction. Fig.9. also shows the cross section of the substrate with initial open porosity of 21.4% after 900 h oxidation, pores covered by oxide scale can be seen.

(a)

(b)
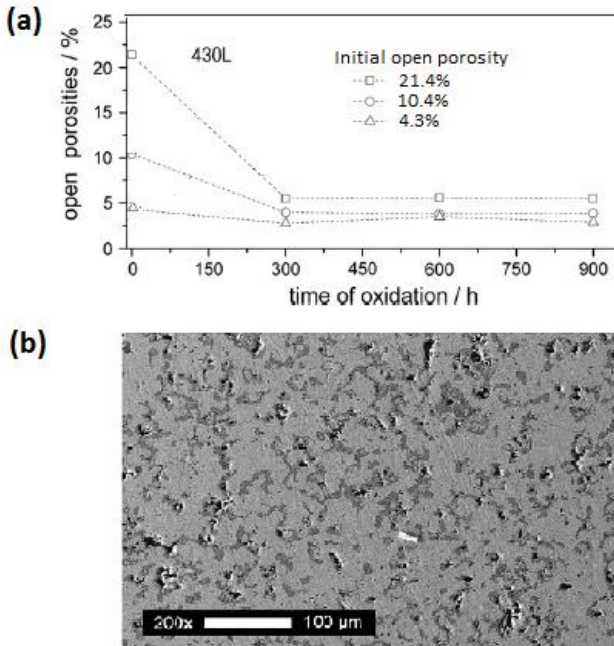
Fig.9. (a) Porosity changes of 430L stainless steel with initial open porosities of 21.4%, 10.4% and 4.3% when oxidized at 800°C in air, (b) Cross section of 430L stainless steel with initial open porosity of 21.4% after 900 h of oxidation at 800°C in air, where the black,dark grey and light grey phases are the pores, chromia scale and steel respectively [20].

2.5.2. Electrolyte Materials

For a material to be considered for electrolyte, it needs to satisfy certain requirements. Material should have high ionic conductivity and low electronic conductivity. It should be stable under both oxidizing (air) and reducing (fuel) environment at elevated temperature. It should be easily producible in the form of thin gas tight film. Also, the thermal expansion coefficient must match at the electrolyte/electrode interface.
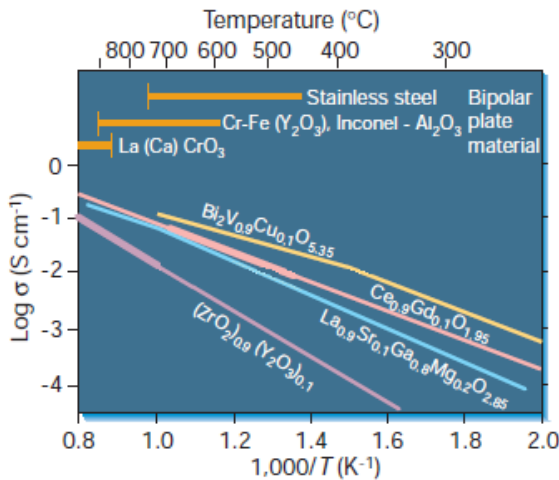
Fig.10. Ionic conductivities of typically used electrolyte materials as a function of temperature [21]

Fig. 10 shows the ionic conductivity of typical electrolyte materials as a function of temperature. Although Y_2O_3 stabilized ZrO_2(YSZ) has the lowest ionic conductivity it is the most widely used electrolyte material due to its excellent stability in both fuel and air environment. The ohmic loss due to low conductivity of YSZ electrolyte can be minimized by reducing its thickness and thus can be used in the temperature range of 700-800°C instead of 1000°C (see section 2.4).Fig.11. provide a qualitative quick reference guide for some of the families of electrolytes, co-relating their conductivity and stability in the temperature range of 600-800°C.Some of these electrolyte materials are discussed individually in context of their application for MS-SOFC.
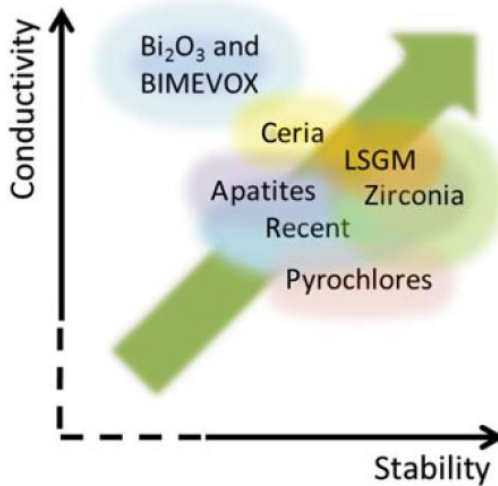
Fig.11.Selected performance indicators for temperature in the range 600-800°C. The green arrow indicates the desirable performance trend [22].

(a) LSGM (Strontium- and magnesium doped-lanthanum gallate)

The chief advantage of this material is that it exhibits decent oxygen ion conductivity at temperature as low as $400^{\circ}C$ due to its nearly pure ionic conducting behavior. However, it is not suitable for long term application because of its reactive nature. LSGM has been shown to react with Cr_2O_3 and Cr containing vapors [23] and therefore not preferred for use with stainless steel supports. LSGM has been applied as an electrolyte on Ni metal supports and on Ni-Fe supports using atmospheric plasma spray (APS) [24] and pulsed laser deposition respectively(PLD [25]. However, LSGM has also been found to react with Ni in the anode or Ni-Fe metal support. Nevertheless, the reaction between the electrolyte and the metal substrate was prevented by introduction of additional thin SDC (Samarium doped ceria) layer between them. Although Cells with these designs showed notable power densities ranging from $100 mWcm^{-2}$ to $1.6\ Wcm^{-2}$ at $400^{\circ}C$ and $600^{\circ}C$ respectively, the power densities dropped by roughly 50% upon a thermal cycle. No long term operation has been reported. Recently, Lanthanum doped ceria (LDC) thin layer was used between LSGM electrolyte and Ni based anode to prevent the reaction of Ni with LSGM [26].

(b) CGO (Gadolinium-doped ceria)

The conductivity of ceria based electrolytes is higher as compared to that of YSZ, and adequate conductivity for CGO can be obtained even at $500^{\circ}C$ [27].The disadvantage of CGO electrolyte is that it is not stable in reducing fuel atmosphere above $600^{\circ}C$ and thus required to operate between $500-600^{\circ}C$.Above $600^{\circ}C$ in reducing fuel atmosphere, Ce^{+4} ions in the CGO is reduced to Ce^{+3} which creates a lattice expansion stress and electrolyte becomes a mixed conductor. This considerably reduces the efficiency and performance of the cell.

Fig.12. shows that open circuit voltage (OCV) can drop below 0.8-0.9 V at 600°C and higher due to mixed conduction in electrolyte, setting this as maximum operating temperature [27] [28]. Nevertheless, the electronic conduction of CGO layer can be blocked by introducing an additional thin electrolyte layer of Sc-stabilized zirconia (ScZr) between anode and CGO as shown by Hui et al [29] [30].This Metal supported cell with additional electrolyte layer showed improved performance. Although the lower operating temperature of 500-600°C is advantageous in terms of stability and performance of the metal support, and the requirement of less expensive balance of plant material, it does not allow the internal reforming of the hydrocarbon fuels [27] [31]. Thus there is a need of pre-reformer which adds up to the cost and the complexity of the system.

An advantage of ceria based electrolytes is that it allows the use of prefabricated metal supports which shrinks very less or does not shrink at all. This is because these electrolytes can be sintered to full density under constraint geometry. Moreover, electrophoretically deposited CGO electrolyte can be sintered to full density at temperature as low as 1000°C [27].Low temperature sintering of CGO electrolyte can also be achieved by appropriate dopants [32] [33] [34]. These low sintering temperatures allows the sintering of CGO electrolyte on stainless steel substrates in air without excessive oxidation of the substrate. Furthermore, dense ceria based electrolytes can be obtained on metal substrates at even lower temperatures by techniques such as RF magnetron sputtering [35], pulsed laser deposition [29] [30], spray pyrolysis [36] and various plasma spray techniques [37] [38] [28]without the need of further heat treatment.

Cells with CGO electrolyte have been prepared on Ni-Fe [39], Hastelloy-X [30] [37] [28] and ferritic stainless steel support [31] [27] [40] [29] [36] [38].
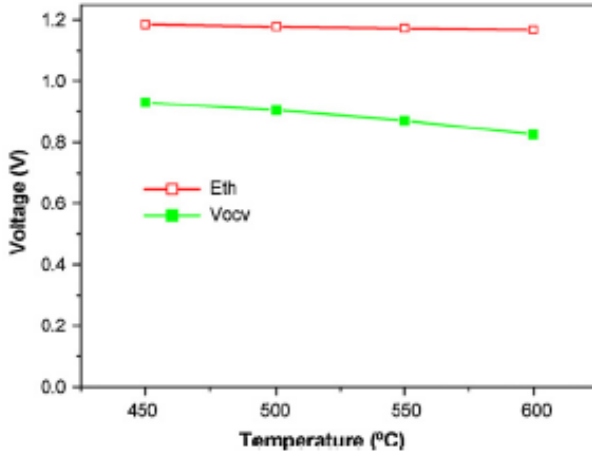
Fig.12.Theoretical open circuit voltage Eth and measured open circuit voltage V_{OCV} over 450-600°C for a metal supported cell with Ni-SD anode, SDC electrolyte, and SSC-SDC cathode operated with humidified hydrogen and air [28]*.*

(c) YSZ (Y_2O_3 stabilized ZrO_2)

Most of the MS-SOFC developers choose to use YSZ electrolyte because it offers crucial advantages over other electrolyte materials such as well-defined cost and demonstrated stability and performance. Moreover, the stability and pure ionic conductivity of YSZ electrolyte allows operation above 650°C, unlike the CGO electrolyte which displays significant electronic conductivity above 600°C. Such high operating temperature (above 650°C) allows the internal reforming of the hydrocarbon fuel thus avoiding the need for external pre-reformer. The main setback associated with YSZ is that it generally cannot be sintered to full density under constraint geometry. Researchers have been trying to address this issue by following ways; deposition of dense YSZ layer by techniques such as plasma

or flame-spray, or co-sintering to full density after colloidal/wet deposition of YSZ on green substrate. These routes to obtain dense electrolyte on metal substrate have their own merits and demerits and are discussed ahead [11].

Plasma spray deposition of YSZ allows the deposition of nearly dense YSZ layer on the prefabricated metal substrate. Complete densification can then be achieved by thermal treatment at relatively lower temperature. This allows the metal substrate to retain high porosity during fabrication. However, electrolyte thickness of 30-70µ is necessary to ensure the gas tightness of the electrolyte layer. Also, the ionic apparent conductivity of plasma deposited YSZ is lower than sintered YSZ [41]. These factors require the cell to operate at least 800°C, which can in turn lead to excessive oxidation of substrate as discussed earlier (see section 2.5.1.b).German aerospace center (DLR) and collaborator have pioneered the plasma deposition of YSZ electrolyte for MS-SOFC [42] [43] [44] [41].Some of the recent works on plasma spray deposition of YSZ for MS-SOFC are [45] [46] [47]. A review on plasma spray deposition technique for various components of SOFC is given by [48] .

In the co-sintering approach, thin porous YSZ layer is first deposited on the green metal substrate by conventional and inexpensive wet/colloidal deposition techniques. These techniques include tape-casting, drip-coating, screen-printing, aerosol spray-coating, dip-coating and spin-coating. The green layers are then co-sintered between 1200-1400°C in order to obtain dense electrolyte. This approach is very attractive for mass production on industrial scale due to the low fabrication cost. Furthermore, unlike plasma spray deposition, the wet/colloidal deposition techniques allows to deposit and sinter thin YSZ layer (10-20 µm). Thus the cell can be operated in relatively lower temperature range (650-700°C) preventing the rapid oxidation of commonly used stainless steel

substrates. YSZ shrinks between 10-25% depending on the green density. It is necessary that the shrinkage of substrate matches with that of the electrolyte or else the electrolyte will be held in tension during co-sintering, forming cracks. It can be very challenging to obtain sufficient shrinkage for substrate while still retaining sufficient porosity. This can be however achieved by care full combination of particle size, granulometery, initial packing density, amount of pore former and amount of binders [49].MS-SOFC fabricated by co-sintering approach have been reported to show good performance [50] [51], stability [52] [51], excellent thermal cycling resistance [53] [54] and good redox cycling resistance [53]. Fig.13 shows power density above 1.2 W/cm^2 at 700°C for a co-sintered MS-SOFC [50].
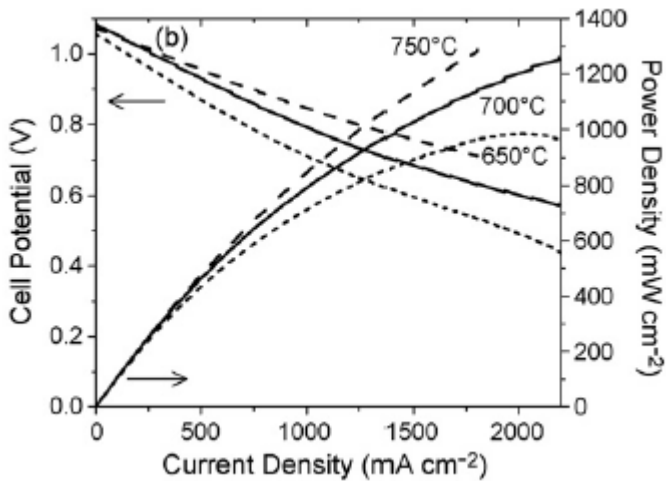

Fig.13. Performance of MS-SOFC with YSZ electrolyte obtained by co-sintering. Measurements were carried out with humidified hydrogen and oxygen. Ni anode catalyst and LSM cathode catalyst were introduced by infiltration [50].

2.5.3. Cathode Materials

Electrochemical reduction of oxygen takes place at cathode/electrolyte interface and therefore the cathode should satisfy the following requirements. It should have high electronic and ionic conductivity and should possess high electrocatalytic activity for cathode oxygen reduction. It should be chemically stable under fabricating and operating conditions. TEC of cathode should match with other cell component and it should be compatible with electrolyte and interconnect materials it is in contact with. Finally, it should have a stable, porous microstructure.

The typical cathodes decompose when sintered in inert or vacuum atmosphere which is necessary to prevent oxidation of metal substrate [55]. Cathodes are therefore restricted for sintering in air below 900°C after all high temperature, non-oxidsing processing steps. Such temperatures are not high enough as the cathode materials like LSM (Sr doped LaMnO$_3$) and LSCF (Lanthanum strontium cobaltite ferrite) requires to be sintered between 1000-1200°C to achieve high performance. Although SDC-Sm$_{0.5}$Sr$_{0.5}$CoO$_3$ (SSC) composite cathodes show good performance when sintered at relatively low temperature of 800°C [56] [29] [36] [30] [37] [38] [28] , they are not suitable due to their high TEC (18.4ppm^{-1}).Moreover, both LSCF and SSC are susceptible to Cr poisoning [23]. LNF (La(Ni)FeO$_3$) cathode is recommended for MS-SOFC application as it is tolerant to presence of Cr [57] [58] [59] and shows good performance at sintering temperature as low as 800°C [60].Lately, some other studies were also carried on cathode material which could be directly sintered in situ during operation for MSOFC. (Bi$_2$O$_3$)$_{0.7}$(Er$_2$O$_7$)$_{0.3}$-Ag composite cathode was sintered in situ at 750°C during operation for a MS-SOFC. The cell showed promising maximum power density of 568 mW cm^{-2} with humidified hydrogen

and air [61]. Kim et.al did a comparative study of unsintered BSCF (Ba-Sr-Co ferrite), LSCF and LSM cathode materials [62]. The study was carried out on ASC having the unsintered cathode materials at 800°C among which BSCF showed the best performance Fig.14.The MS-SOFC with unsintered BSCF showed maximum power density of 820 mW cm^{-2} at 800°C with H$_2$-3%H$_2$O and air.

Nonetheless, the above mentioned processing limitations can be overcome by catalyst infiltration approach for cathode fabrication. In this route the molten salt of metal that comprise the catalyst is infiltrated in 'porous support/porous YSZ/dense YSZ' geometry after its processing at high temperature in reducing atmosphere. The salts can then be decomposed between 400-600°C to give the desired oxide catalyst composition [63].

It should be noted that deposition of cathode materials like LSM or LSCF for MS-SOFC have also been done by plasma spray [42] [41].
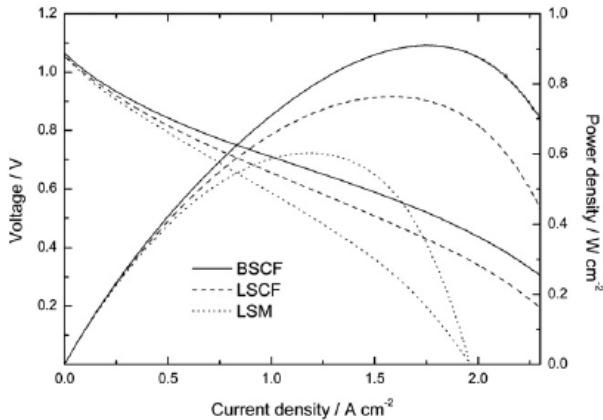

Fig.14. Performance of ASC with unsintered BSCF, LSM and LSCF cathodes at 800°C with H$_2$-3%H$_2$O and air at anode and cathode respectively [62].

37

2.5.4. Anode Material

The function of the anode material is to provide sites for the oxidation of fuel and to enable the charge neutralization by electronic conduction. The anode must be an excellent catalyst for the oxidation of fuel. It should be: electronically conducting, sufficiently porous, stable in oxidizing and reducing atmosphere, and have TEC closely matching with that of electrolyte and substrate. Furthermore it should be chemically stable with components it is in contact with, such as substrate and the electrolyte. Finally it should be applicable with various fuel and impurities like sulphur.

Ni/YSZ cermet has been the most preferred anode material for the previous generations of SOFCs. Same anode material has been considered for the MS-SOFC by most of the developers. Ni/YSZ cermet, however imparts some fabrication issues. Any MS-SOFC fabrication approach involving temperature above $900^{o}C$ should be carried out in inert atmosphere (typically Ar-3%H_2) or high vacuum to prevent excessive substrate oxidation. Such condition leads to reduction of NiO (initially used) during fabrication itself and causes coarsening of Ni phase in the anode. For instance, Fig.15. shows the microstructure of a cell fabricated at $1400^{o}C$ in H_2 and cell fabricated at high temperature in air and then reduced at $800^{o}C$ in H_2 [64].Coarsened Ni grains with non-homogenous microstructure can be seen for cell sintered at $1400^{o}C$ in H_2. Ni coarsening decreases the number of triple phase boundaries (sites active for oxidation of fuel), and can also decrease the electrical conductivity of the anode due to the loss in connectivity and percolation of Ni phase. Moreover, there is this problem of interdiffusion of Ni and Fe, Cr from the anode and the stainless steel substrate respectively during high temperature fabrication (more worse) and during operation [65] [66] [43]. Fe and Cr can form intolerable oxide phases in the anode material whereas Ni can lead to austenisation of ferritic stainless steel substrate.

38

Austenisation of ferritic stainless steel is problematic because it can cause the mismatch in TEC of substrate with that of other cell components. The interdiffusion and coarsening due to high temperature fabrication processes can be avoided by using low temperature processes such as plasma spray for the deposition of anode and electrolyte. However, interdiffusion still occurs during the long term operation of the cell as shown in Fig.16. [43].
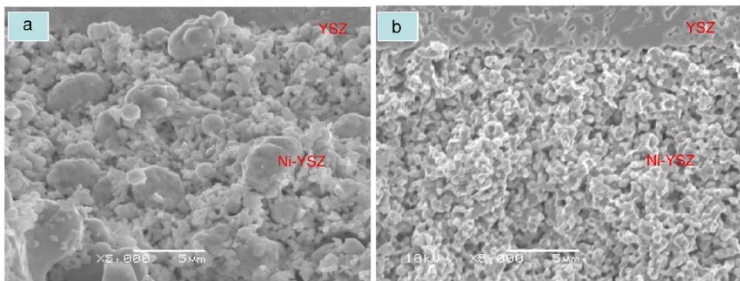
Fig.15. Electrolyte and anode microstructure of (a) Cell sintered at 1400°C in H$_2$ and (b) Cell sintered at high temperature in air and then reduced at 800°C in H$_2$.Comparatively large (coarsened) Ni grains with non-homogenous microstructure can be seen for cell sintered at 1400°C in H$_2$. [64].
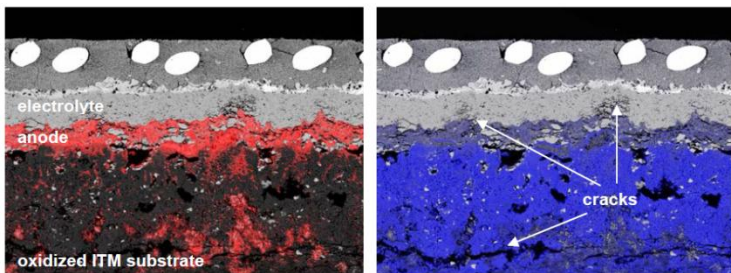
Fig.16. EDAX/SEM composite image of cross-section of MS-SOFC produced by plasma spray processing after 1500 H operation at 800°C (Left: Ni distribution in red, Right: Fe distribution in blue [43].

Nevertheless, the issues of high temperature coarsening and interdiffusion have been addressed by infiltration approach for anode. Use of diffusion barrier layer (DBL) between anode and steel substrate has also shown to prevent interdiffusion. These topics will be addressed in detail in section 2.6.2.
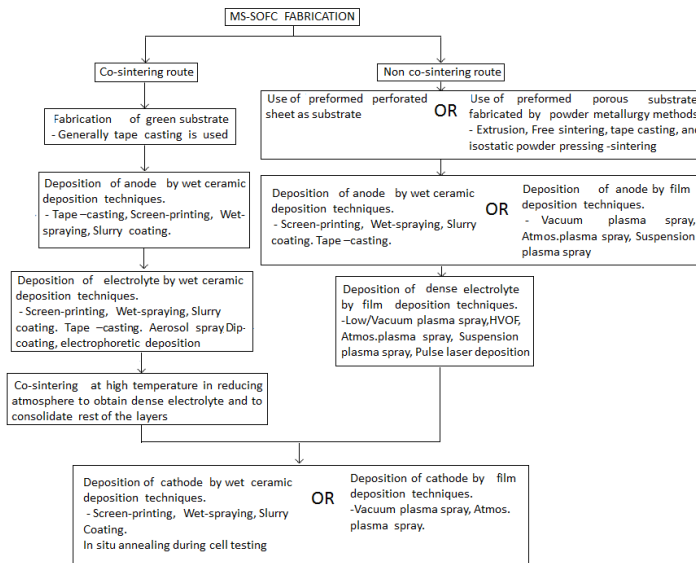
2.6. Fabrication of MS-SOFC

The presence of metallic substrate in the design makes the fabrication of MS-SOFC quite challenging. Unlike the conventional ceramic or cermet supported SOFC, care should be taken that high temperature fabrication steps for MS-SOFC is carried out in inert atmosphere or vacuum to prevent substrate oxidation. Also, the sintering temperature may not be too high (necessary to obtain gas tight electrolyte) which otherwise can lead to limited porosity or the melting of the substrate. Moreover, the less or no shrinkage exhibited by the substrate during fabrication demands to employ expensive and advanced fabrication approaches. Different approaches and techniques have been employed by developers to overcome the fabrication issues and will be discussed ahead.

In general, the MS-SOFC fabrication can be distinguished into fabrication by non-cosintering and fabrication by co-sintering route. Fig.17. shows the schematic representation of techniques used for MS-SOFC fabrication by the two approaches.

2.6.1. Fabrication by non-co-sintering routes

In the non-cosintering approach, MS-SOFC is fabricated by using film deposition techniques for the deposition of functional layers on the prefabricated substrate. The prefabricated substrate can be a preformed perforated sheet or a porous substrate produced by powder metallurgy methods (Extrusion, free sintering, tape casting and isostatic powder pressing-sintering).Fig.18. show the SEM images of perforated and porous substrates [67]. Prefabricated substrates are especially suitable for the film deposition techniques. This is because the prefabricated substrate does not shrink during sintering and the film deposition technique deposits electrolyte in a

dense or nearly dense state; it does not require the high temperature sintering step and shrinkage for densification. The film deposition technique for depositing functional layers include physical / vapor / plasma deposition methods. This fabrication route is often called as "low temperature route" as the layers are produced at lower temperature. Fig.19. shows the SEM image of the MS-SOFC fabricated by plasma spray deposition of active layers on the porous stainless steel 430 substrate [47]. This approach is actively developed by different groups for e.g. National Research Council

Fig.17. Schematic representation of techniques used for MS-SOFC fabrication by the two approaches. It should be noted that 1) For co-sintering route, the sequence of deposition can be substrate.=>anode=>electrolyte or electrolyte=>anode=>substrate depending on the type of wet deposition technique employed. 2) Ceria based electrolytes can be deposited by wet ceramic deposition

42

techniques on the preformed substrate as it can be constraint sintered (see section 2.5.2.b)

Canada (NRC) using PLD [37] [30] and HVOF [68], and Aerospace Research Center and Space Agency (DLR) in Germany using APS and VPS [41] [42]. These fabrication processes allows fabrication of MS-SOFC in a single step by consecutively coating all the functional layers on the substrate. Another advantage is that these processes limits the coarsening of Ni in the anode and interdiffusion of Ni and Fe,Cr between anode and the substrate during fabrication. Ni coarsening and interdiffusion is a critical issue when single step co-sintering approach is considered for MS-SOFC fabrication.
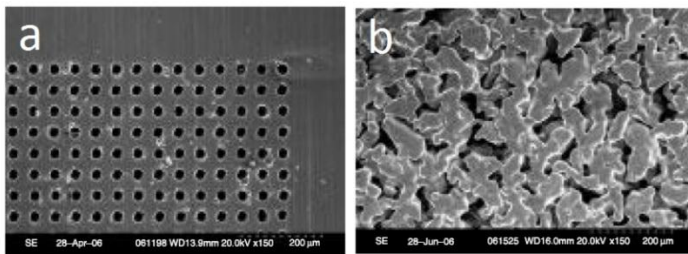
Fig.18.SEM images of two different substrates: (a) perforated sheet and (b) porous one.

The major drawback of this approach is the high cost and limited flexibility associated with the deposition techniques. Use of plasma spray deposition requires the sufficiently smooth surface of the underlying layer to be coated. Preformed perforated sheet gives smooth surface and therefore they are preferred. For substrates produced by powder metallurgy, surface with small pores and roughness require small grained alloy powder for production. This

causes the substrate to have enhanced surface area and can lead to Cr depletion from bulk which is not favorable (see section 2.5.1.a)
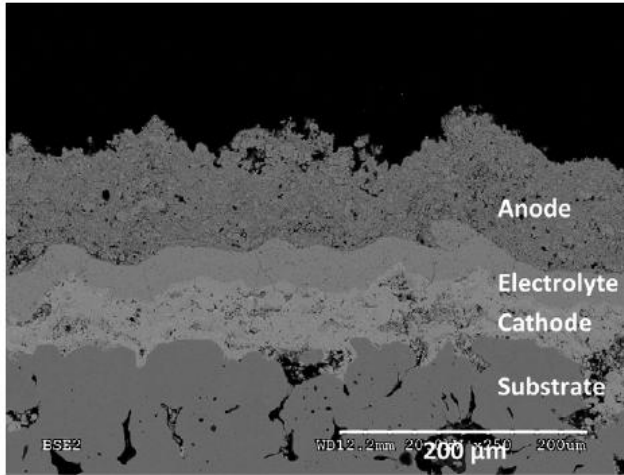
Fig.19. SEM image of MS-SOFC fabricated by plasma spray deposition of LSM/8YSZ cathode, 8YSZ electrolyte and NiO/8YSZ anode on the prefabricated porous ferritic stainless steel 430 substrate [47].

High temperature sintering can also be avoided by employing the film deposition techniques just for the electrolyte while wet ceramic deposition techniques can be used for the electrodes. Screen printing or spray coating can be used to deposit the active functional layers (AFL) with smooth surface and small pores which is necessary to obtain gas tight electrolyte. Use of screen printing for deposition of AFL and atmospheric plasma spray for electrolyte is reported in [69]. [37] [30] employed screen printing for AFL coating and SPS for electrolyte deposition. This approach is however not preferred and not suitable for mass production on industrial because it involves multiple steps of coating and annealing which makes it time and energy consuming.

44

2.6.2. Fabrication by co-sintering routes

MS-SOFC fabrication by co-sintering route employs wet ceramic deposition techniques (tape-casting, screen-printing, wet powder spraying and spray/spin/dip- coating) for the deposition alloy substrate and the active functional layers (anode and electrolyte). The assembly is subjected to one or more co-sintering steps at high temperature in reducing atmosphere to densify the electrolyte and consolidate the AFL and substrate. The cathode layer is then deposited usually by screen printing and sintered in situ at lower temperature to avoid its decomposition (see section 2.5.3.). Since the electrolyte layer is deposited by the wet ceramic technique, high sintering temperatures are required for the densification of electrolyte. This route is therefore often called as "high temperature process". The main advantage of this processing route is that it is economical, flexible and easy to upscale for mass production on industrial scale. However, there some serious issues related to this fabrication route.

The electrolyte has to shrink considerably so as to fully densify during cosintering, alloy substrate also is therefore required to have sufficient shrinkage. It is quite challenging to obtain such shrinkage and at the same time maintain sufficient porosity for the substrate even when produced by wet deposition technique such as tape casting. However, particle size and granulometry of the starting alloy powder, use of binder, additives and pore formers can be carefully optimized to give sufficient shrinkage and the required porosity [49]. Another problem is that, the different sintering profiles and the variations in TEC of different layers lead to delamination, cracking and bending of the cells. Besides this, the major drawback of the co-sintering route is associated with the anode and anode-substrate interactions (see section 2.5.4.). This includes Ni coarsening in the anode and Ni [64] and Fe, Cr interdiffusion between

anode and substrate [43] [65] [66]. The developers have employed approaches such as infiltration and the use of diffusion barrier layer to overcome these issues.

(a) Infiltration approach for co-sintering

Lawrence Berkeley National Laboratory (LBNL) in USA was the first one to come up with infiltration route [11] [53] [50]. In this approach, first the porous YSZ anode (without the catalyst) is co-sintered with metal support, electrolyte and possibly other layers at high temperature in reducing atmosphere. Catalyst (Ni) is then infiltrated by precursor method at lower temperature. The catalyst is therefore never exposed to high temperature in reducing atmosphere thus preventing coarsening and interdiffusion upon fabrication. In this approach, the anode catalyst coats the metal support as well and so, inclusion of rare earth in the precursor can improve the oxidation resistance of the support. The catalyst forms a thin layer on the porous YSZ and porous metal support backbone, and does not play any role in the mechanical integrity. Thus, catalyst with significant TEC mismatch or volume change upon redox cycling can be employed. Similarly, infiltration route can be, and is also employed for the cathode material to overcome its limitations during high temperature co-sintering (see section 2.5.3.). The infiltration route is also investigated by Riso National Laboratory in Denmark with Karlsruhe Institut fur Technologie (KIT) in Germany [51] [70]. A setback of this approach is the need for multiple-annealing cycles to achieve sufficient connectivity between catalyst particles, thereby making the process tedious. Fig.20. shows the microstructure of the cell fabricated at LBNL by co-sintering before the catalyst infiltration [11], and the microstructure of anode after Ni infiltrations [50].
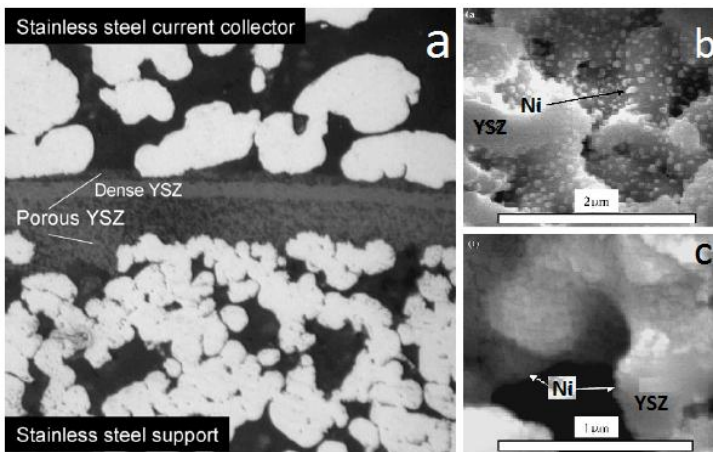
Fig.20. (a) Microstructure of the cell fabricated at LBNL by cosintering *before the catalyst infiltration* [11]*, and the microstructure of anode after Ni infiltration (b)once and (c)5 times* [50]*.*
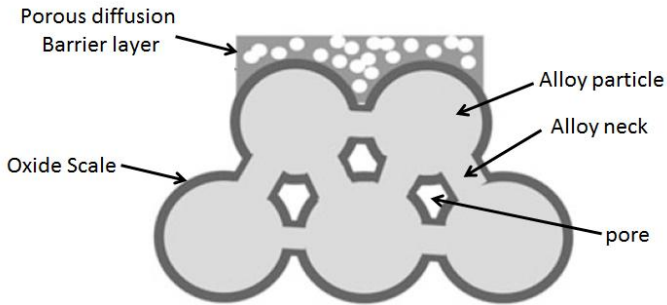
(b) Diffusion Barrier Layer (DBL)

One way to prevent Ni and Fe,Cr interdiffusion is by insertion of DBL between substrate and the anode (Fig.21.) [3]. DBL should prevent interdiffusion of elements while allowing the electron and gas transport. It should have a TEC matching with that of other components, and should be stable and compatible with operating and processing conditions. The challenges are to make the layer porous enough to ensure gas transport and at the same time to cover all points between electrode particles and the substrate particles to inhibit interdiffusion.

Some of the efficient DBLs are the compositions including: $La_{0.6}Sr_{0.2}Ca_{0.2}CrO_3$ and $La_{1-x}Sr_xMnO_3$ [43] [44] [41]; CeO_2 and $Ce_{0.8}Gd_{0.2}CrO_3$ [69]; and undisclosed compositions [65]. Fig.22. shows a MS-SOFC with CeO_2 DBL between CroFer22APU substrate and Ni/YSZ anode after 165 h of operation at 800^oC, CeO_2 was found

to be an efficient DBL [69]. It should be noted that compositions similar to LSM are expected to be unstable in fuel atmosphere [55]. Although Cr_2O_3 also was used as DBL, it was not very effective due to reduction of Cr_2O_3 layer during cell fabrication at high temperature in reducing atmosphere [69].

DBL addresses to the issue of elemental interdiffusion, however, it does not prevent Cr evaporation from the bulk of the substrate, and due to its porous structure cannot solve the problem of electrode poisoning by Cr.

Fig.21. Schematic representation of a porous diffusion barrier layer coated in the surface of the alloy [3].
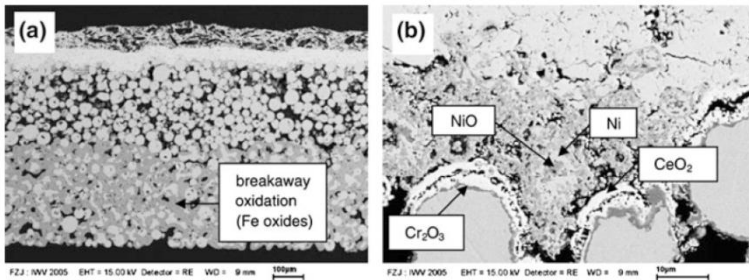
Fig.22. MS-SOFC with CeO_2 DBL between CroFer22APU substrate and Ni/YSZ anode after 165 h of operation at 800°C at (a) low magnification and (b) high magnification [69].

2.7. Powder consolidation by tape casting for SOFCs

Tape casting belongs to the wet powder processing technique for green forming (the other main techniques include slip casting, filter pressing, gel casting and electrophoretic deposition).It is a highly productive technique for the fabrication of flat, single or multilayered ceramics with thickness ranging from about 5µ to over 1mm for a layer, and is widely used in the electronic industry. It is a well-established ceramic forming technology, but can be also used in powder metallurgy as a powerful, versatile and low-cost shaping process. It has been successfully demonstrated to produce thin sheets of stainless steel [71]. Fig.23. outlines the basic principle of tape casting. The first and probably the most important step is the preparation of the slurry with the powder under consideration. It involves preparation of slurry with powder of appropriate grain size distribution and morphology in a dispersing fluid, with addition of additives like, a dispersant, a binder and sometimes a plasticizer [72] [73]. The slurry is then cast on a stationary or moving flat surface with help of a blade also known as doctor-blade. The wet cast tape then enters the evaporation chamber where the solvent from the cast evaporates by means of heat and air circulation to give strong and flexible tape. The tape is cut or punched into desired shapes and then peeled from the carrier before de-binding and sintering. For mass production on industrial scale, moving polymeric carrier (such as PET, PE, PP) is generally used, whereas, for a lab scale production the doctor blade is moved over a fixed surface (eg glass or a metal blade).The carrier is usually covered with a release agent in order facilitate the peeling of the dry tape.
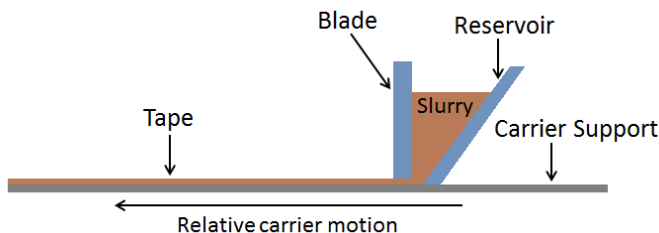
Fig.23. Schematic overview of a typical tape casting system equipped with a Doctor Blade.

Preparation of a suitable formulation for casting is the most challenging task in the tape casting process. The liquid carrier is usually non-aqueous, although recently water-base suspensions are gaining more and more interest. In this work, water base suspensions were used due to their lower environmental impact and lower cost compared to organic solvents, in terms of purchasing, handling, recycling, disposing and protecting the working environments. The slurry is prepared by mixing the components by ball milling or ultrasonicating. In this step the soft agglomerates are broken down and the powder surface is covered by dispersant to keep them dispersed. The milling step can however be avoided when the layer of coarse particles is being deposited. For instance, in the current thesis for the casting of stainless steel support layer the milling step was avoided and the slurry was prepared simply by mechanical stirring. The function of the binder which is an organic polymer is to give strength and the flexibility to the green tapes. Plasticizer is added to modify the mechanical properties of the green tapes and for the relaxation of drying stresses. Examples of common binders are: vinyl binders (PVA, PVB), acrylic (PEMA, PMMA, acrylic emulsions), polyolefin and cellulose based. The binder is usually added after the milling process in order to prevent the degradation of polymer chain

50

due to high impact force during milling, and also because it is more effective when it covers the well dispersed particles rather than the agglomerates. Other additives such as antifoaming agent, rheology modifiers and surfactants may be added to the slips in order to get the desired properties.

The thickness of the dry tape results from the combination of different parameters. In general, the tape thickness increases with increase in blade gap, slurry level in the reservoir and solid loading in suspension, while increasing the casting speed and the viscosity of the slurry decreases the tape thickness. Usually the thickness of the dry tape often lies in the range of one third to two third of the blade gap.

Typical defects which can affect the quality of the dried tape are large voids caused by air bubble entrapment or rapid evaporation, and presence of agglomerates or impurities. The drying stresses in the tapes can induce cracks nucleating from the defects, and are detrimental for the mechanical resistance of the final sintered product. In addition, there can be a problem of segregation of the particles with different sizes and densities, and segregation of binders at the top in the case of thick tapes. This can lead to differential density in the green tape which in turn leads to bending and cracking during sintering. Although these problems cannot be completely avoided, it can be reduced to great extent. The reader in suggested to refer [72] [73] for deeper knowledge.

SOFC production involving the use of tape casting technique can be achieved either by conventional processing route or by sequential tape casting. Fig.24a. illustrates the manufacturing process of conventional SOFC production, where the first step consist of tape casting of substrates and subsequent sintering (pre-sintering) before application of functional layers by screen printing. Fig.24.b. illustrates cell manufacturing by sequential tape casting in which the

51

binder burnout and pre-sintering step can be avoided. Additionally, the time for the half cell production can be reduced significantly.
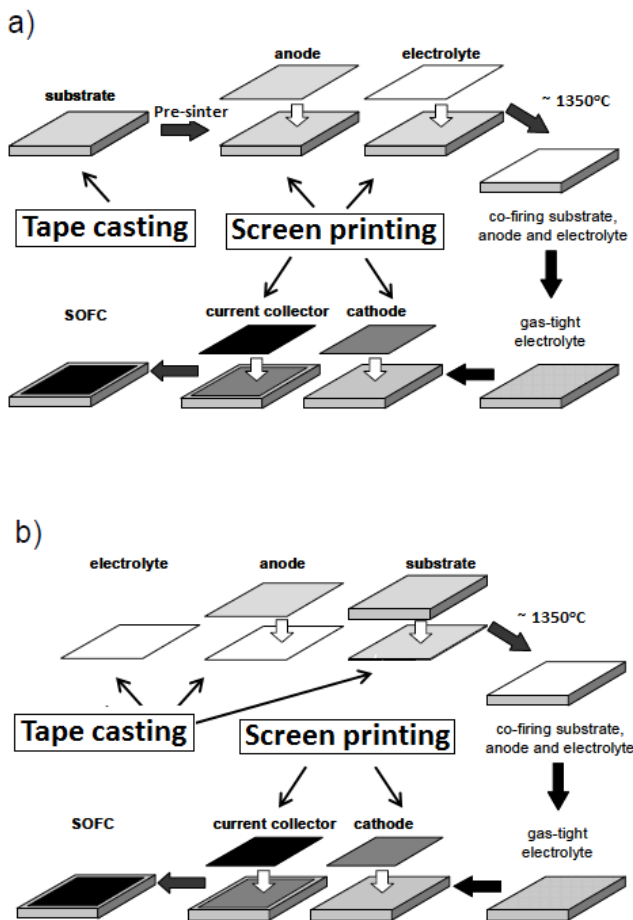
Fig.24. Illustration of fabrication routes of SOFC involving tape casting technique.

In this thesis, keeping in mind the economic feasibility and processing constraints (pre-sintered substrate exhibits less or no shrinkage), sequential tape casting route has been employed for the production of MS-SOFC. The route however gets modified for MS-SOFC in comparison to conventional AS-SOFC, involving change in sintering atmosphere and introduction of additional layers due to the presence of the metal support (see section 2.6.).

2.8. De-binding and sintering

Once the green sample is produced, the next step is the heat treatment in order to consolidate and to obtain desired microstructure. During firing the green sample shrinks, reducing the porosity and increasing the mechanical properties. The first step is usually the loss of organic binders which is then followed by sintering during heat treatment. The binder loss is carried out by slowly heating a green sample, and it takes place usually between 400-700°C.During sintering, the joining of the particle and the reduction of porosity of the body occurs by atomic diffusion in the solid state. In the following section just a brief overview of sintering process is given, however there are numbers of books which covers the complex aspects of powder sintering [74] [75] [76] [77].

2.8.1. Driving force for sintering

For the sintering to take place the free energy of the system must be reduced. The sources which lower the free energy of the system provide the driving force for sintering. The possible driving forces for sintering are:

1. Curvature of the particle surface
2. Externally applied pressure
3. Chemical reaction

In the absence of chemical reactions and externally applied pressure, the decrease in surface free energy E_s of a system is given by [75]:

$$E_S = \frac{3\gamma_{sv}V_m}{a}$$

Where a is the radius, V_m is the molar volume and γ_{sv} is the specific surface energy of the particles comprising the system.

The decrease in surface energy is therefore inversely proportional to particle radius.
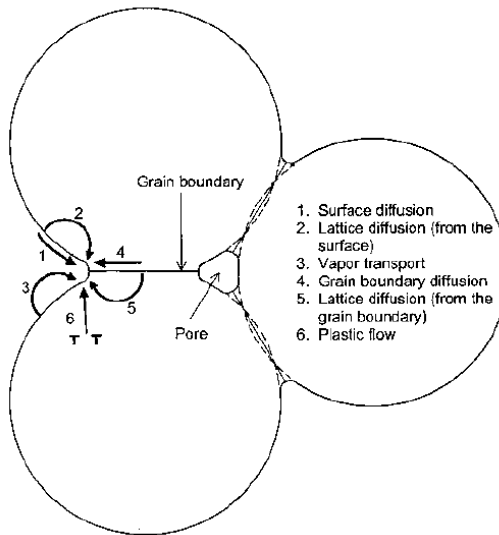
2.8.2. Matter transport

Driving force stimulates the sintering, but the actual sintering process requires matter transport to take place. In crystalline solids the matter transport takes place via diffusion process involving atoms, ions or molecules [75]. The presence of defects in the crystal lattice allows the mass transport to take place. The defects can be classified in 3 types; 1) point defects such as vacancies, interstitial atoms, and substitutional atoms, 2) line defects (dislocations) and 3) planar defects such as free surfaces, grain boundaries, stacking faults, and crystallographic shear planes. Point defects govern the rate of matter transport through the lattice, and the concentration of such defects can be controlled by variables such as temperature, oxygen partial pressure (for oxides) and dopant concentration.

2.8.3. Mechanism of sintering

Mechanism of sintering in crystalline solids is defined by the path via which the diffusion of matter takes place. The matter is transported from region of higher chemical potential (referred to as the source) to region of lower chemical potential (referred to as the sink). Fig.25. shows the assembly of 3 particles in which six different mechanisms of sintering are represented by numbers. In all the cases, the sink for the matter is the neck whereas the source may be different. The neck of the particles has lower energy and thus will

always be the sink for matter transport. Hence the mechanism is defined depending on the source of the matter and the path it follows to the sink. Table 3. describes the six different sintering mechanisms out of which only few contributes for densification as indicated in the table [77].

Fig.25. Path of matter transport during sintering [77].

Mechanism	Source of Matter	Sink of matter	Densifying
1. Surface diffusion	Surface	Neck	No
2. Lattice diffusion	Surface	Neck	No
3. Vapor transport	Surface	Neck	No
4.Grain boundary diffusion	Grain boundary	Neck	Yes
5. Lattice diffusion	Grain boundary	Neck	Yes
6 Plastic flow	Dislocations	Neck	Yes

Table 3. Mechanisms of sintering in polycrystalline solids [77].

56

2.9. Constrained sintering

Almost all the sintering systems are constrained to some extent. For instance, sintering of a pure single phase powder is constrained by inhomogeneity such as agglomerates in the green sample. The term constraint is however used when the constraint is del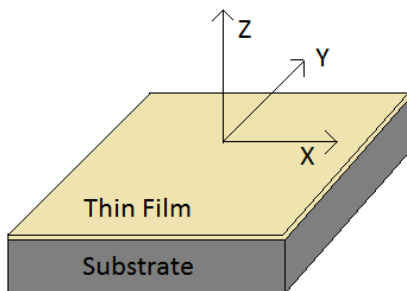iberately involved as it forms the necessary part of the system. Four important cases of constrained sintering in powder science and technology are: 1) composites where porous matrix densifies around rigid inclusions or agglomerate which densifies at a different rate, 2) densification of a thin film on a rigid substrate, 3) sintering of multilayers of different materials where each material densifies at a different rate and 4) compact with density variation [78]. These cases of constrained sintering are illustrated in fig.26. Sintering of multilayers is thoroughly involved in SOFC fabrication, and, sintering of thin films on rigid substrate is especially involved in fabrication of MS-SOFC where in some cases the functional layers are made to sinter on rigid prefabricated metal support. Due their criticality in SOFC fabrication, only these two cases of constrained sintering will discussed ahead.
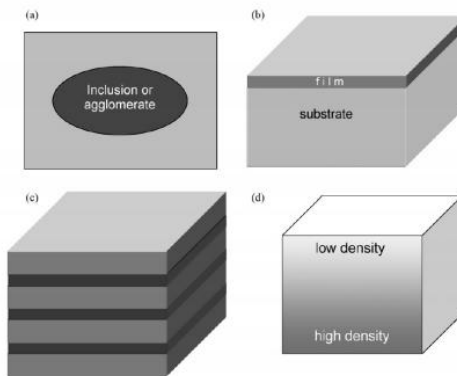
Fig.26. Schematic illustrations of structures which undergo differential densification: (a) composite material where porous matrix densifies around rigid inclusion or agglomerate, (b) thin film densifying on rigid substrate, (c) sintering of multilayers with different densification rates and (d) structure with density gradient [78].

2.9.1. Constrained sintering of thin film on a rigid substrate

Areas of electronic and optical ceramics involves this case of constrained sintering where thin film is deposited on a substrate which is followed by drying and sintering. Usually the film adheres to the substrate and is too thin to cause it to deform, so the substrate can be considered as rigid. If the film remains attached to the substrate during sintering with no cracks, shrinkage in the plane the substrate is inhibited, and stresses arise in the substrate and the film. The shrinkage occurs in the film in the direction perpendicular to the plane (Fig.27.), far from the edges. The film experiences tensile stress in order to maintain the strain compatibility with the substrate, subjecting the film to simultaneous creep. The densification rate of constrained film is thus reduced due the stresses when compared to free sintering of the film, and can lead to the growth of the flaws [77].

The volumetric densification rate of the constrained film on a rigid substrate can be given as [77]

$$\left(\frac{\rho^{\cdot}}{\rho}\right)_c = -\left[\frac{1+v_p}{3(1-v_p)}\right]3\dot{\varepsilon_f}$$

where ρ is the relative density of the film, and the dot denotes the derivative with respect to time. v_p is the Poisson's ratio of the porous film and $\dot{\varepsilon_f}$ is the linear densification rate of the free or unconstrained film.

Since the densification rate of the unconstrained film is given by

$$\left(\frac{\rho^{\cdot}}{\rho}\right)_u = -3\dot{\varepsilon_f}$$

the function of v_p in the square brackets of equation for volumetric densification rate of the constrained film represents the amount by which the densification rate of the film is retarded by the substrate.

Substantial stresses are generated in adherent film during constrained sintering. If the film is sufficiently thin, then the stress distribution normal to the plane of film surface can be considered uniform. The interfacial adhesion or the shear strength should be high enough to overplay the stresses. For a fixed interfacial strength, there is a critical thickness of the film (typically <50μ for sintering of particulate film on rigid substrate) above which the interfacial strength can no longer withstand the tensile stresses. This leads to interfacial

59

failure such as delamination. The tensile stresses can also lead to failure by cracking initiated in the film itself by the growth of preexisting flaws. The growth of the preexisting crack is favored if the initial crack length is high, whereas high interfacial strength and small film thickness does not allow the crack to grow.

2.9.2. Constrained sintering of multilayers

When the green multilayers are co-sintered, the difference in sintering rates of different layers imparts transient stresses that inhibit the densification of individual layer. These stresses can lead to the growth of microstructural flaws (cracking, delamination), as well to anisotropic shrinkage (warping of the multilayered structure). Cracking, delamination, limited densification and warping during co-sintering can however be avoid by carefully matching the sintering rate of each layer through control of powder characteristics, green density, and sintering program [77].
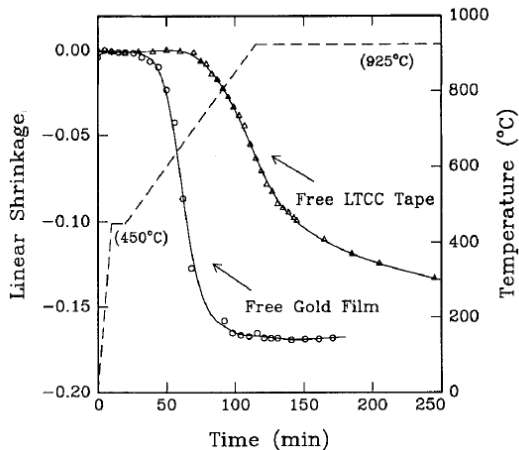
Fig.28. Shrinkage kinetics for unconstrained thick film of gold particles and LTC tape consisting of cordierite and glass particles.

60

Fig.28. shows the plot for the unconstrained sintering shrinkage of thick films of gold particles and the ceramic (LTCC particles tape consisting of cordierite and glass particles) [79].When the two films are bonded and co-sintered, since the gold film begins to shrink first, its densification will be constrained by the ceramic tape. The gold film will thus experience a tensile stress and the bilayer will wrap towards the gold side. Later when the ceramic tape tries to shrink, its densification will be constrained by the gold tape.

3. Experimental procedure and results

3.1. General experimental methods and techniques

3.1.1. Preparation of Al and Ce doped NiO

$Al(NO_3)_3.9H_2O$ (Fluka, Germany) was used as precursor to produce Al-doped NiO (doping = 0, 2, 3 and 5 wt%). NiO (J.T.Baker, USA), $Al(NO_3)_3.9H_2O$ and water were ball milled for 20 h in a plastic jar containing zirconia balls (Inframat Advanced Materials, USA) and then dried at $110^{o}C$ overnight. The powder was manually ground in mortar, calcined at $900^{o}C$ for 10 h and then again manually ground to avoid any agglomerate.

Ce-doped NiO powder was produced in similar way for which $Ce(NO_3)_3.6H_2O$ (Alfa Aesar, Germany) was used as precursor.

3.1.2. Techniques and Instruments

Scanning Electron Microscope (SEM):
SEM (JEOL JSM 5500, Japan) equipped with Energy Dispersive X-ray Spectroscopy (EDXS) probe was used to determine the microstructure and the chemical composition of the samples. In some case the samples were mounted in epoxy resin and polished using diamond paste down to 1 μm for detailed microstructural analysis.

X-ray diffraction (XRD):

XRD measurements were performed by a Rigaku Geigerflex X-ray Powder Diffractometer (Japan) for phase identification. For all the samples, XRD scanning was carried out between 25° to 90° with step interval of 0.05^o and hold of 8 s for each step.

Dilatometer:

Dilatometer (Linseis GmbH, Germany) was used to monitor the change in dimension of samples as a function of temperature under different atmospheres. The samples of desired dimensions for dilatometery were produced by machining the pellets made by uniaxial pressing. In some cases dilatometry was also performed on tape cast samples produced by carefully rolling the tapes.

Tubular furnace:

Tubular furnace (HTRH 100-300/18, GERO Hochtemperaturofen GmbH, Germany) was used to carry out heat treatment processes on samples under different atmospheres. In some cases, sintering profile of cells was also monitored with the help of CCD camera and optical/thermal filters during sintering in the tubular furnace.

TG/DTA:

TG/DTA instrument (NETZSCH, Geraetebau, GmbH, Germany) was used to study the binder loss process during sintering of green cells produced by tape casting. The binder loss study was carried out in different atmospheres.

Planetary mixer and ball miller:

Planetary mixer (Turbula, Switzerland) and ball miller were used for preparation of doped NiO powders, anode powders, composite powders, slurries for tape casting and doped YSZ powders.

Tape casting:
Laboratory scale tape casting set up in SOFCPOWER, Mezzolombardo, Italy was used for casting of the monolithic tapes and the multilayers.

Screen printing:
Screen printing instrument, screen with mesh size 120 (Gabbrieli technology, Italy) were used for deposition of the cathode.

Keithley:
Keithley multimeters, K2000 and K2100, U.S.A were used for the electrical conductivity measurements of the anode materials.

Archimede's method:
Gibertini instruments, Italy were used to measure the bulk/aparent densitiy of the samples by Archimede's method.

Press:
Manual hydraulic press (Specac, UK) was used to consolidate the powder.

CCD camera:
CCD camera (Imaging Source, DMK 41 AU02) was used in some cases to monitor the sintering.

Optical filters:

CCD camera was focused on the sample through optical filter (Edmund Optics Ltd) and fused silica window (Edmund Optics Ltd) to capture the images during sintering.

3.2. Al dopant effect on Ni/YSZ anode

3.2.1. Introduction and aim of the analysis

In previous works [80] [81] [82] [83], Al doped Ni/YSZ anode material has been shown to be beneficial for the realization of AS-SOFC where the high temperature processing is carried out in air. He et al. found that the addition of Al_2O_3 significantly enhances the flexural strength of Ni-YSZ anode material for up to 3wt% of Al_2O_3 [80]. Cologna et al. demonstrated that the sintering profile of the anode material can be controlled by Al and Ce doping, and high quality flat cells can be obtained by reducing the sintering mismatch among the different layer [81]. In addition, Larsen et al. proposed Al_2O_3 as one of the oxides to prevent Ni coarsening in the anode material by acting as Ni-particle growth inhibitor [82]. Conversely, MS-SOFC fabrication by co-sintering up to around 1350^oC, necessary to obtain dense YSZ electrolyte, must be carried out in non-oxidizing atmosphere to avoid excessive oxidation of the metal. No investigations have been so far performed on the effect of Al doping on Ni/YSZ anode material upon the high temperature sintering in reducing atmosphere. On this basis, the aim of the present work is to analyze the effect of Al doping on Ni/YSZ anode material under conditions for MS-SOFC fabrication by co-sintering.

3.2.2. Materials and methods

(a) Preparation of anode materials

55 g of 0-5 wt% Al-doped NiO (see section 3.1.1.) and 45 g of 8YSZ (8 mol% yttria stabilized zirconia) powder were placed in a plastic jar containing zirconia balls and water and mixed for 3 h using

planetary mixer. The powders were dried overnight at 110°C and then manually ground. In order to study the effect of dopant only, no binder or pore former was used. The obtained anode powders were labelled as 0Al-NiO/YSZ, 2Al-NiO/YSZ, 3Al-NiO/YSZ and 5Al-NiO/YSZ.

(b) Consolidation and sintering

2 g of anode powder were pressed in a 20 mm diameter circular steel dye at 63 MPa for 2 min to produce cylindrical pellets (height = ~2 mm).The obtained pellets were sintered at 1350°C for 4 h (heating rate = 2°C/min) in Ar – 3 vol% H_2 atmosphere in a tubular furnace, these being the typical conditions for the fabrication of MS-SOFC by co-sintering [49].

(c) Characterization

X-ray diffraction measurements were performed on doped NiO and anode powders before sintering and after sintering (by using crushed pellets) for mineralogical phase identification.

SEM equipped with EDXS probe was used to determine the microstructure and the chemical composition of the samples. The samples were mounted in epoxy resin and polished using diamond paste down to 1 μm for detailed microstructural analysis.

Density and electrical conductivity of the samples were also measured.

(d) Electrical conductivity and density

In order to measure the electrical conductivity, sintered samples were cut and polished to realize bar-shaped samples with length of 16 mm, width of 3 mm and thickness of 1.5 mm. The density of the bar-shaped samples previously produced was measured by the Archimede's method.

A standard four- electrodes setup was used for the DC conductivity measurements similar to the procedure reported in [84]. Fig.29. shows the set up for the measurements. Silver (Ag) wires were used for current and voltage electrodes. Two current electrodes were wrapped for 2-3 times around the bar shaped sample at the extreme ends. In order to ensure proper contact, Silver (Ag) paste was applied over the wrapped portion and the samples were kept in oven at 80^oC overnight. The potential probes fixed in the DC set up were used. The distances between the probes was 5mm and were contacted to the center of the bar by applying load from the top. The electrical conductivity was measured at room temperature from the current-voltage characteristics measured in the current range of 0.2 mA to 2 A using a Source-Meter (Keithley). All samples showed ohmic behavior and the electrical resistance were measured from slope of the curve estimated by the least squares method.
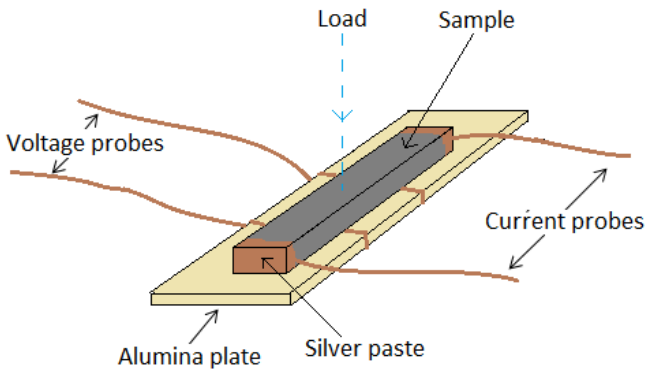

Fig.29. Setup for electrical conductivity measurements.

3.2.3. Results and Discussion

(a) XRD Characterization

The XRD pattern of pure and Al-doped NiO powder is shown in Fig.30.The peaks corresponding to pure NiO are detected; in addition, for Al-doped NiO powders, additional peaks corresponding to $NiAl_2O_4$ (PDF 10-0339) are identified, their intensity increasing with Al content.
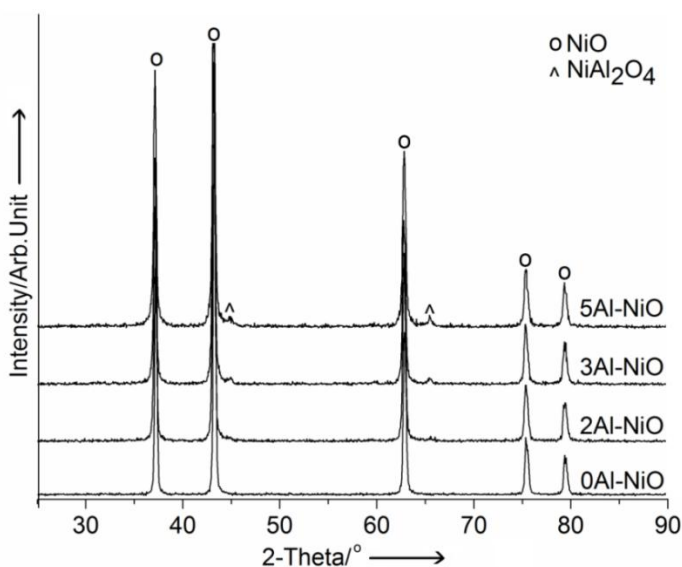
Fig.30. XRD spectrum of pure and Al-doped NiO powders synthetized in this work.

Fig.31. shows the XRD spectrum of Al-doped NiO/YSZ anode materials after sintering at 1350^oC for 4 h in Ar-3 vol% H_2, XRD pattern of as prepared 5Al-NiO/YSZ composite powder is also shown for reference. As prepared 5Al-NiO/YSZ composite powder shows the as expected peaks corresponding to YSZ (PDF 30-1468),

NiO (PDF 47-1049) and $NiAl_2O_4$. Conversely, for the sintered anode materials the NiO peaks disappear completely and additional peaks corresponding to metallic Ni (PDF 04-0850) can be detected. This means that NiO is completely reduced to Ni in anode material when sintered in Ar-3vol%H_2 atmosphere. In addition to Ni peaks, other small intensity peaks corresponding to Al_2O_3 (PDF 46-1212) are present in Al-doped anode sintered materials, their intensity increasing with the Al content. Also, the peaks corresponding to $NiAl_2O_4$, which are detected in the as prepared 5Al-NiO/YSZ powder, completely disappear in the Al-doped sintered material. Therefore, one can conclude that the oxygen partial pressure was sufficiently low in Ar-3vol%H_2 sintering atmosphere when the Al-doped anode materials were sintered to determine the reduction/decomposition of $NiAl_2O_4$ into Ni and Al_2O_3 [85]. The fact that the solubility of Ni and Al_2O_3 in YSZ is negligible accounts for the fixed position of the peaks associated to YSZ before and after sintering for all the considered anode materials [86] [87].

For the conventional AS-SOFC, co-sintering is typically carried out at high temperature, around $1350^{\circ}C$ -$1400^{\circ}C$, in ambient air. The sintered NiO/YSZ composite is then reduced at lower temperature between $600^{\circ}C$ and $1000^{\circ}C$ in either pure H_2 or diluted H_2 to produce Ni/YSZ cermet. Alumina-doped Ni/YSZ material for AS-SOFC was carefully studied in a previous work [80] and it was found that Al_2NiO_4 phase, which is formed during sintering at $1350^{\circ}C$ in air, cannot be decomposed upon the reduction process of the anode material in pure H_2 at $850^{\circ}C$; this was found to be responsible for the limited electrical conductivity of the anode. In another work concerning Al_2O_3-doped Ni/YSZ for AS-SOFC the formation of $NiAl_2O_4$ was described and its reduction to Ni and alumina was shown only at high temperature ($1100^{\circ}C$) in N_2-$10\%H_2$ [83]. This is substantially in agreement with the results obtained in the present work, where $NiAl_2O_4$ is decomposed/reduced to Ni and Al_2O_3 during MS-SOFC co-sintering in Ar-$3\%H_2$ atmosphere at $1350^{\circ}C$.

(b) Microstructure

Fig.32. shows EDXS scan on sintered 5Al-NiO/YSZ showing the distribution of Al, Ni and Zr. Homogenous distribution of Al can be seen throughout Ni/YSZ cermet which means that Al_2O_3 which is formed during sintering is well dispersed in the Ni/YSZ cermet.

The microstructure of sintered 5Al-NiO/YSZ is shown in Fig.33. : on the basis of EDXS analyses, the black regions are the pores filled with epoxy resin, the dark grey phase is Al_2O_3, the light grey phase is 8YSZ and the brightest phase is Ni. One can observe

that sub-micron Al_2O_3 particles are segregated at the grain boundary of both nickel and zirconia grains and most of the alumina particles can be associated with a pore close to them. This suggests that Al_2O_3 inhibits sintering and also coarsening of Ni and YSZ in the composite by segregating on the grain boundaries.

Fig.34. shows the microstructures of the sintered samples. In the case of 0Al-NiO/YSZ and 2Al-NiO/YSZ large Ni grains (~4 μm) can be ide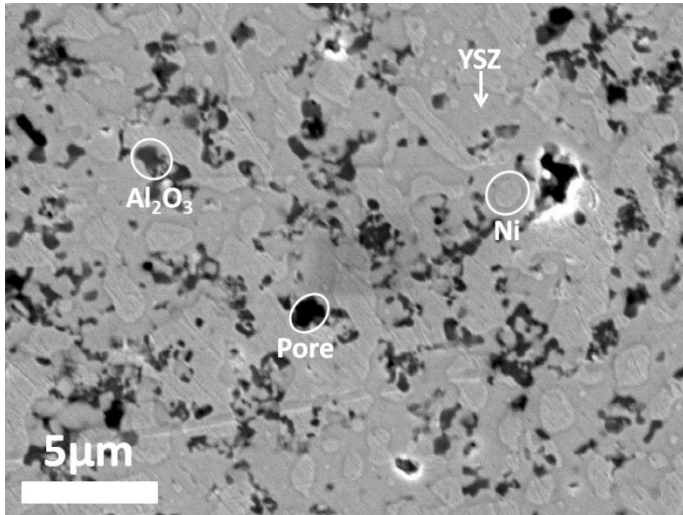ntified. In both cases the microstructure is coarse with isolated Ni grains within the YSZ matrix. Conversely, in the case of 3Al-NiO/YSZ and 5Al-NiO/YSZ the coarsening of both Ni and YSZ is inhibited to some extent and an improved connectivity among Ni grains is developed; the microstructure is finer and Ni grains are well dispersed in the YSZ matrix especially in the latter material. On the basis of such observations, one can conclude that alumina segregation at the Ni and YSZ grain boundary prevents their extensive coarsening and a fine microstructure can be obtained even after sintering at 1350°C for 4 h. Such fine microstructure is expected to improve the electrochemical performance of the cell by increasing the active three-phase boundaries specifically in the case of MS-SOFC where the anode layer only acts as the Active Functional Layer (AFL) and not as support.
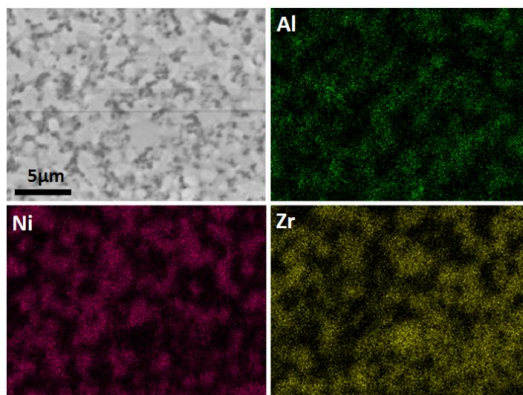
Fig.33. SEM micrograph showing the microstructure on a polished
surface of sintered 5Al-NiO/YSZ.
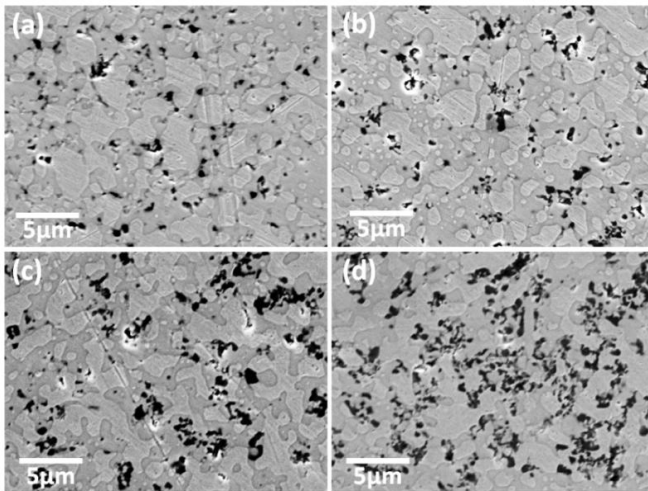
73

(c) Density and Electrical Conductivity

Density and electrical conductivity for the sintered samples are shown in Fig.35. as function of Al concentration. Bulk density slightly increases for 2Al-NiO/YSZ with respect to 0Al-NiO/YSZ; then it decreases considerably for 3Al-NiO/YSZ and 5Al-NiO/YSZ. The initial increase could be related to the effect of Al_2O_3 acting as a sintering aid thus promoting densification of YSZ. It has been shown previously (Fig.36.) [87] that alumina acts as a sintering aid and increases density in YSZ for concentration as high as 2 wt%; conversely, at higher concentrations alumina was found to limit the densification of YSZ. The real density was measured by the so called specific density bottle method after sintering the pellets of Al_2O_3 doped YSZ at $1600^{o}C$ for 20 h [87].

The electrical conductivity of Ni/YSZ cermet depends on the connectivity and percolation of the conducting metallic Ni phase in the porous YSZ matrix. At higher temperature coarsening of Ni particles takes place within the YSZ matrix; as a result, the conducting Ni grains loose connectivity among them, thus degrading the electrical conductivity of the cermet. The electrical conductivity generally increases also with density, and conductivity of at least 100 S cm^{-1} has to be guaranteed throughout the lifetime of the cell to ensure efficient anode current collection [88] [89] [90].

The limited electrical conductivity shown in Fig.35 can be accounted for by the extensive coarsening of Ni phase due to high temperature sintering in reducing atmosphere; this is different with respect to previous studies where the reduction was carried at

maximum temperature of 1000°C after sintering the NiO/YSZ composite at 1350-1400°C in air. One can observe that the electrical conductivity in 2Al-NiO/YSZ sintered sample is slightly lower that in 0Al-NiO/YSZ and this can be related to the formation of insulating alumina upon sintering, although 2Al-NiO/YSZ is denser. In addition, the electrical conductivity of 3Al-NiO/YSZ and 5Al-NiO/YSZ sintered samples increases considerably although their density decreases and the concentration of insulating alumina is higher. This trend can be explained on the basis of the microstructure of the sintered samples as reported above. In 3Al-NiO/YSZ and 5Al-NiO/YSZ sintered samples the microstructure is finer and this improves the connectivity of the conducting Ni phase due to inhibited coarsening of both Ni and YSZ. Therefore, the effect of improved connectivity associated to finer microstructure suppresses the effect of both density and alumina concentration. As a matter of fact, in Ref. [90] lower electrical conductivity is observed for Ni/YSZ with coarser Ni grains although the cermet is denser if compared to the material with finer Ni grains.

Fig.37. [90] shows the electrical conductivity of different Ni/YSZ cermets at 800°C in 10% H_2 balance argon as a function of relative bulk density of their respective sintered NiO-YSZ composite. The relative bulk density of Ni-YSZ cermet can be calculated by simply multiplying the bulk density of NiO-YSZ composite by 0.77.The different cermets were produced from the combination of Fine YSZ and Coarse NiO (FC), Fine YSZ and Fine NiO (FF) and, Coarse YSZ and Fine NiO (CF) starting powders. NiO powders with 3 different average particle size (d_{50}) were tested in the coarse NiO class, and NiO powders with 2 different average particle size (d_{50}) were tested in the fine NiO class. The mixing ratio of YSZ and NiO was fixed to 45:55 for all the samples. Carbon black was used as pore forming agent, and lead to the relative sintered density for the samples depending upon the amount of carbon black used and also on the

75

type of powders. Table.4. [90] gives the average particle size (d_{50}) of the starting powders, amount of carbon black used and the relative sintered density of NiO/YSZ. The uniaxially pressed samples of NiO, YSZ and carbon black mixture were sintered at 1400°C for 3 h. The samples were reduced at 900°C in H_2 to give the respective cermets. The electrical conductivity of the Ni/YSZ cermet was found by four-probe dc method whereas the bulk density of NiO/YSZ was found by Archimede's method. The microstructure of the cermets were found to represent the starting powders used, i.e. samples with fine or coarse NiO starting powders gave fine or coarse Ni grains respectively in the Ni/YSZ cermets. Similarly, samples with fine or coarse YSZ powders gave fine or coarse YSZ grains respectively in the cermet.

It can be seen from Fig.37. [90] that for samples from CF-series (coarse YSZ and fine NiO) the electrical conductivity increases as the relative density of NiO/YSZ (or Ni/YSZ) increases, as expected. For the samples from FC-series (fine YSZ and coarse NiO),it can be seen that the electrical conductivity is lower than that of samples from CF series which have lower relative density. In principle the samples having higher relative density should show higher electrical conductivity. For the samples from FF-series (fine YSZ and fine NiO) it can be seen that the electrical conductivity increases with relative density, and also these series shows the highest values of conductivity. These results clearly show that although density influences the electrical conductivity, it is the microstructure which plays a major role in determining the electrical conductivity of the cermet. In order to have good electrical conductivity the microstructure should be fine with fine Ni and YSZ grains, or at least, the conducting Ni grains should be fine to from well-connected and percolated network. The electrical conductivity decreases considerably when the microstructure becomes coarse, specially the conducting Ni grains.

With respect to above discussion, Al doped Ni/YSZ seems to be a suitable anode material as a microstructure with fine Ni and YSZ is obtained even after sintering at high temperature in reducing atmosphere.
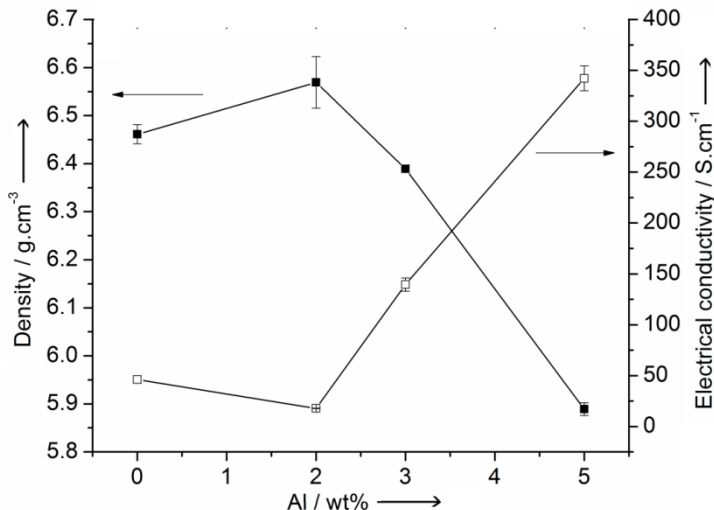

Fig.35. Electrical conductivity at room temperature and bulk density of sintered anode material as function of Al load.
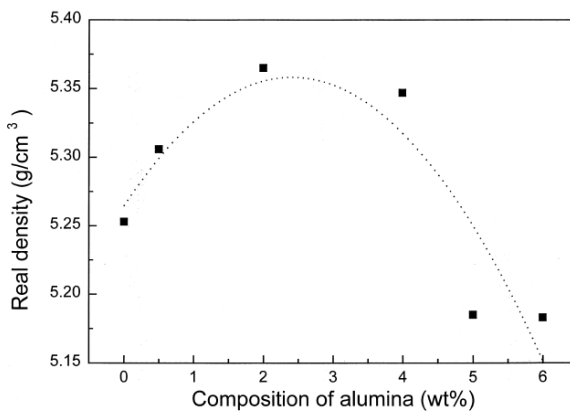
Fig.36. Real density of YSZ as a function of Alumina load [87].
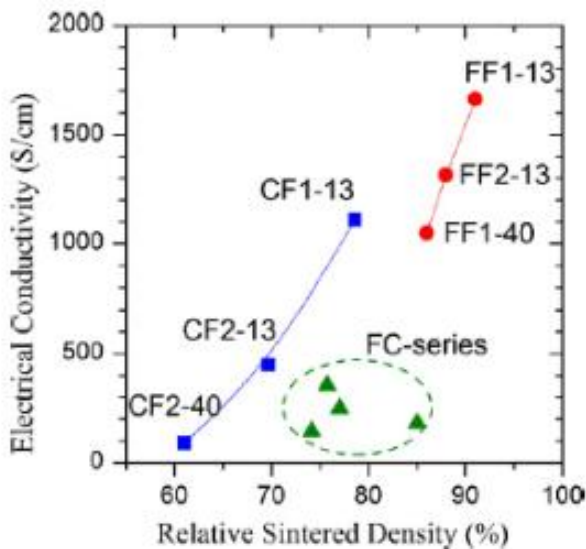
Fig.37. Electrical conductivity of Ni-YSZ cermets prepared from a
variety of powders plotted as a function of the sintered density of NiO-
YSZ [90].

8YSZ		NiO		Carbon black addition (vol%)	Sample notation	Relative sintered density (%)
	Average particle size (μm)	Starting powders	Average particle size (μm)			
Fine class		Coarse class				
	0.762		6.789	13	FC1-13	86
				40	FC1-40	76
			5.006	40	FC2-40	77
			9.964	40	FC3-40	74
Fine class		Fine class				
	0.762		0.878	13	FF1-13	91
				40	FF1-40	86
			0.839	13	FF2-13	88
Coarse class		Fine class				
	7.798		0.878	13	CF1-13	79
			0.839	13	CF2-13	70
				40	CF2-40	61

Table.4. The samples notation, the commercial powders (NiO and
YSZ), the amount of carbon black added as a pore former, and the
relative sintered density of NiO-YSZ composites used for the study
(all the samples were sintered at 1400°C) [90].

78

3.2.4. Conclusion

Al-doped Ni-YSZ cermet was found to be a suitable anode material for MS-SOFC fabrication by co-sintering. $NiAl_2O_4$ which is formed in Al-doped NiO is decomposed/reduced giving Al_2O_3 when the anode material is sintered by using typical MS-SOFC co-sintering conditions, i.e. in reducing atmosphere at relatively high temperature. Al_2O_3 was found to segregate at the grain boundaries of both Ni and 8YSZ grains, thus inhibiting sintering and leading to finer microstructure. Such fine microstructure is expected to improve the electrochemical performance of the anode material in MS-SOFC due to larger number of active three-phase boundaries. The electrical conductivity of the cermet increases for Al doping equal to 3 and 5 wt% and this is attributed to the finer microstructure that accounts for improved connectivity and percolation of the conducting Ni phase in spite of the lower density. The current study was carried out on the anode materials without any binders or pore formers in order to solely analyze the effect of Al doping; nevertheless, similar effects are expected for the porous samples. The effect of Al addition on the polarization resistance and the electrochemical activity of the anode material is the matter of future studies. In any case, from the current work it is clear that Al-doped Ni-YSZ cermet allows the realization of a fine microstructure when MS-SOFC co-sintering conditions are used.

3.3. Investigation of anode/steel interface and dopant effect

3.3.1. Introduction and aim of the analysis

Reduction and oxidation kinetics of metal oxides involve the diffusion of metal cations and oxygen anions through the oxide lattice and along high diffusivity pathways, such as grain boundaries. The contribution of different transport mechanisms depends on temperature [91]. The RedOx behavior of nickel oxide was found to be tunable by the addition of reactive elements (RE), usually rare-earths, which have a high affinity for oxygen [91, 92, 82].Reactive element addition to Ni limits NiO scale growth probably operating by inhibiting grain boundary transport. On the other hand, RE additions may increase the oxidation rate of Ni at higher temperatures (1100-1200°C) [92]. Additions of RE to improve the RedOx tolerance in SOFC anodes have been proposed by Larsen et al. [93, 94]. Tikekar et al. studied the reduction and re-oxidation kinetics of Ni/YSZ anode material and demonstrated that small amount of stable oxides like CaO, MgO and TiO prevent Ni re-oxidation under transient operating conditions [95]. Despite several findings on the beneficial effect of doped-NiO on the anode RedOx behavior under SOFC operating conditions (600-800°C), no investigations have been so far performed on the effect of doping elements on the reduction and coarsening mechanism of NiO upon the high temperature and inert atmosphere sintering conditions.

During co-sintering, the interdiffusion of species at the metal/anode interface can be limited by the addition of a diffusion barrier layer between the metal and the anode. Such extra-layer is often made by CeO_2 due to its low reactivity with the adjacent layers

and its good electrical conductivity (0.89 S/cm at 800^0C) under typical anode operating condition [69]. Nevertheless, although inhibiting solid state interdiffusion, CeO_2 alone is not sufficient to prevent NiO reduction by the chromium contained in the steel, because the oxygen partial pressure in the furnace can be controlled by the release of O_2 due to NiO reduction and, therefore, it does not need a direct interface between the two phases. For this reason, while interdiffusion of Fe, Cr and Ni species can be prevented by the addition of the barrier layer, Cr-NiO RedOx reaction and Ni coarsening still represents a problem to solve.

Thus the aim of the current work is to study the interaction between the anode and steel during the fabrication of MS-SOFC by co-sintering in Ar. Doping elements such as Al and Ce were considered for modification of RedOx kinetics of NiO powder used for anode. Effect of these dopants on anode/steel interaction during co-sintering in Ar atmosphere was also studied.

3.3.2. Materials and methods

(a) Preparation of anode slurries for screen printing

50 g of 0-5wt% Al-doped NiO (see section 3.1.1.) and 50 g of 8YSZ (8 mol% yttria stabilized zirconia) powder were placed in a plastic jar containing zirconia balls and water, and mixed for 3 h using planetary mixer. The powders were dried overnight at 110^oC and then manually ground.

Anode powders composed of Ce doped NiO and YSZ were produced in similar way by using Ce doped NiO powders instead of Al doped NiO. See the general experimental section (3.1.1.) for production of Ce doped NiO powders.

For the preparation of anode slurries, 50g of anode powders were mixed with 50 g of organic vehicle (Terpineol with 3 wt% ethyl cellulose) with the help of magnetic stirrer until a homogenous mixture was obtained.

(b) Preparation of NiO/YSZ/steel powder composites

0-5 wt% Al doped NiO (see section 3.1.1.), 8YSZ and ferritic stainless steel powder containing 22 wt% Cr were used to produce the NiO/8YSZ/steel (1:1:2 wt%) composites. The composites were produced by energetic mixing of powders in a plastic jar containing zirconia balls and water for 6 h. The powders were dried overnight at 110°C and then manually ground.

(c) Experiments

For the initial studies, anode ink composed of NiO/YSZ with pure, Al- and Ce- doped NiO was screen printed on the dense Crofer 22 APU substrates (1 mm thick). Samples were then heated at 2^{0}C/min up to 1400^{0}C and sintered for 2 h under Ar atmosphere.

In order to simulate the interaction occurring at the anode/metal interface, composite materials were analyzed by dilatometry. Specimens were prepared by pressing 2.5 g of the composite powders in a 20 mm diameter circular dye at 100 MPa for 2 min, reaching the thickness of about 2 mm. The resulting pellets were then cut into rectangular bars with size 12 x 5 x 2 mm^3 and used for the dilatometry. The heating profile used was 2°C/min up to 1400°C in Ar condition at flow rate of 400 ml/min.

In order to evaluate the effect of each material on the composite mixture, dilatometric analyses were also performed on single-phase specimens containing only steel and YSZ subjected to same milling conditions used for NiO-YSZ-steel composite.

X-ray diffraction measurements were performed on the composites heat treated in the dilatometer under the same heating rate and Ar flow rate to investigate the phase transformations taking place in NiO-8YSZ-steel composite. Samples were prepared by heating in the dilatometer and stopping the cycle at temperatures corresponding to selected discontinuities observed in the dilatometric curve. After cooling down at room temperature the XRD measurements were taken on crushed sample.

3.3.3. Results and discussion

(a) Anode-steel interaction

The dilatometric plot in Fig.38. shows the behavior of the samples heat treated under Ar and air atmosphere. When pure steel sample is heat treated in air, it shows a volume expansion obviously related to oxidation, but when heated in Ar it shows a conventional sintering behavior with a shrinkage onset at 1170^{0}C. On the other hand, it can be observed that NiO/YSZ/Steel composite shows a sudden volume expansion above 800°C followed by a substantial shrinkage after 1200°C in Ar. The fact that the steel shows conventional sintering behavior when sintered in Ar, allows to exclude that the volume expansion in the composite could be related to oxidation of steel due to oxygen impurities in the Ar atmosphere. This volume expansion in the composite heated in Ar can be attributed to the oxidation of steel due to the redox reaction between NiO and steel. It is well known from the Ellingham diagram [96] that Fe and Cr oxides are thermodynamically more stable than NiO; therefore, there is a thermodynamically favored oxidation of steel due to the redox reaction between steel and NiO, producing Ni. From these results it is proposed that steel-NiO RedOx reactions involving volume changes

at the interface between Ni-based anode and the metal substrate could be the key sources for major issues like coarsening, delamination and cracking of MS-SOFC. As shown in Fig. 38, YSZ shows the onset of sintering at around $1200^{\circ}C$ accounting for shrinkage in the composite above $1200^{\circ}C$. It is worth to notice that the net shrinkage of the NiO/YSZ/steel sample, at $1400^{\circ}C$, is almost zero, such value being definitely not suitable for cells fabrication, where at least 20% volume reduction is required for the co-sintering with the electrolyte. It is also interesting to observe the two slight rate changes in the volume increase for the pure steel when fired under Air atmosphere. This result suggests a change of the oxidation mechanism of the steel as a function of the temperature and it could be related to the formation of Cr-Fe oxides with different structure, on the metal particle surface. Therefore, the change of slope in the curve suggests 3 ranges of steel oxidation, between 800°-$1050^{\circ}C$, 1050°-$1150^{\circ}C$ and above $1150^{\circ}C$.
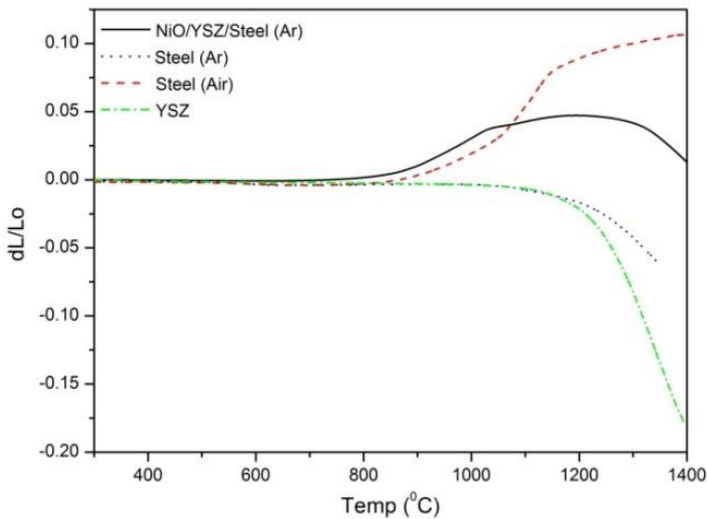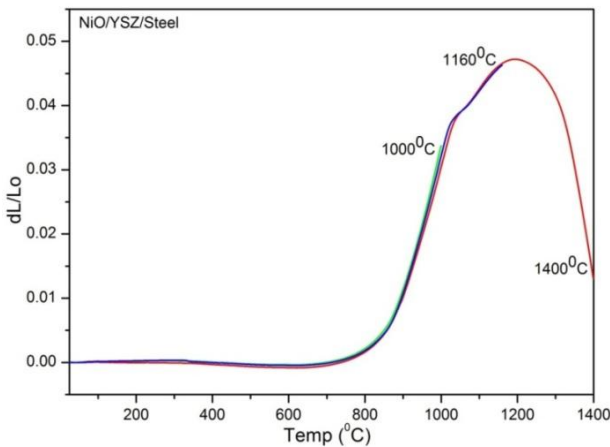

Fig.38. Change in relative length (dL/L$_0$) as a function of temperature for pure materials and composite under different atmosphere.

It is observed in Fig.39. (and also Fig.38.) that the sintering curve for NiO/YSZ/steel composite follows a non-monotonic behavior, displaying a step at about 1000°C, a maximum volume expansion at ~1160°C and a continuous behavior up to 1400°C. As described before, XRD measurements of as prepared NiO/YSZ/steel composite and composites from dilatometer were taken after heat treating at such characteristic temperatures and then cooling down to room temperature. The XRD pattern related to these three samples is shown in Fig.40. For the as-prepared sample, the XRD pattern of the composite shows NiO peaks; the intensity of these peaks decreases when the sample is fired up to 1000°C and then disappears at 1160°C. It should be noted that peaks corresponding to Ni appear at 1000°C, this pointing out that, at such temperature, NiO already starts to reduce, producing Ni. The peaks corresponding to Fe_2O_3 are also observed at 1000°C and, as expected, the peaks intensities for steel decreases as Fe_2O_3 increases with temperature. At 1160^{0}C, the peaks for Ni decreases and there is the appearance of new Fe-Cr-Ni phase. We can speculate that Ni, produced from the redox reaction, rapidly diffuses into the steel to form the new Fe-Cr-Ni phase or mixed oxides, leading to the disappearance of the Ni phase. Conversely, no single Cr_2O_3 phase was observed. However, due to the low intensity of the peaks, an unambiguous identification of the minor phases was not achieved.

These findings are also supported by EDXS maps (Fig.41) recorded on the three samples. Almost no interdiffusion was observed at 1000°C, where only the formation of a thin Cr-rich scale is clearly visible on the surface of metal particles. This scale increases in thickness when the sample is heated up to 1160°C but, at this temperature, some spherical Ni-rich particles are observed, together with a slight Fe diffusion in the ceramic phase. At 1400°C, the extent

of Fe and Cr outward diffusion from the steel to the ceramic matrix is huge, forming a thick layer containing Cr, around the metal particle. From the SEM images, since the edges of the metal particle are quite sharp, this Cr-rich phase seems to be not an oxide scale adherent to the metal particle but a mixed new phase formed through the ceramic network. It is also interesting to observe that, while Cr diffusion is limited to this reaction layer, Fe is homogeneously distributed in the ceramic matrix, forming alloys and/or mixed oxides with Ni. On the other hand, Ni diffusion through the steel is not significant enough to be recorded by EDXS maps. We could speculate that the fast formation of the Cr scale on the steel surface, already below 1000°C, prevents further Ni diffusion in the steel, even at high temperature. However, such Cr-rich scale, is not able to block Fe outward diffusion or, being composed of a mixed Cr-Fe oxide, it releases Fe in the ceramic phase as the temperature increases above 1000°C.

Fig.39. Change in relative length (dL/Lo) as a function of temperature for NiO/YSZ/steel composite when heat treated in Ar. The three curves correspond to three different samples heated up to each selected temperature and then cooled down and used for XRD analysis.
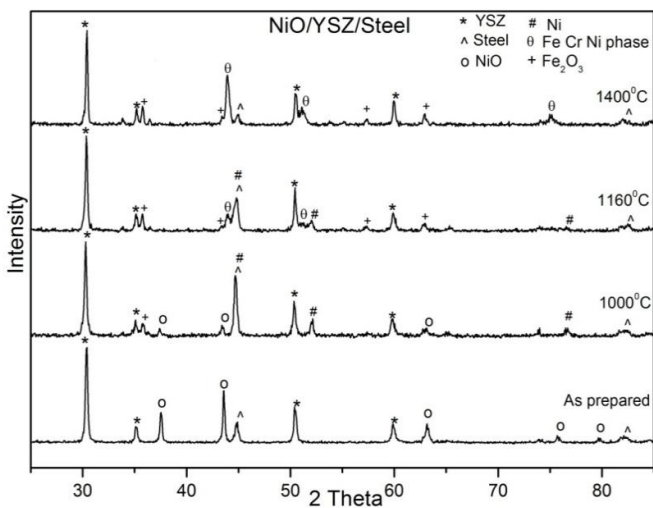
86

Fig.40. XRD pattern of NiO/YSZ/steel composite samples after heating at different temperatures in Ar.
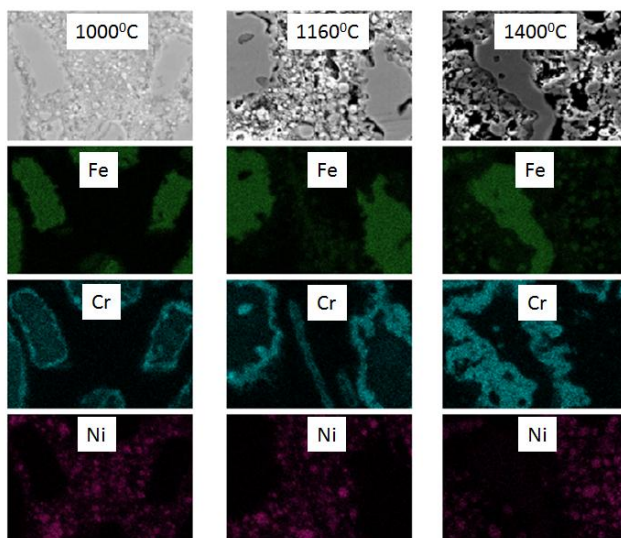

Fig.11. EDXS maps of NiO/YSZ/steel composite samples after heating at different temperature in Ar.
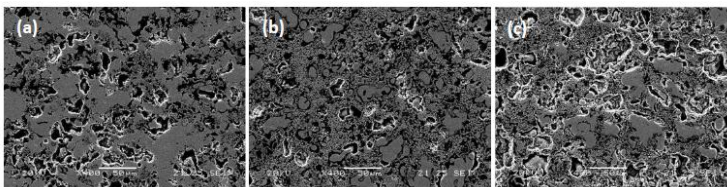
(b) Effect of doped-NiO

In order to limit the steel-induced NiO reduction and, consequently, the associated sudden volume change, NiO redox kinetic was modified by the addition of reactive doping element, Al and Ce, to NiO powder. A preliminary investigation was carried out by printing NiO/8YSZ layers on dense Crofer 22APU plates and sintering under Ar atmosphere, 2 h at 1400°C. The microstructure of samples with pure-NiO, 2wt%Al-NiO and 3wt%Ce-NiO after sintering is shown in Fig.42. This preliminary test shows that, in the case of pure NiO, the adhesion between substrate and anode material is not uniform, with the formation of cavities at the interface, probably due to Cr evaporation and diffusion through the ceramic layer. In addition, several Cr-rich oxide grains, probably related to a mixed Ni-Cr-Fe spinel phase, were observed in the bulk of the anode layer. On the other hand, in the case of Al-doped-NiO, the anode shows good adhesion to the substrate, with a limited occurrence of voids at the interface. Similar results were observed in the case of Ce-doping. An increased porosity was observed in the case of Al-NiO, while both pure- and Ce-NiO containing layers showed similar microstructural density.

Composite mixtures of steel/8YSZ with doped and undoped NiO were prepared and sintered at 1350°C under Ar atmosphere. The resulting microstructure of the samples is shown in Fig. 43. The sample prepared with pure NiO showed the coarsest grain structure, due to the extent of densification at high temperature. On the other hand, the two samples prepared with Al and Ce doping retain a quite fine ceramic microstructure, the composite with Al-NiO possessing the finest structure (Fig.43b). In addition, large metal grains are distinctly visible only in the case of Al-NiO, while they appear in a continuous network with the ceramic phase in pure and Ce-doped

samples. On this basis, the successive investigation was focused on Al-NiO only.
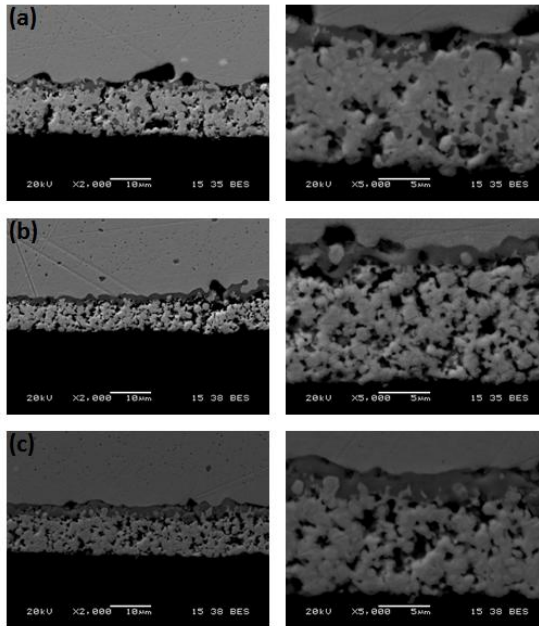

Fig.42. SEM images showing the microstructure between anode and substrate at different magnification. (a) Pure NiO; (b) 2 wt% Al doped NiO; (C) 3 wt% Ce doped NiO.

Fig.43. Microstructure of NiO/8YSZ/steel composite after sintering at 1350°C for 2 h under Ar atmosphere. Composite were prepared by using: (a) pure NiO; (b) Al-doped NiO; (c) Ce-doped NiO.

In order to study the effect of increasing dopant concentration on the consolidation behavior and to optimize the NiO powder composition, composites containing increasing amounts of aluminum were prepared and analyzed at the dilatometer. The sintering temperature for such experiment was set to 1350°C (under Ar atmosphere) to propose a cell production process involving less severe sintering conditions. Results are given in Fig. 44. The shrinkage of the composites drastically changes up to 3 wt% Al doping, while the increase of Al content from 3 to 5 wt% does not significantly change the sintering profile. The occurrence of the step at about 1000°C is still unclear, but probably it does not depend on the dopant since this behavior was observed even for undoped NiO. It is worth to note that Al-doping up to 3 wt%, significantly reduces the volume expansion in the composites, leading to a larger final shrinkage
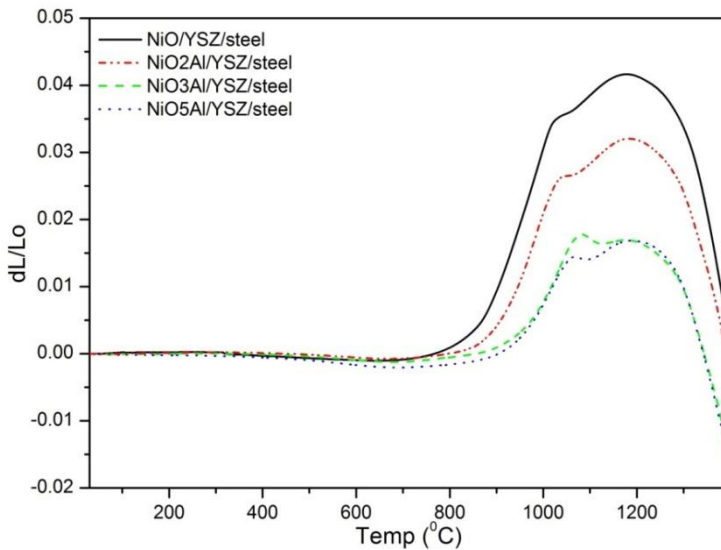
Fig.44. Change in relative length as a function of temperature for NiO/YSZ/steel composite with pure and Al-doped NiO.

3.3.4. Conclusion

High temperature co-sintering of metal/ceramic layers under inert atmosphere, in MS-SOFC, leads to problems associated to volume change and different shrinking behaviour of the layers, resulting in Ni-coarsening, cracking and delamination of the electrodes.

In the present work, steel oxidation by oxygen provided by nickel oxide was identified as the main source for volume expansion. In addition, intense Cr-Fe-Ni interdiffusion and Ni coarsening were observed when the different materials are co-sintered. The Cr oxide formed on the steel surface at 1000°C seems to limit Ni diffusion through the steel, but it cannot prevent Fe outward diffusion when the temperature is further increased.

It was found that the addition of doping elements (Al and Ce) to NiO significantly reduces steel oxidation and volume expansion, probably affecting the NiO reduction rate. This work was focused on Al-doping and it was observed that aluminum additions up to 3 wt% significantly reduce the volume expansion.

3.4. Optimization of sintering conditions and multilayer design

3.4.1. Introduction and aim of the analysis

Co-sintering of multilayers for MS-SOFC encounters various problems such as delamination, cracking, bending, and interdiffusion of Fe,Cr and Ni between anode and the substrate. The cracking in the multilayers can be because of the stresses generated due to binder loss events, mismatch in sintering profile or mismatch in TEC of different layers. The delamination of ceramic layers from the substrate is also a problem when these stresses overpower metal-ceramic interlayer bonding. In this work, the multilayers were produced by tape casting for the fabrication of MS-SOFC half-cell by co-sintering. The binder loss step during co-sintering has been optimized in order to prevent the cracking of the multilayers due to the binder loss events. Intermediate layers composed of metal-ceramic powder composite are also investigated in the current study to prevent delamination and to inhibit interdiffusion of the elements. CeO_2-steel, YSZ-steel, and LDC(La doped Ceria)-steel powder composites are considered for investigation to use as intermediate layer. Depending on the type of intermediate layer 3 different designs of multilayers are considered wherein an additional CeO_2 diffusion barrier layer (DBL) is used when CeO_2-steel is used as intermediate layer. The three designs are YSZ/(Al-NiO)-YSZ/CeO_2/CeO_2-steel/steel, YSZ/(Al-NiO)-YSZ/YSZ-steel/steel and YSZ/(Al-NiO)-YSZ/LDC-steel/steel. Where YSZ is 8 mol% yttria stabilized zirconia electrolyte, steel is the ferritic stainless steel support and, (Al-NiO)-YSZ is the composite of 8 mol% Al doped NiO and YSZ as the anode. Since previous studies in this work showed that Al doped NiO is suitable for anode material,

92

commercially available 8mol% Al doped NiO was used instead of pure NiO in the current study. The aim of the analysis is to optimize the co-sintering condition and the multilayer design, in order to obtain crack and camber free half-cell, with good bonding between the layers and minimal interdiffusion of elements.

3.4.2. Materials and methods

(a) Starting powders

In this work, YSZ (8 mol% yttria stabilized zirconia), ferritic stainless steel, and 50:50 by weight composite of 8 mol% Al doped NiO (commercially available) and YSZ were used for electrolyte, anode and the support respectively. CeO_2 was considered for Diffusion barrier layer (DBL). For the intermediate layer, 70:30 by weight composite of stainless steel and ceramic powders such as CeO_2, YSZ and LDC (La doped CeO_2) were considered. Hence the three different intermediate layers studied in the current work were the composite of CeO_2-steel, YSZ-steel and LDC-steel.

(b) Tape casting procedure

Preparation of water based slurries for electrolyte, anode and DBL followed the same procedure, whereas the slurries for intermediate layer and the substrate were prepared in a slightly different manner. For preparation of electrolyte, anode and DBL slurries, first the powders were added to the solution of deionized water and ammonium polyacrylate dispersant, and mixed for 2 h with zirconia balls using planetary mixer. The suspension was then filtered to 100μ and de-aired by a low vacuum pump for 30 min. Required amount of acrylic emulsion binder was then added to the suspension and stirred for 90mins with help of a mechanical stirrer. The slurry was then again filtered to 100 μ before casting. Slurry for the substrate was prepared by adding stainless steel powder to the

solution of water and polyvinylic emulsion binder, and then stirring for 30min. The slurry was then filtered to 500 µm. For the slurry preparation of the intermediate layer the mixture of stainless steel powder and ceramic powder was added to solution of deionized water, ammonium polyacrylate dispersant and acrylic emulsion binder, and stirred for 60 min. The suspension was then filtered at 230 µ before casting. The compositions of the slurries for different layers are given in Table .5.
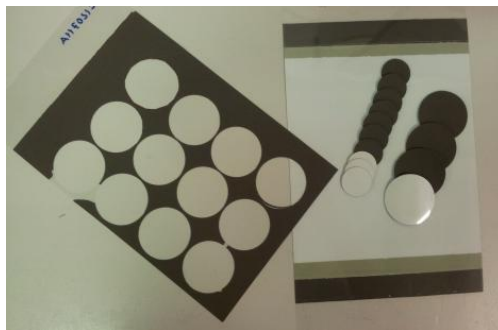
Raw material (wt %)	Electrolyte	Anode	DBL	Intermediate layer	Support
YSZ	--	--			
Al-NiO		--			
CeO$_2$			58.2		
Steel(<53µ)+ceramic 70:30 by wt				76	
Steel (<75µ)					75.9
Water	--	--	23.3	7.6	3.0
Dispersant	--	--	1.7	1.1	
Polyvinylic emulsion binder					21.1
Acrylic emulsion binder	--	--	16.7	15.2	

Table.5. Composition of slurries for different layers in half-cell of MS-SOFC.

The slips were cast on a silicone coated PET film by a laboratory scale tape caster, with a double blade apparatus. Thanks to low water solubility of the binders, it was possible to cast one suspension on top of the previous dried one without layer mixing. The green half-cell for MS-SOFC was obtained by first casting a thin electrolyte, and then the anode, DBL, intermediate layer and finally

94

the thick layer of steel substrate. The DBL and the intermediate layer were optional in some cases depending on the design. The different designs of MS-SOFC half cells produced by sequential tape casting in the current study are given below, and the gap of the doctor blade for each layer is given in the brackets. These multilayers were then punched and peeled off before analysis. Picture of the tapes produced in this study is shown in Fig.45.

- $YSZ / (Al\text{-}NiO)\text{-}YSZ / CeO_2 / steel$
  (30μ)   (150μ)   (150μ) (700μ)

- $YSZ / (Al\text{-}NiO)\text{-}YSZ / CeO_2 / CeO_2\text{-}steel / steel$
  (30μ)   (200μ)   (200μ)   (300μ)   (900μ)

- $YSZ / (Al\text{-}NiO)\text{-}YSZ / YSZ\text{-}steel / steel$
  (30μ)   (150μ)   (200μ)   (900μ)

- $YSZ / (Al\text{-}NiO)\text{-}YSZ / LDC\text{-}steel / steel$
 (30μ)   (150μ)   (200μ)   (900μ)

Fig.45. Picture of the tapes produced in the current study.

In order to study the sintering profile of electrolyte, anode, DBL and support alone, same slurries used for the half-cell

95

preparation were casted separately for each of the material. However, the blade gap used was 300 μ for all the layers in order to obtain thicker tapes for better handling. The tapes were then rolled carefully in order to give samples (as shown in Fig.46.) for dilatometric studies. The dilatometric studies were carried up to 1400°C at heating rate of 2°C/min in argon atmosphere.
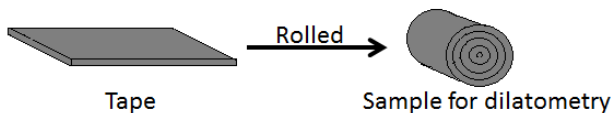

Fig.46. Samples made for dilatometric studies by rolling the tapes.

(c) Other experiments

Thermal analysis was carried on a small piece of YSZ/(Al-NiO)-YSZ/CeO$_2$/steel multilayers with the help of TG instrument in order to study the binder loss. The experiments were carried up to 700°C with the heating rate of 2°C/min in both air and argon atmospheres.

The in situ sintering behavior of YSZ/(Al-NiO)-YSZ/CeO$_2$/steel multilayers was also studied by optical microscopy. The multilayers were sintered in a tubular furnace under different sintering conditions. The furnace was specifically adapted for in-situ observation of the samples upon sintering: a silica glass window and a heat absorbing filter were sealed at one end of the alumina tube and the pictures were recorded at 60 s intervals with help of a CCD camera (10X macro zoom). Fig.47. shows the set-up and the sketch for the optical observation of sintering.

The other half cell multilayers were analyzed by SEM and EDXS after sintering to study the microstructure and interdiffusion of elements.
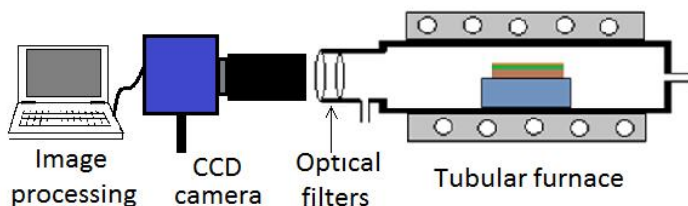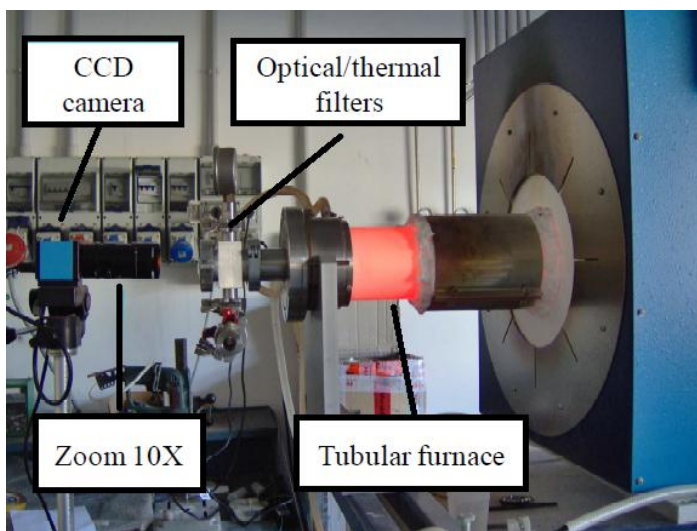
*Fig.47. Set-up and the sketch for optical observation during sintering.*

3.4.3. Results and discussion

(a) Binder loss study

Fig.48. shows the thermal analysis of green tape cast multilayers composed of YSZ/(Al-NiO)-YSZ/CeO$_2$/steel carried out in air and in argon. The steel layer is composed of polyvinylic binder whereas rest of the ceramic or cermet layers are composed of acrylic binder.

In air atmosphere the binder loss is complete at $450^\circ C$ with 13.4% of weight loss. At temperatures above $450^\circ C$ the there is a slow and very slight increase in weight. This increase can be attributed to the oxidation of stainless steel substrate i.e. the formation of chromia scale in the air atmosphere. In the case of argon atmosphere, at temperature of $450^\circ C$ only around 90% (12.1 wt%) of binder is lost. However at temperatures above $450^\circ C$ there is a slow
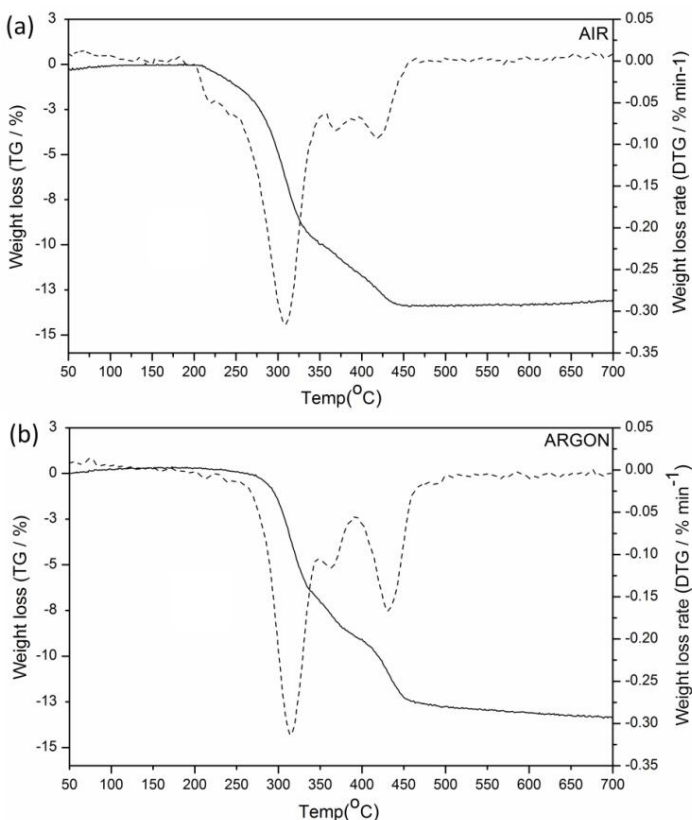

Fig.48. TG curves for YSZ/(Al-NiO)-YSZ/CeO₂/steel green tape cast multilayers carried out in (a)air and (b)argon

increase in weight loss completing the binder loss. Following these results, the de-binding step for binder removal was decided which will

98

be discussed ahead. De-binding step is one of the critical steps in a firing process, since stresses are developed in the layers as the organic polymers burnout. Slow heating rate is generally advised for the binder loss step followed by an isotherm to remove all waste gaseous products. When the de-binding step is out of control, the stresses may lead to green cracking and to warping.

(b) Optimization of de-binding step

The YSZ/(Al-NiO)-YSZ/CeO$_2$/steel green tape caste multilayers were sintered in the Gero furnace and the sintering behavior was monitored with the help of CCTV camera. Initially the sintering profile used was, 2°C/min up to 1350°C for 2 h including a 1 h isotherm at 450°C during heating. Isotherm at 450°C was selected based on previous binder loss studies. Ar atmosphere was used during the entire sintering process. Fig.49. shows the sintering profile used.
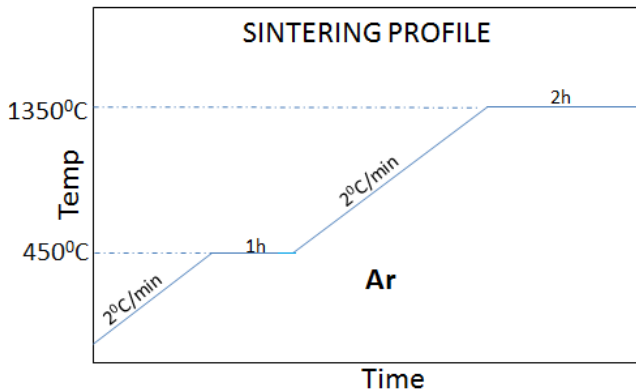
Fig.49. Sintering profile used initially

Fig.50. shows the selected images of the cell at different temperatures taken by CCTV camera during sintering process. It can

be seen that at 565°C cracks are visible on the surface of the cell and these cracks grow and tear the cell at higher temperature as can be seen at 605°C.The final picture of the completely cracked cell after the completion of sintering process is also shown in Fig.50.The cracks became visible at low temperature of 565°C which means that crack was initiated at even lower temperature. Such temperatures are very low for any sintering process to occur and thus it can be concluded that cracking is related to the de-binding step.
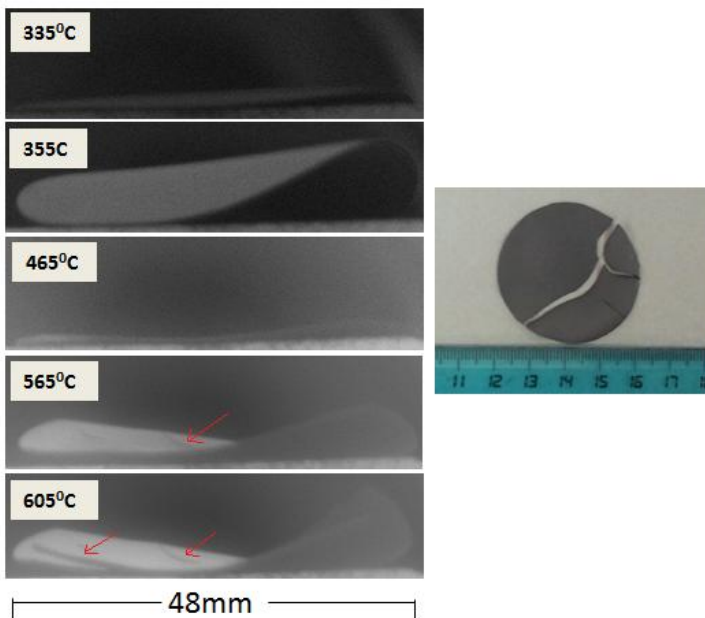
Fig.50. Showing the images taken by CCTV camera during the sintering of YSZ/(Al-NiO)-YSZ/CeO$_2$/steel multilayers with sintering profile including isotherm at 450°C. The picture of cell taken after sintering process is also shown.

Fig.51. shows the relative change in length (dL/L_o) as a function of temperature in Ar atmosphere for the tapes of steel and Al-NiO/YSZ anode. Anode tape was selected to represent the CeO_2 and the YSZ layer as they were made from same formulation. For the anode it can be seen that there is a small linear shrinkage (~5.8% of the total shrinkage, $dL/Lo=-0.01$) between 300^oC to 600^oC due to loss of acrylic binders in the anode layer. For the steel, considerably higher linear shrinkage (~41.9% of the total shrinkage, $dL/Lo=-0.07$) is observed up to 300^oC which is due to loss of polyvinylic binder from steel layer. Following this results, an isotherm at 300^oC (2h) instead 450^oC was given in the next attempt in order to facilitate the binder loss from the steel layer without leading to cracks. Air was used up to the isotherm at 300^oC for 1st hour and the gas was then switched to argon and allowed to run for another 1 hour to make sure that all the air in the furnace is replaced by argon. Fig.52. shows the sintering profile used and, Fig.53. shows the images taken by CCTV camera during sintering .The pictures of cell taken after sintering process are also shown. From Fig.53. it can be seen that no cracks are visible on the surface of the cell even up to 1350^oC and the cell is intact throughout. This means that there were no cracks generated due to binder loss event when an isotherm at 300^oC was given. If there had to be crack during the binder loss stage, then it would propagate and tear the cell apart as seen in Fig.50. Therefore an isotherm at 300^oC is necessary to prevent cracking, and this seems to be related in some way to the higher linear shrinkage associated with loss of polyvinylic binder at 300^oC in the steel. However, the cell deforms at 1350^oC which is due to the over sintering of the steel substrate. The cell also showed the problem of delamination of ceramic layers from the metal substrate.

Fig.51. Relative change in length (dL/Lo) as a function of temperature for tapes of steel and the anode.

Fig.52. Sintering profile used in the next attempt
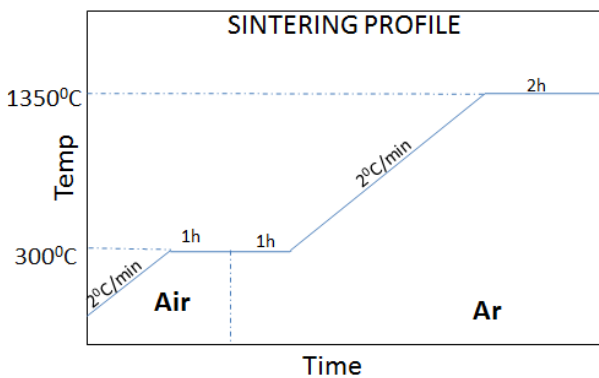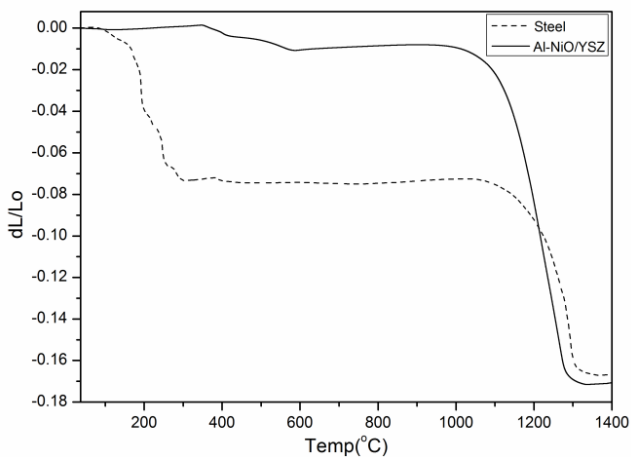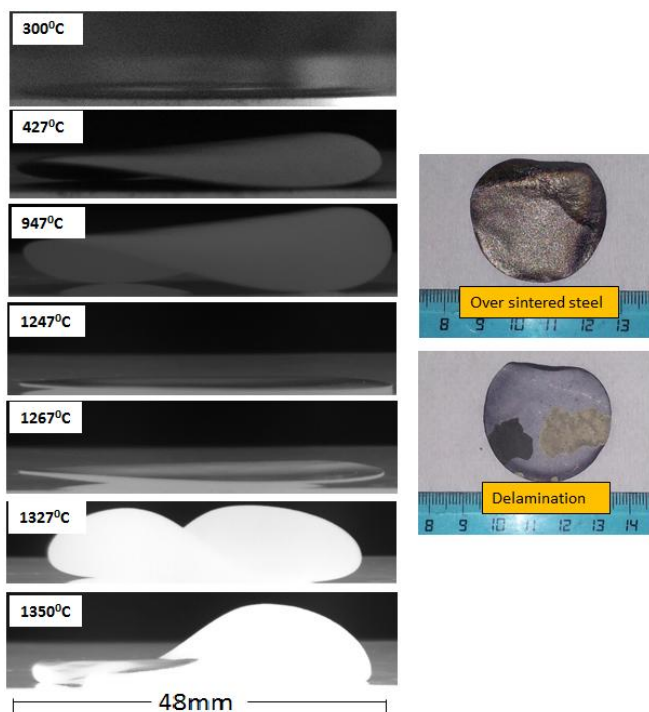
Fig.53. Showing the images taken by CCTV camera during the sintering of YSZ/(Al-NiO)-YSZ/CeO$_2$/steel multilayers with sintering profile including isotherm at 300°C. The pictures of cell taken after sintering process are also shown.

(c) Use of Intermediate layer to improve steel-ceramic adhesion and to prevent interdiffusion

In order to improve the adhesion between steel substrate and rest of the layers, an intermediate layer was introduced between them. The idea was to introduce an intermediate layer of steel and ceramic mixture so that it adheres the steel substrate on one side and ceramic layer on the other. 3 designs considered were YSZ/(Al-NiO)-

YSZ/CeO$_2$/CeO$_2$-steel/steel, YSZ/(Al-NiO)-YSZ/YSZ-steel/steel and YSZ/(Al-NiO)-YSZ/LDC-steel/steel. Fig.54. shows the schematics of the three designs in which CeO$_2$-steel, YSZ-steel and LDC-steel composite mixtures were used as intermediate layers. The green multilayers were then sintered using the same sintering profile as shown in Fig.52. except that the final sintering temperature was 1330°C instead of 1350°C. The lower sintering temperature was used in order to prevent oversintering/melting of the substrate as discussed previously.

| ELECTROLYTE (YSZ)	ELECTROLYTE (YSZ)	ELECTROLYTE (YSZ)
ANODE (Al-NiO) -YSZ	ANODE (Al-NiO)-YSZ	ANODE (Al-NiO)-YSZ
DBL(CeO$_2$)	YSZ-Steel	LDC-Steel
CeO$_2$-Steel		
STAINLESS STEEL	STAINLESS STEEL	STAINLESS STEEL
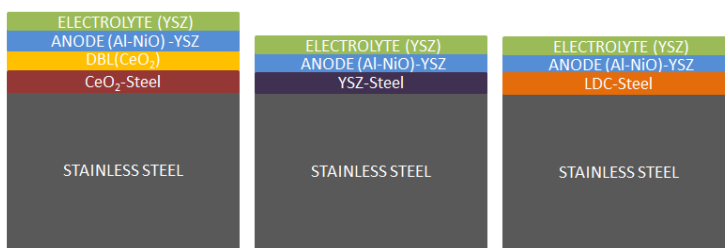
Fig.54. Showing the schematics of 3 different designs with different intermediate layers considered for co-sintering, (from left to right) YSZ/(Al-NiO)-YSZ/CeO$_2$/CeO$_2$-steel/steel, YSZ/(Al-NiO)-YSZ/YSZ-steel/steel and YSZ/(Al-NiO)-YSZ/LDC-steel/steel.

Fig.55. shows the SEM images, EDXS line scan across the multilayer and the picture of the YSZ/(Al-NiO)-YSZ/CeO$_2$/CeO$_2$-steel/steel half-cell after sintering. It can be seen that LDC-steel intermediate layer forms good bondage with steel substrate on one side and CeO$_2$ diffusion barrier layer (DBL) on the other. For an EDXS line scan across the multilayers it can be seen that there is heavy diffusion of Cr from the steel particle into the ceria layer. However ceria efficiently prevents the diffusion of Cr further into the anode layer. Quantitative analysis by EDXS showed presence of only ~0.3wt% of Cr in the anode layer. Similarly no diffusion of Ni in the

steel particle is observed. Although this design is good enough to prevent delamination and interdiffusion, the cell showed camber (also shown in Fig.55.) and the electrolyte layer was not gas tight.
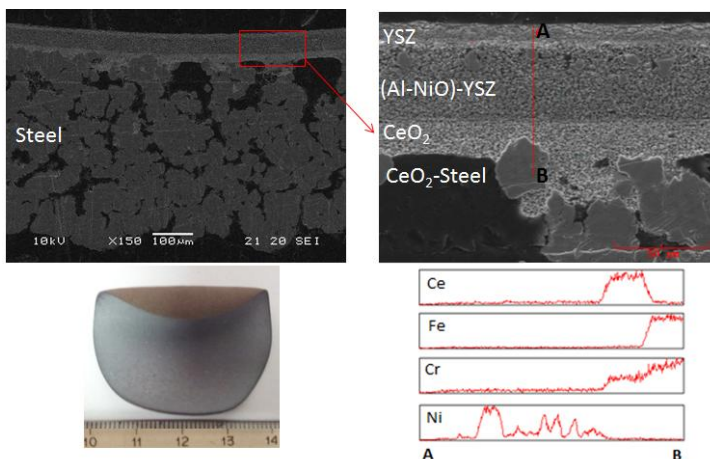
Fig.55. SEM images, EDXS line scan across the multilayer and the picture of the YSZ/(Al-NiO)-YSZ/CeO$_2$/CeO$_2$-steel/steel half-cell after sintering.

Fig.56. shows the relative change in length as a function of temperature in argon atmosphere for tapes of steel, anode, YSZ and CeO$_2$ .For the steel, YSZ and anode the onset of sintering occurs at around same temperature, and all have similar final shrinkage. However, for ceria the onset of sintering occurs at higher temperature compared to the other materials. Also, CeO$_2$ has considerably lower shrinkage than other materials at 1400°C.This is the reason why CeO$_2$ layer was avoided in other designs although it was found to be a good diffusion barrier layer.

Fig.56. Relative change in length (dL/Lo) as a function of temperature in argon atmosphere for tapes of different materials.
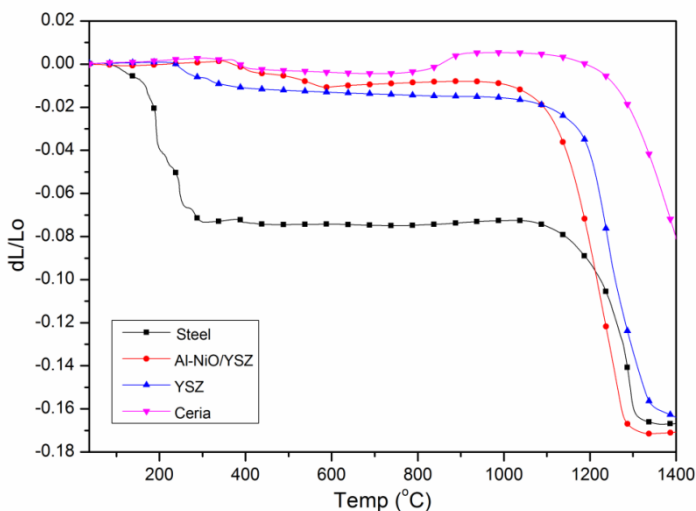
Fig.57. shows the SEM images, EDXS line scan across the multilayers and the picture of the YSZ/(Al-NiO)-YSZ/YSZ-steel/steel half-cell after sintering. YSZ-steel intermediate layer shows good adhesion with steel substrate and the anode layer as seen in the SEM image. However, from the EDXS line scan it can be seen that there is a heavy diffusion of Fe and Cr in the anode layer. For the line scan in the anode region it can be seen that the high intensity peaks of Fe, Cr and Ni are in the same region thus indicating the formation Fe-Cr-Ni alloy or mixed metal oxide. Slight diffusion of Ni in the steel particle is also observed. The interdiffusion of elements is considerable although the steel particle over which the line scan is measured is covered by YSZ, hence YSZ seems to be a poor material to prevent interdiffusion. The quantitative analysis by EDXS showed presence of 6.7wt% of Cr and 13.5wt% of Fe in the bulk of the anode layer. The steel particle showed presence of 5.3wt% of Ni.

It is interesting to note that the cell is flat, and this could be because of absence of the CeO$_2$ layer.

Fig.57. SEM images, EDXS line scan across the multilayer and the picture of the YSZ/(Al-NiO)-YSZ/YSZ-steel/steel half-cell after sintering.
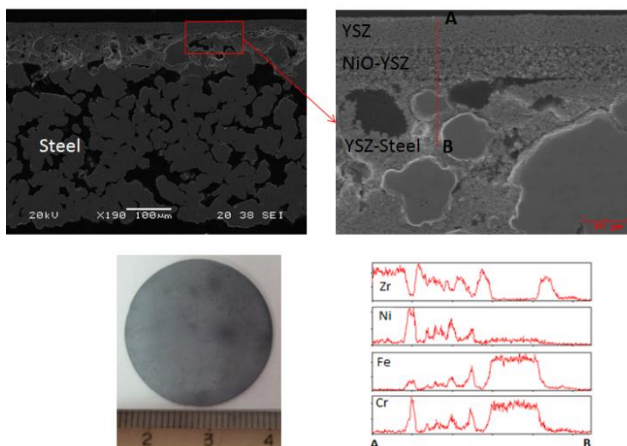
Fig.58. shows the SEM images, EDXS line scan across the multilayers and the picture of the YSZ/(Al-NiO)-YSZ/LDC-steel/steel half-cell after sintering. The bonding between the layers is good enough to prevent delamination. The EDXS line scan was performed where it seemed that steel particle is in direct contact with the anode layer. However from the EDXS measurement it is found that the steel particle is covered with ~2 μm thick LDC layer. It can be seen that diffusion of Ni in the steel particle in negligible. Also, the diffusion of Fe and Cr in the anode layer is less in comparison to when YSZ-steel is used as intermediate layer. 5.9 wt% and 9.6 wt% of Cr and Fe is found to be present in the bulk of the anode layer. The half-cell did not show any camber but however, the electrolyte was not dense.
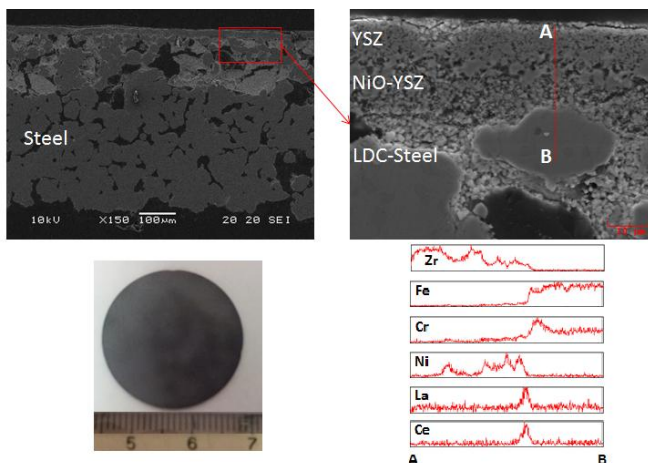
Fig.58. SEM images, EDXS line scan across the multilayer and the picture of the YSZ/(Al-NiO)-YSZ/LDC-steel/steel half-cell after sintering.

Although the multilayer design consisting of YSZ/(Al-NiO)-YSZ/CeO_2/CeO_2-steel/steel was the best with no interdiffusion and delamination, it was not considered for further investigation as it showed camber. YSZ/(Al-NiO)-YSZ/LDC-steel/steel design was however considered over YSZ/(Al-NiO)-YSZ/YSZ-steel/steel design because it showed less severe interdiffusion of elements. Also, it was found that LDC in the LDC-steel layer becomes porous due to reduction when H_2 is fed from the anode side during operation. This increase in porosity can be crucial to facilitate gas diffusion.

3.4.4. Conclusion

In this study, the binder loss from the multilayers during co-sintering, and the use of different intermediate layer to prevent delamination and to inhibit interdiffusion between substrate and

108

anode were investigated. At 300°C the polyvinylic binder from the steel substrate is decomposed whereas the acrylic binder from rest of the ceramic or cermet layers are decomposed above 450°C. It is found that an isotherm at 300°C instead 450°C is necessary to prevent cracking of the cell due to binder loss events. The binder loss from steel substrate is accompanied by considerably high linear shrinkage and this could be the reason why an isotherm is necessary at 300°C. Three multilayer designs with different intermediate layers were considered for investigation. YSZ/(Al-NiO)-YSZ/LDC-steel/steel was found to be a good compromise so as give a half-cell, with good bonding between the layers, is camber free, and shows moderate interdiffusion of elements between the substrate and the anode. YSZ/(Al-NiO)-YSZ/LDC-steel/steel multilayer design was considered for further investigation in order to achieve gas tight dense YSZ electrolyte.

3.5. Effect of Fe dopant on YSZ electrolyte

3.5.1. Introduction and aim of the analysis

From earlier discussions in section 2.5.2 it is clear that Y_2O_3 stabilized ZrO_2 (YSZ) is the most preferred electrolyte material for SOFC. YSZ material however requires high sintering temperature ranging from 1300^oC to 1400^oC in order to achieve gas tightness. Such high sintering temperature can be detrimental to other components of cell when co-sintering of multilayers is considered for the fabrication of SOFC. The detrimental effects can be even more severe in particular for MS-SOFC where inert or reducing atmosphere is used for fabrication by co-sintering. Complete densification, enough to prevent gas permeability is also difficult to achieve under constrained geometry for YSZ, unlike the ceria based electrolyte materials. In short, reducing the sintering temperature can facilitate the fabrication of SOFCs to a great extent.

One of the ways to reduce the sintering temperature and to improve the 'sinterability' of YSZ material is by the use of sintering aid. Although other methods such as sol gel, hydrothermal synthesis and microwave sintering can be used to reduce the sintering temperature, they are not preferred due to relatively high cost of industrial scale up. Thus, use of sintering aid remains to be the most viable option provided it does not degrade the electrical properties of YSZ and its function in SOFC. Different sintering aids for YSZ investigated by researchers include $Sr_2Ga_2O_5$ [97], Bi_2O_3 [98], CuO [99] [100], Co [101] [102], Al_2O_3 [87], MnO_2 [103] and Fe [104] [105] [106]. Fe as a sintering aid is studied by many researchers and has shown to improve the electrical properties of YSZ. SOFCs with Fe

doped YSZ electrolyte has been demonstrated to show enhanced performance as compared to when pure YSZ is used [104].

All the previous research on Fe doped YSZ is in perspective of Anode supported-solid oxide fuel cells (AS-SOFCs) where the cell is fabricated by sintering in air atmosphere. However, MS-SOFC fabrication by co-sintering has to be performed in reducing or inert atmosphere to prevent the oxidation of substrate. Thus the aim of the current work is to analyze the effect of Fe dopant on YSZ when sintered in inert argon atmosphere. A comparative study of Fe doped YSZ for sintering in air and argon has been carried out in this work.

3.5.2. Materials and methods

(a) Preparation of Fe doped YSZ

$Fe(NO_3)_3.9H_2O$ was used as source of Fe for the preparation of 0,1,2 and 3 mol% Fe doped YSZ.YSZ (Baikowski, France), $Fe(NO_3)_3.9H_2O$ (Farmitalia Carlo Erba, Milan), zirconia balls and water were taken together in a plastic jar and mixed for 2hrs with help of a planetary mixer. The slurry obtained was dried overnight at $140^{\circ}C$ and the solid mass obtained was then manually ground with the help of a mortar and pestle. The powder was then calcined at $600^{\circ}C$ for 2hrs allowing the formation of Fe oxide in the mixture. This powder was once again mixed in the planetary mixer along with water and zirconia balls to ensure homogenization. The slurry obtained was dried overnight and finally ground manually to give fine powder.

(b) Sintering and other experiments

In order to prepare the samples for sintering, 2.5g of the powders were pressed in a cylindrical dye with 13mm diameter at 75MPa for 2mins. The samples were sintered at a heating rate of

5°C/min up to 1350°C for 2hrs in air and argon atmosphere. A digital camera was used take the picture of the sintered samples in order to compare the colors. The density of the samples was measured by Archimede's method.

For the XRD and grain growth analysis of the sintered samples the cylindrical pallets were cut into half, along the diameter of the circular section. XRD was carried on the flat surface between 20 to 80° with a step of 0.05^o and a hold time of 8sec.For the grain growth analysis the samples were etched at 1300°C for 20 mins in air and argon and then observed under SEM. The grain size was measured by lineal intercept method.

(c) Fabrication and testing of MS-SOFC with Fe-doped YSZ electrolyte

(Al-NiO)-YSZ/LDC-steel/steel half cells were prepared by water-based tape casting technology (see section 3.4.2).

The anode was based on Aluminum-doped-NiO and 8mol%Y_2O_3 stabilized zirconia (8YSZ) in a NiO/YSZ=1 ratio. The electrolyte was based on 8YSZ with the addition of 2 mol % Iron as sintering aid. A mixed LDC/steel intermediate layer was placed between the anode and the metal support in order to provide a good adhesion at the interface between the two layers.

Metal support, intermediate layer and anode were prepared by sequential tape casting of water based suspensions and presintered at 1100°C. The electrolyte was applied by screen printing and the half-cell was then sintered at 1320°C.The cathode, consisting of $La_{0.6},Sr_{0.4}CoO_{3-\delta}$ (LSC40) was then applied by screen printing and sintered in situ at 850°C during the electrochemical test. The electrochemical characterization, comprising i-V curves and Electrochemical Impedance Spectroscopy was performed on a 35 mm cell with active area 3.14 cm². Gold and Nickel meshes were

used to collect the current at the cathode and the anode, respectively. The cell testing was carried at a local company SOFCPOWER in Mezzolombardo, Italy.

The microstructure of the multilayers half-cells was observed by scanning electron microscope.

3.5.3. Results and discussion

(a) XRD analysis

Fig.59. shows the XRD patterns of pure and Fe doped YSZ samples after sintering in air and argon atmospheres. The peaks in all the XRD patterns correspond to cubic YSZ. Also, no additional peaks accounting for a secondary phase such Fe oxides or Fe is observed for the samples sintered in either of the atmospheres for all the Fe concentrations. The solubility of Fe in YSZ was studied by Wilhelm et al. [107]and they demonstrated that 8.06 mol% Fe dissolves in YSZ matrix which is in good agreement with the current results. The fact that no secondary phase of Fe and/or its oxides is observed for samples sintered in argon atmosphere confers that dissolution of Fe dopant in YSZ is not affected by the sintering atmosphere. If at all there is any effect of sintering atmosphere on the solubility of Fe in YSZ, it is very low so as to get detected by XRD.

From the XRD patterns, however, a shift to higher 2θ values with the increase in Fe concentration is observed for the samples sintered in air and argon atmosphere. The shift to higher 2θ with increasing Fe concentration means that lattice parameter of YSZ is decreasing because the Zr^{+4} ions (ionic radius=0.84 A^{o}) are substituted by undersized Fe^{+3} ions (ionic radius=0.55-0.78 A^{o}) [104] [105]. Fig.60. shows the change in lattice parameter for pure and Fe doped YSZ samples after sintering in air and argon atmosphere.
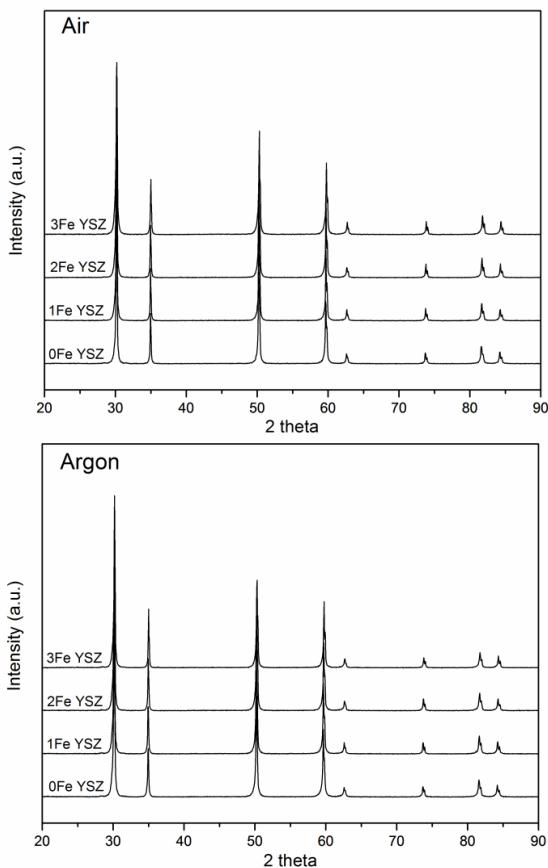
Fig.59. XRD patterns of 0-3 mol% Fe doped YSZ
samples after sintering in air and argon atmosphere

From Fig.60. it can be seen that lattice parameter of YSZ decreases with increasing Fe concentration in both the sintering environment, however, for the samples sintered in argon it is found that lattice parameter is always higher than the respective sample sintered in air. This expansion of YSZ lattice parameter can be attributed to the formation of positively charged oxygen vacancies ($V_O^{\bullet\bullet}$) due to low

114

oxygen partial pressure in argon atmosphere. There occurs a relaxation of lattice due to the electrostatic repulsion between the positively charged oxygen vacancy and the cations surrounding it [108].
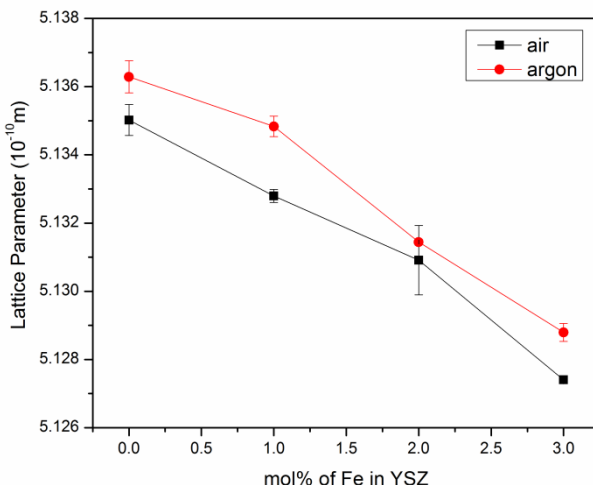
Fig.60. Lattice parameter as a function of Fe concentration
for samples sintered in air and argon atmosphere

(b) Density and Grain growth analysis

Fig.61. shows the density of Fe doped YSZ samples as function of Fe concentration for sintering in air and argon atmosphere. As expected, for samples sintered in air atmosphere Fe acts as a sintering aid considerably increasing the densification up to 2mol% of Fe, the density only slightly increases for further increase in Fe concentration. What is interesting is that for the samples sintered in argon atmosphere, their density is always higher than the respective sample sintered in air. This suggests that Fe retains its "sintering aid effect" for sintering in argon atmosphere. Previously it has been reported for pure YSZ that the density is generally higher for samples

sintered in argon than for those in air [109]. Similar result is observed in the current work for both pure and Fe doped YSZ. It appears that effect of both, Fe concentration and sintering atmosphere occurs simultaneously.

The increase in sinterability of YSZ with Fe dopant can be explained based on the work of Guo et al. [105]. As Fe^{+3} ion dissolves in zirconia, it can occupy substitutional and interstitial sites in the structure generating defects. However, in cubic YSZ it is the substitutional defects which predominate. The two defect reactions for susbtitutional and interstitial occupation are represented by Kroger-vink notation. The substitution of Fe^{+3} ion in Zirconia is similar to that of of Y^{+3} and is given as:

$$Fe_2O_3 \xrightarrow{ZrO_2} 2Fe'_{Zr} + V_O^{\bullet\bullet} + 3O_0^x$$
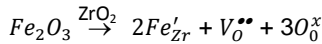
The equation for Fe^{+3} ion interstitial doping defect in YSZ can be given as:

$$2Fe_2O_3 \xrightarrow{ZrO_2} 3Fe'_{Zr} + Fe_i^{\bullet\bullet\bullet} + 6O_0^x$$
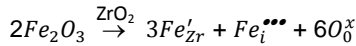
Densification is a matter diffusion process and in the case of YSZ it depends on the diffusion rate of Zr^{+4} ions. Since dissolution of Fe^{+3} in YSZ increases the densification of YSZ, it indicates that defects generated by Fe^{+3} doping increases the diffusion rate of Zr^{+4}. It is believed that Fe^{+3} ion migrate by vacancy diffusion mechanism. However, as mentioned before, co-existence of Fe^{+3} substituents and Fe^{+3} interstitials in Fe_2O_3 doped YSZ indicate that Fe^{+3} ion can also migrate by interstitial diffusion mechanism during sintering. When the Fe^{+3} ion migrate from substitutional site to the interstitial site a cation vacancy will be generated because the radius of Fe^{+3} ions (0.55 A^o) are much smaller than that of Zr^{+4} ions (0.84 A^o). In other words for every Fe^{+3} substituent a cation vacancy is generated if it migrates to the interstitial site during sintering. This increase in cation vacancy will increase the Zr^{+4} ion jump frequency thereby increasing its diffusion

rate. Thus, interstitial defects of Fe^{+3} ions partially contribute to an increase in the diffusion coefficient D.

The diffusion coefficient D also depends on the activation energy which in turn depends on the bond strength of the cations and the anions. In the case of Fe_2O_3 doped YSZ, since Fe^{+3} ions (0.55 A^o) is much smaller than Zr^{+4} ions (0.84 A^o) and Y^{+3} ions (1.019 A^o), it weakens the Zr-O bond strength. In addition a greater activation energy is associated with larger ionic radius, and thus the activation energy of Fe^{+3} diffusion is lower than that of Zr^{+4} and Y^{+3}. Duly, the presence of Fe-O and Zr-O bonds with weakened bond strengths lower the activation energy, which partially contribute to increase in diffusion coefficient D.

Thus, the increase in diffusion coefficient of Zr^{+4} ion due to increase in its jump frequency and due to decrease in activation energy leads to higher densification rate for Fe_2O_3 doped YSZ.
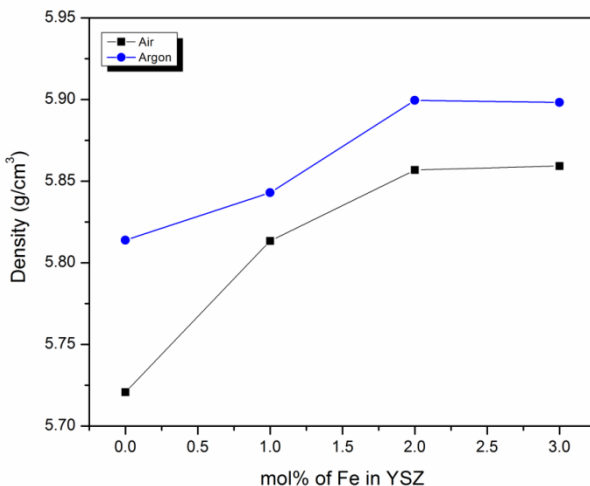
Fig.61. Density of pure and Fe doped YSZ samples as a function of Fe concentration after sintering in air and argon atmosphere.

Fig.62. shows the grain size of Fe doped YSZ samples after sintering in air and argon atmosphere. Since grain growth is also a diffusion controlled process, as expected, grain size increases with increasing Fe concentration. However, it can be seen that the grain size of samples sintered in argon is slightly higher than the respective samples sintered in air. As this effect is also observed for the pure YSZ samples sintered in air and argon, it indicates that the effect is related to the influence of sintering atmosphere on the YSZ rather than Fe dopant. Fig.63. shows the microstructures of the samples. It can be seen that, a small amount of secondary phase having size of few hundred of nanometers can be easily observed for Fe doped samples sintered in argon. This secondary phase is observed at grain boundaries as well as within the grains. Concentration of the secondary phase is high in the samples sintered in argon although small amount of this phase can also be seen in the air sintered samples.
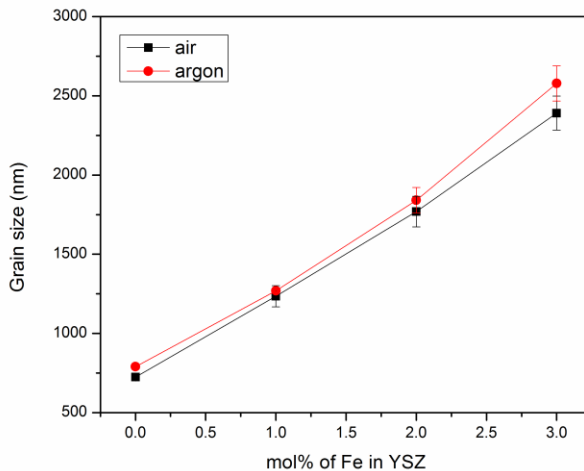
Fig.62. Grain size as a function of Fe concentration for YSZ samples after sintering in air and argon atmosphere.
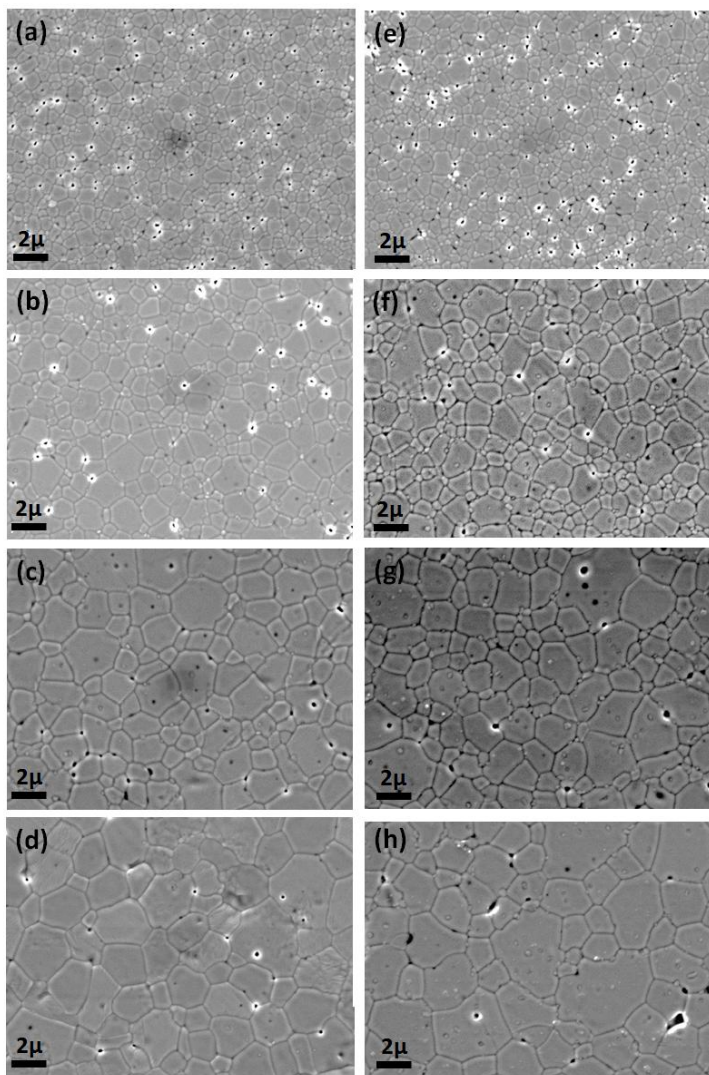
*Fig.63. Microstructure of (a-d) 0-1mol% Fe doped YSZ sintered in air
and, (e-h) 0-1mol% Fe doped YSZ sintered in argon*

Fig.64. shows the digital photographs of the samples. Fe^{+3} ions when dissolved evenly in crystal matrix is known to give yellowish-brown color to the matrix. Such color is observed for Fe doped samples sintered in air and this color becomes darker with increase in Fe concentration as expected. However, for the samples sintered in argon it can be seen that the color is slightly greyish as compared to the respective air sintered sample. Among the argon sintered samples, the greyish nature of the color increases with the Fe concentration. This greyish color can be because of reduction and/or precipitation of Fe dopants in the oxygen deficient argon atmosphere.
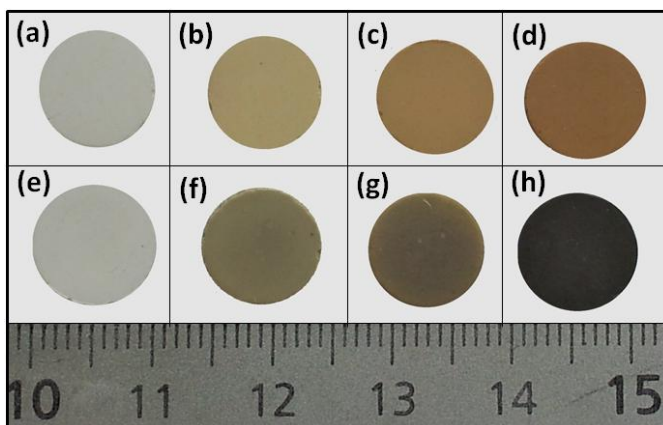
Fig.64. Digital photographs of of (a-d) 0-1mol% Fe doped YSZ sintered in air and, (e-h) 0-1mol% Fe doped YSZ sintered in argon.

(c) Microstructure and testing of the cell

The microstructure of metal supported cell produced in the present work is shown in Fig.65. From the microstructure it can be seen that good adhesion between the layers is obtained. The electrolyte layer is completely dense (note that such dense electrolyte could not be obtained when pure YSZ is used: see section 3.4.3) as can be seen in image taken at higher magnification. However, few pin

holes can be observed on the surface of the electrolyte layer as seen in the image taken from top, before embedding the cell in epoxy resin.
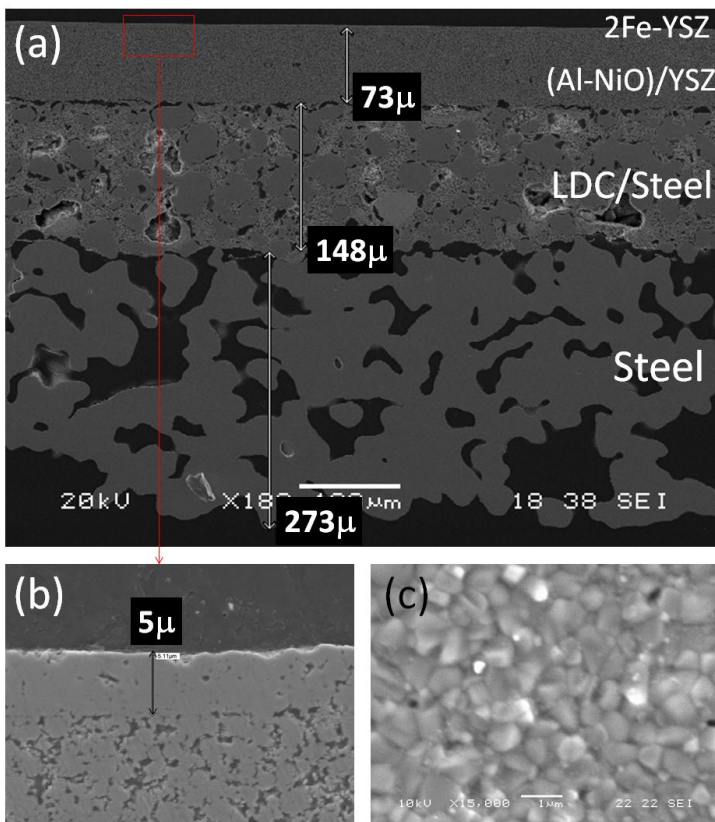
Fig.65. SEM image of (a) half-cell showing all the layers, (b) electrolyte layer (top) and a part of the anode layer (bottom) taken at higher magnification and (c) top surface of the electrolyte.

Despite the very attractive microstructure, the electrochemical performances of the cell observed by IV curves and EIS analyses were quite poor (Fig.66).The maximum current densities

obtained at 0.7V operating potential were 0.21 A/cm^2 and 0.125 A/cm^2, respectively. In addition, the open circuit voltage was slightly below the expected theoretical potential, being this mismatch probably due to the occurrence of pin-holes in the electrolyte layer.

Fig.66. Showing (a) Polarization curves for MSSOFC at 800°C and 750°C and (b) Nyquist plot at 800°C and 750°C.

On the other hand, the results of EIS analysis suggest that one of the main contributions which limit the electrochemical performances is the ohmic resistance (R_Ω ca. 0.8 Ωcm^2 at 750°C). In comparison the value of R_Ω for conventional anode supported cells under the sam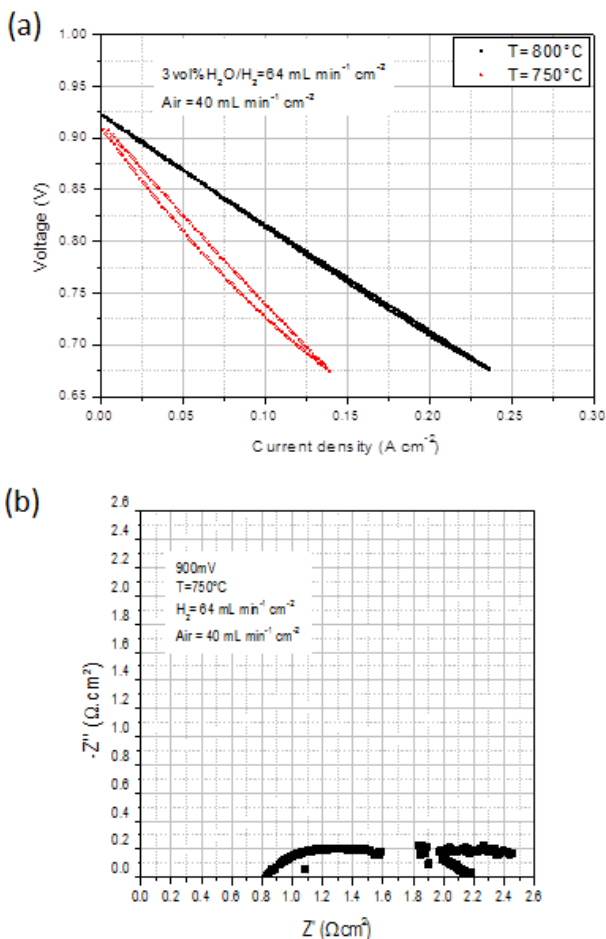e conditions is ca. 0.2 Ωcm^2. This very large ohmic contribution can be associated to a poor percolation of Ni phase, resulting from Ni coarsening. However, since in this case no barrier layer was applied between the cathode and the electrolyte, a large resistance is also expected to be related to zirconates formation from the solid state reaction between $(La_{0.6}Sr_{0.4})CoO_3$ and zirconia. EIS spectra become poorly reliable at low frequency due to large noise, probably related to the instability due to some leakages in the electrolyte. However, the polarization resistance was observed to be R_p=1.4 Ωcm^2.

3.5.4. Conclusion

In this work, a comparative study was done on Fe doped YSZ samples for sintering in air and argon atmosphere, with the aim to analyze the effect of Fe as sintering aid under MS-SOFC fabrication by co-sintering conditions. Samples showed enhanced densification with increasing Fe concentration in both the sintering atmospheres thus concluding that Fe can be used as a sintering aid for YSZ even under argon. The samples sintered in argon atmosphere were however characterized by larger lattice parameter, and higher density and grain size. The increase in lattice parameter is attributed to the oxygen vacancies generated under low $p(O_2)$ in argon atmosphere. The oxygen vacancy causes the relaxation of the lattice due to electrostatic repulsion between positively charged vacancy and the surrounding cations. The microstructural analysis showed the presence of small amount of secondary phase, and the

concentration of such phase was seen to be higher in the argon sintered samples. Comparison of colors of argon and air sintered samples indicates the reduction and/or precipitation of Fe dopant in the argon. Although Fe seems to be a suitable sintering aid for YSZ under argon atmosphere, the effect on conductivity still needs to be analyzed. The conductivity is expected to be affected due to the presence of high concentration of the secondary phase and the oxygen vacancies in the argon sintered samples. Nevertheless, gas tight dense electrolyte could be obtained for MS-SOFC fabricated by co-sintering when Fe doped YSZ is employed for electrolyte, although the performance of the cell was quite poor.

3.6. General Conclusion

Cost-effective co-sintering approach was considered for the fabrication of MS-SOFCs in the current work. Ferritic stainless steel, Ni-YSZ cermet and YSZ were considered for support, anode and electrolyte respectively. The anode and the electrolyte materials were suitably doped, and the multilayer design and sintering conditions were optimized so as to address the generally encountered problems during co-sintering.

It was found that Al doped Ni-YSZ anode materials acquires a finer microstructure if compared to pure Ni-YSZ anode when sintered under MS-SOFC co-sintering conditions. The fine microstructure in Al doped anode materials is attributed to the segregation of Al_2O_3, which is formed during the course of sintering, on both Ni and YSZ grains, thus inhibiting sintering. Such fine microstructure is expected to improve the electrochemical performance of the cell as the number of triple phase boundaries increases. Moreover, it was also found that the electrical conductivity of the anode material increases considerably for the Al doped anode materials, although these materials have lower density than the pure Ni-YSZ anode materials. The improved electrical conductivity is explained on the basis of the fine microstructure which leads to improved connectivity and percolation of conducting Ni grains.

The modification of the reduction kinetic of NiO and the interaction between the anode and steel during the fabrication of Metal Supported Solid Oxide Fuel Cells (MS-SOFC) was also studied in this work. With the aim to limit NiO reduction under inert atmosphere at high temperature, doping elements such as Al and Ce were considered for NiO powders modification and anode production. A sudden volume expansion above 1000^0C followed by substantial shrinkage above 1200^0C was observed to occur at anode-steel interface during sintering in Ar up to 1400^0C. Such volume expansion

can be related to the oxidation of steel due to the RedOx reaction between NiO and steel. Moreover, it was found that the volume expansion, i.e. the steel oxidation, can be minimized to a good extent when Al-doped NiO is used. Hence it is proposed that Al-doped NiO is a promising candidate material to be used for anodes in high temperature sintering of MS-SOFC.

Green multilayers were produced by tape-casting for the fabrication of MS-SOFC half-cell by co-sintering. The binder loss step during co-sintering was optimized so as to prevent the cracking of the multilayers due to the binder loss events. Intermediate layers (layer between metal support and rest of the layers) composed of metal-ceramic powder composite were investigated to prevent delamination and to inhibit interdiffusion of the elements. CeO_2-steel, YSZ-steel, and LDC(La doped Ceria)-steel powder composites were considered for investigation to use as intermediate layer. Out of the different multilayer design considered for investigation, YSZ/(Al-NiO)-YSZ/LDC-steel/steel multilayer design was found to be a good compromise so as give a half-cell with good bonding between the layers, camber free cell, and moderate interdiffusion of elements between the substrate and the anode. It was however found in all the designs that complete densification of YSZ electrolyte could not be obtained.

In order to address the issue of limited densification of YSZ electrolyte during co-sintering, Fe was considered for doping YSZ. A comparative study was done on Fe doped YSZ samples for sintering in air and argon atmosphere, with the aim to analyze the effect of Fe as sintering aid under MS-SOFC fabrication by co-sintering conditions. Samples showed enhanced densification with increasing Fe concentration in both the sintering atmospheres thus concluding that Fe can be used as a sintering aid for YSZ even under argon. The samples sintered in argon atmosphere were however characterized

by larger lattice parameter, and higher density and grain size. The increase in lattice parameter is attributed to the oxygen vacancies generated under low $p(O_2)$ in argon atmosphere. The microstructural analysis showed the presence of small amount of secondary phase, and the concentration of such phase was seen to be higher in the argon sintered samples. Comparison of colors of argon and air sintered samples indicates the reduction and/or precipitation of Fe dopant in the argon. Gas tight dense electrolyte could be obtained for MS-SOFC fabricated by co-sintering when Fe doped YSZ is employed for electrolyte. The performance of the cell obtained was quite poor nevertheless; the results are encouraging for further research.

Bibliography

[1]   K. Huang and J. B. Goodenough, Solid Oxide Fuel Cell
        Technology,Priciples,   Performance   and   Operations,
        Boca Raton, Florida, USA: Woodhead Publishing Ltd.,
        2009.

[2]   I. EG&G Technical Services, Fuel Cell Handbook (Seventh
        Edition), West Virginia, USA: U.S. Department of Energy,
        2004.

[3]   J. T. Irvine and P. Connor, Solid Oxide Fuel Cells: Facts
        and Figures, Verlo, London: Springer, 2013.

[4]   J. Larminie and A. Dicks, Fuel Cell Systems Explained
        (Second Edition), West Sussex PO19 8SQ, England: John
        Wiley & Sons Ltd, 2003.

[5]   M. Cologna, "Advances in the Production of Planar and
        Micro-Tubolar Solid Oxide Fuel Cell," University of
        Trento, Trento, Itlay, 2009.

[6]   A. A. Thomas, J. Nease, D. Tucker and P. I. Barton,
        "Energy Conversion with Solid Oxide Fuel Cell Systems:
        A Review of Concepts and Outlooks for the Short- and
        Long-Term," *Industrial & Engineering Chemistry
        Research,* vol. 52, pp. 3089-3111, 2013.

[7]   A. Choudhury, H. Chandra and A. Arora, "Application of
        Solid Oxide Fuel Cell Technology for Power Generation-

A Review," *Renewable and Sustainable Energy Reviews,* vol. 20, pp. 430-442, 2013.

[8]   M. C. Williams, "Solid Oxide Fuel Cells: Fundamentals to Systems," *Fuel Cells,* no. 1, pp. 78-85, 2007.

[9]   P. W. Atkins, Physical Chemistry, Third Edition ed., New York: W.H. Freeman and Company, 1986.

[10] L. Blum, W. A. Meulenberg, H. Nabielek and R. Steinberger-Wilckens, "Worlwide SOFC Technology Overview and Benchmark," *International Journal of Applied Ceramic Technology,* vol. 6, no. 2, pp. 482-492, 2005.

[11] M. C. Tucker, "Progress in Metal-Supported Solid Oxide Fuel Cells: A Review," *Journal of Power Sources,* vol. 195, pp. 4570-4582, 2010.

[12] J.-W. Kim, A. V. Virkar and F. Kuan-Zong, "Polarization Effects in Intermediate Temperature, Anode-Supported," *Journal of The Electrochemical Society,* vol. 146, no. 1, pp. 69-78, 1999.

[13] Z. G. Yang, J. W. Stevenson and e. al., "Material properties database for selection of high temperature alloy and concepts of alloy design for SOFC applications," U.S. Department of Energy under contract DE-AC06-76RL01830, 2002.

[14] H. Kurokawa, K. Kawamura and T. Maruyam, "Oxidation behavior of Fe–16Cr alloy interconnect," *Solid State*

Ionics, vol. 168, p. 13 – 21, 2004.

[15] P. Y. Hou and J. Stringer, "The Effect of Reactive Element Additions on the Selective Oxidation, growth and adhesion of chromia scale," *Materials Science & Engineering A,* vol. 202, pp. 1-10, 1995.

[16] N. Shaigan, W. Qu, D. G. Ivey and W. Chen, "A review of recent progress in coatings, surface modifications and alloy developments for solid oxide fuel cell ferritic stainless steel interconnects," *Journal of Power Sources,* vol. 195, p. 1529–1542, 2010.

[17] Z. Yang, G. Xia, X. Li and J. W. Stevenson, "(Mn,Co)3O4 spinel coatings on ferritic stainless steels for SOFC interconnect applications," *International Journal of Hydrogen Energy,* vol. 32, no. 16, pp. 3648-3654, 2007.

[18] X. Montero, F. Tietz, D. Sebold, H. P. Buchkremer, A. Ringuede, L. Villarreal, A. Laresgoiti and M. Cassir, "MnCo1.9Fe0.1O4 spinel protection layer on commercial ferritic steels for interconnect applications in solid oxide fuel cells," *Journal of Power Sources,* vol. 184, pp. 172-179, 2008.

[19] M. C. Tucker, T. Z. Sholklapper, G. Y. Lau, L. C. De Jonghe and S. J. Visco, "Progress in Metal-Supported SOFCs," *ECS Transactions,* vol. 25, no. 2, pp. 673-680, 2009.

[20] S. Molin, M. Gazda and P. Jasinski, "High temperature oxidation of porous alloys for solid oxide fuel cell applications," *Solid State Ionics,* vol. 181, pp. 1214-1220,

2010.

[21]   B. C. H. Steele and A. Heinzel, "Materials for Fuel Cell Technologies," *Nature,* vol. 414, pp. 345-352, 2001.

[22]   F. M. L. Figueiredo and F. M. B. Marques, "Electrolyes for Solid Oxide Fuel Cellls," *WREs Energy and Environment,* vol. 2, pp. 52-72, 2013.

[23]   M. C. Tucker, H. Kurokawa, C. P. Jacobson, L. C. De Jonghe and S. J. Visco, "A fundamental study of chromium deposition on solid oxide fuel cell cathode materials," *Journal of Power Sources,* vol. 160, p. 130–138, 2006.

[24]   C. Hwang, C.-H. Tsai, C.-H. Lo and C.-H. Sun, "Plasma sprayed metal supported YSZ/Ni–LSGM–LSCF ITSOFC with nanostructured anode," *Journal of Power Sources,* vol. 180, pp. 132-142, 2008.

[25]   T. Ishihara, J. Yan, M. Enoki, S. Okada and H. Matsumoto, "Ni–Fe alloy-supported intermediate temperature SOFCs using LaGaO3 electrolyte film for quick startup," *Journal of Fuel Cell Science and Technology,* vol. 5, pp. 031205-1-031205-1-3, 2008.

[26]   C.-H. Tsai, C.-s. Hwang, C.-L. Chang, J.-F. Yu and S.-H. Nien, "Post-heat treatment pressure effect on performances of metal-supported solid oxide fuel cells fabricated by atmospheric plasma sparying," *Journal of Power Sources,* vol. 197, pp. 145-153, 2012.

[27] P. Bance, N. P. Brandon, B. Girvan, P. Holbeche, S. O'Dea and B. C. Steele, "Spanning-out a fuel cell company from a UK University- 2 years of progeress at Ceres Power," *Journal of Power Sources,* vol. 131, pp. 86-90, 2004.

[28] Q.-A. Huang, B. Wang, Q. Wei and R. Hui, "Impedance diagnosis of metal-supported SOFCs with SDC as electrolyte," *Journal of Power Sources,* vol. 191, pp. 297-303, 2009.

[29] S. Hui, D. Yang, Z. Wang, S. Yick, C. Deces-Petit, W. Qu, A. Tuck, R. Maric and D. Ghosh, "Metal-supported solid oxide fuel cell operated at 400-600C," *Journal of Power Sources,* vol. 167, pp. 336-339, 2007.

[30] Q.-A. Huang, J. Oberste-Berghaus, D. Yang, S. Yick, Z. Wang, B. Wang and R. Hui, "Polarization analysis for metal-supported SOFCs from different fabrication processes," *Journal of Power Sources,* vol. 177, pp. 339-347, 2008.

[31] N. P. Brandon, A. Blake, D. Corcoran, D. Cumming, A. Duckett, K. El-Koury, D. Haigh, C. Kidd, R. Leah, G. Lewis, C. Mathews, N. Maynard, N. Oishi, T. McColm, R. Trezona, A. Selcuk, M. Schmidt and L. Verdugo, "Developement of metal-supported solid oxide fuel Cells for operation at 500-600 C," *Journal of Fuel Cell Science and Technology,* vol. 1, pp. 61-65, 2004.

[32] C. Kleinlogel and L. J. Gauckler, "Sintering and properties of nanosized ceria solid solutions," *Solid*

State Ionics, vol. 135, pp. 567-573, 2000.

[33] G. S. Lewis, A. Atkinson, B. C. Steele and J. Drennan, "Effect of Co addition on the lattice parameter, electrical conductivity and sintering of gadolinia-doped ceria," *Solid State Ionics,* vol. 152 – 153, p. 567 – 573, 2002.

[34] J. D. Nicholas and L. C. De Jonghe, "Prediction and evaluation of sintering aids for Cerium Gadolinium Oxide," *Solid State Ionics,* vol. 178, p. 1187–1194, 2007.

[35] Y. Lee and M. C. Gyeong, "Ceria film supported on Ni-Fe metal film cell designs, processing and performance," *ECS Transactions,* vol. 25, no. 2, pp. 727-730, 2009.

[36] Y. Xie, R. Neagu, C.-S. Hsu, X. Zhang and C. Decès-Petit, "Spray Pyrolysis Deposition of Electrolyte and Anode for Metal-Supported Solid Oxide Fuel Cell," *Journal of The Electrochemical Society,* vol. 155, pp. 4 B407-B410, 2008.

[37] Z. Wang, J. O. Berghaus, S. Yick, C. Deces-petit, W. Qu, R. Maric and D. Ghosh, "Dynamic evaluation of low-temperature metal-supported solid oxide fuel cell oriented to auxiliarry power units," *Journal of power sources,* vol. 176, pp. 90-95, 2008.

[38] R. Hui, J. Oberste Berghaus, C. Decès-Petit, W. Qu, S. Yick, J.-G. Legoux and C. Moreau, "High performance metal-supported solid oxide fuel cells fabricated by thermal spray," *Journal of Power Sources,* vol. 191, p.

371–376, 2009.

[39] H. C. Park and A. V. Virkar, "Bimetallic (Ni–Fe) anode-supported solid oxide fuel cells with gadolinia-doped ceria electrolyte," *Journal of Power Sources,* vol. 186, p. 133–137, 2009.

[40] R. T. Leah, N. P. Brandon and P. Aguiar, "Modelling of cells, stacks and systems based around metal-supported planner IT-SOFC cells with CGO electrolytes operating at 500-600oC," *Journal of Power Sources,* vol. 145, pp. 336-352, 2005.

[41] P. Szabo, J. Arnold, T. Franco, M. Gindrat, A. Refke, A. Zagst and A. Ansar, "Progress in the Metal Supported Solid Oxide Fuel Cells and Stacks for APU," *ECS Transactions,* vol. 25, no. 2, pp. 175-185, 2009.

[42] G. Schiller, R. H. Henne, M. Lang, R. Ruckdäschel and S. Simone, "Development of vacuum plasma sprayed thin-film SOFC for reduced operating temperature," *Fuel Cells Bulletin,* vol. 21, pp. 7-12, 2000.

[43] T. Franco, K. Schibinger, I. Zeynep, G. Schiller and A. Venskutonis, "Ceramic Diffusion Barrier Layers for Metal Supported SOFCs Cell Design, Processing, and Performance," *ECS Transactions,* vol. 7, no. 1, pp. 771-780, 2007.

[44] T. Franco, M. Brandner, M. Rüttinger, G. Kunschert, A. Venskutonis and L. Sigl, "Recent development aspects of metal supported thin-film SOFC:Cell Designs, Processing

and Performance," *ECS Transactions,* vol. 25, no. 2, pp. 681-688, 2009.

[45]   A. Macwan, D. L. Chen, M. Marr and O. Kesler, "Residual stresses in suspension plasma sprayed electrolytes in metal-supported solid oxide fuel half cells," *Journal of Power Sources,* vol. 221, pp. 397-405, 2013.

[46]   S. Wolf, R. Adam, F. Lars, S. A. Ansar and F. K. Andreas, "Characterization of electrolyte layers of plasma-sprayed metal supported solid oxide fuel cells," *Solid State Ionics,* vol. 243, pp. 30-35, 2013.

[47]   D. Waldbillig and O. Kesler, "Electrochemical testing of suspension plasma sprayed solid oxide fuel cell electrolytes," *Journal of Power Sources,* vol. 196, pp. 5423-5431, 2011.

[48]   R. Henne, "Solid Oxide Fuel Cells: A challenge for plasma deposition processes," *Journal of Thermal Spray Technology,* vol. 16, no. 3, pp. 381-403, 2007.

[49]   H. Kurokawa, G. Y. Lau, C. P. Jacobson, L. C. De Jonghe and S. J. Visco, "Water-based binder system for SOFC porous steel substrate," *Journal of Materials Porcessing and Technology,* vol. 182, pp. 469-476, 2007.

[50]   M. C. Tucker, G. Y. Lau, C. P. Jacobson, L. C. DeJonghe and S. J. Visco, "Performance of metal-supported SOFCs with infiltrated elecrode," *Journal of Power Sources,* vol. 171, pp. 477-482, 2007.

[51] P. Blennow, J. Hjelm, T. Klemensø, A. Persson, K. Brodersen, A. Srivastava, H. Frandsen, M. Lundberg, S. Ramousse and M. Mogensen, "Developement of planer metal supported SOFC with novel cermet anode," *ECS Transactions,* vol. 25, no. 2, pp. 701-710, 2009.

[52] L. M. Rodriguez-Martinez, L. Otaegi, M. Alvarez, M. Rivas, N. Gomez, A. Zabala, N. Arizmendiarrieta, I. Antepara, A. Urriolabeitia, M. Olave, , I. Villarreal and A. Laresgoiti, "Degradation Studies on Tubular Metal Supported SOFC Cell Designs, Processing and Performance," *ECS Transactions,* vol. 25, no. 2, pp. 745-752, 2009.

[53] M. C. Tucker, G. Y. Lau, C. P. Jacobson, L. C. DeJonghe and S. J. Visco, "Stability and robustness of metal-supported SOFCs," *Journal of Power Sources,* vol. 175, p. 447–451, 2008.

[54] M. C. Tucker, C. P. Jacobson, L. c. De Jonghe and S. J. Visco, "A braze system for sealing metal-supported solid oxide fuel cells," *Journal of Power Sources,* vol. 160, pp. 1049-1057, 2006.

[55] N. Q. Minh and T. Takahashi, Science and technology of ceramic fuel cells, The Netherlands: Elsevier, 1995.

[56] N. Oishi and Y. Yoo, "Fabrication of Cerium Oxide based SOFC having a Porous Stainless Steel Support:Cell Designs, Processing and Performance," *ECS Transactions,* vol. 25, no. 2, pp. 739-744, 2009.

[57] T. Komatsu, H. Arai, R. Chiba, K. Nozawa, M. Arakawa and K. Sato, "Cr Poisoning Suppression in Solid Oxide Fuel Cells Using LaNi (Fe) O3 Electrodes:Batteries, Fuel Cells, and Energy Conversion," *Electrochemical Solid State Letters,* vol. 9, p. A9, 2006.

[58] T. Komatsu, H. Arai, R. Chiba, K. Nozawa, M. Arakawa and K. Sato, "Long-Term Chemical Stability of LaNi (Fe) O3 as a Cathode Material in Solid Oxide Fuel Cells:Fuel Cells and Energy Conversion," *Journal of Electrochemical Society,* vol. 154, no. 4, p. B379, 2007.

[59] M. K. Stodolny, F. P. Van Berkel and B. A. Boukamp, "La(Ni,Fe)O3 Stability in the Presence of Cr Species-solid-state Reactivity Study:Cathode Materials, Processing and Performance," *ECS Transactions,* vol. 25, no. 2, pp. 2915-2922, 2009.

[60] H. Orui, K. Watanabe, R. Chiba and M. Arakawa, "Application of LaNi (Fe) O 3 as SOFC Cathode:BATTERIES, FUEL CELLS, AND ENERGY CONVERSION," *Journal of The Electrochemical Society,* vol. 151, no. 9, pp. A1412-A1417, 2004.

[61] Y. Zhou, Z. Zhang, C. Yuan, J. Li, C. Xia, Z. Zhan and S. Wang, "Metal-supported solid oxide fuel cells with in-situ sintered (Bi2O3)0.7(Er2O7)0.3-Ag composite cathode," *Hydrogen Energy,* vol. 38, no. 36, pp. 16579-16583, 20013.

[62] Y.-M. Kim, P. Kim-Lohsoontorn, B. Seung-Wook and B.

Joongmyeon, "Electrochemical performance of unsintered Ba0.5Sr0.5Co0.8Fe0.2O3−δ, La0.6Sr0.4Co0.8Fe0.2O3−δ, and La0.8Sr0.2MnO3−δ cathodes for metal-supported solid oxide fuel cells," *International Journal of Hydrogen Energy,* vol. 36, no. 4, pp. 3138-3146, 2011.

[63]   T. Z. Sholklapper, C. Lu, C. P. Jacobson, S. J. Steven and L. C. De Jonghe, "LSM-infiltrated solid oxide fuel cell cathodes: Batteries, Fuel Cells, and Energy Conversion," *Electrochemical Solid State Letters,* vol. 9, no. 8, pp. A376-A378, 2006.

[64]   H. J. Cho, Y. M. Park and G. M. Choi, "Enhanced power density of metal-supported solid oxide fuel cell with a two-step firing process," *Solid State Ionics,* vol. 192, pp. 519-522, 2011.

[65]   I. Villarreal, M. Rivas, L. M. Rodriguez-Martinez, L. Otaegi, A. Zabala, N. Gomez, M. A. Alvarez, I. Antepara, N. Arizmendiarrieta, J. Manzanedo, M. Olave, A. Urriolabeitia, N. Burgos, F. Castro and A. Laresgoiti, "Tubular Metal Supported SOFC Development for Domestic Power Generation," *ECS Transactions,* vol. 25, no. 2, p. 689–694, 2009.

[66]   H. J. Cho, Y. M. Park and G. M. Choi, "A Flexible Solid Oxide Fuel Cell Supported on the Thin Porous Metal," *ECS Transactions,* vol. 25, no. 2, p. 695–699, 2009.

[67]   S. P. Jiang and Y. Yan, Materials for High Temperature

Fuel Cells, Germany: Wiley-VCH, 2013.

[68] J. O. Berghaus and J. G. Legoux, "Suspension HVOF spraying of reduced temperature solid oxide fuel cell electrolytes.," *Journal of Thermal Spray Technology,* vol. 17, pp. 700-707, 2008.

[69] M. Brandner, J. Froitzheim, M. Bram, H. P. Buchkremer and D. Stover, "Electrically conductive diffusion barrier layers for Metal-Supported SOFC," *Solid State Ionics,* vol. 179, pp. 1501-1504, 2008.

[70] P. Blennow, J. Hjelm, T. Klemenso, S. Ramousse, A. Kromp, A. Leonide and A. Weber, "Journal of Power Sources," *Journal of Power Sources,* vol. 196, pp. 7117-7125, 2011.

[71] M. Rauscher, G. Besendorfer and R. Andreas, "Steel-sheet fabrication by tape casting," *International Journal of Powder Metallurgy,* vol. 44, no. 6, pp. 39-48, 2008.

[72] D. Hotza and P. Greil, "Review: aqueous tape casting of ceramic powders," *Materials Science and Engineering A,* vol. 202, pp. 206-217, 1995.

[73] R. E. Mistler and E. R. Twiname, Tape casting, theory and practice, Westerville, OH: The Americal Ceramic Society, 2000.

[74] J. S. Reed, Principles of ceramics processing, 2nd Edition, USA: John Wiley & Sons, 1995.

[75] M. N. Rahaman, Ceramic processing and sintering, New York: Marcel Dekker, 2003.

[76] A. G. King, Ceramic technology and processing, Norwich, NY: William Andrew, 2002.

[77] M. N. Rahaman, Sintering of ceramics, Boca Raton, USA: CRC Press, 2008.

[78] D. J. Green, O. Guillon and J. Rodel, "Constrained sintering: A delicate balance of scales," *Journal of Europeon Ceramic Society,* vol. 28, pp. 1451-1466, 2008.

[79] G.-Q. Lu, R. C. Sutterlin and T. K. Gupta, "Effect of mismatched sintering kinetics on camber in a low-temperature cofired ceramic package," *Journal of American Ceramic Society,* vol. 76, no. 8, pp. 1907-1914, 1993.

[80] C. R. He and W. G. Wang, "Alumina doped Ni/YSZ anode materials for solid oxide fuel cells," *Fuel Cells,* no. 5, pp. 630-635, 2009.

[81] M. Cologna, A. R. Contino, D. Montinaro and V. M. Sglavo, "Effect of Al and Ce doping on the deformation upon sintering in sequential tape cast layers for solid oxide fuel cells," *Journal of Power Sources,* vol. 93, p. 80–85, 2009.

[82] P. H. Larsen, C. Chung and M. Mogensen.United States Patent US 2008/0166618 A1, 2008.

[83] E. Chinarro, F. M. Figueiredo and G. C. Mather, "Combustion synthesis and characterisation of Ni-MO-YSZ(M = Mg, Ca, Al2/3) cermet anodes for SOFCs," *Journal of European Ceramic Society,* vol. 27, p. 4233–4236, 2007.

[84] T. Klemenso and M. Mogensen, "Ni-YSZ Solid Oxide Fuel Cell Anode Behavior Upon Redox Cycling Based on Electrical characterization," *Journal of American Ceramic Society,* vol. 90, no. 11, pp. 3582-3588, 2007.

[85] T. Sekino, T. Nakajima, S. Ueda and K. Niihara, "Reduction and Sintering of a Nickel-Dispersed-Alumina Composite and its Properties," *Journal of American Ceramic Society,* vol. 80, no. 5, pp. 1139-1148, 1997.

[86] A. Lefarth, B. Butz, H. Stormer, A. Utz and D. Gerthsen, "Impact of Ni on Accelerated Degradation of 8.5 mol% Y2O3-Doped Zirconia," *ECS Transactions,* vol. 35, no. 1, pp. 1581-1586, 2011.

[87] Y. Ji, J. Liu, Z. Lu, X. Zhao, T. He and W. Su, "Study on the properties of Al2O3-doped (ZrO2)0.92 (Y2O3)0.08," *Solid State Ionics,* vol. 126, p. 277–283, 1999.

[88] D. Simwonis, F. Tietz and D. Stover, "Nickel coarsening in annealed Ni/8YSZ anode substrates for solid," *Solid State Ionics,* vol. 132, pp. 241-251, 2000.

[89] M. H. Pihlatie, A. Kaiser, M. Mogensen and M. Chen, "Electrical conductivity of Ni–YSZ composites: Degradation due to Ni particle growth," *Solid State*

Ionics, vol. 189, pp. 82-90, 2011.

[90] J. H. Yu, G. W. Park, S. Lee and S. K. Woo, "Microstructural effects on the electrical and mechanical properties of Ni-YSZ cermet for SOFC anode," *Journal of Power Sources,* vol. 163, pp. 926-932, 2007.

[91] R. Haugsrud, "On the high temperature oxidation of nickel," *Corrosion Science,* vol. 45, pp. 211-235, 2003.

[92] D. P. Moon, "The Reactive Element Effect on the Growth Rate," *Oxidation of metals,* pp. 47-66, 1989.

[93] Larsen and e. al.United States Patent US 2008/0188818 A, 2008.

[94] A. R. Contino, M. Cologna, S. Modena and V. M. Sglavo, "Effect of Doping Elements on the Redox Kinetics of NiO-YSZ Powders for SOFC Applications,," in *ECS Transections*, 2009.

[95] N. M. Tikekar, T. J. Armstrong and A. V. Virkar, "Reduction and Reoxidation Kinetics of Nickel-Based SOFC Anodes," *Journal of The Electrochemical Society,* vol. 153, pp. A654-A663, 2006.

[96] H. Ellingham, *J Soc Chem Ind (London),* vol. 63, p. 125, 1944.

[97] M. Feng and J. B. Goodenough, "Improving Stabilized Zirconia with Strontium Gallate," *Journal of the*

American Ceramic Society, p. 1954, 1994.

[98] K. Keizer, A. J. Burggraaf and De With, "The effect of Bi2O3 on the electrical and mechanical properties of ZrO2-Y2O3 ceramics," *Journal of Materials Science,* vol. 17, p. 1095, 1982.

[99] J. R. Seidensticker and M. J. Mayo, "Thermal Analysis of 3-mol%-Yttria-Stabilized Tetragonal Zirconia Powder Doped with Copper Oxide," *Journal of American Ceramic Society,* vol. 79, p. 401, 1996.

[100] C. Bowen, S. Ramesh, C. Gill and S. Lawson, "Impedance spectroscopy of CuO-doped Y-TZP ceramics," *Journal of Materials Science,* vol. 33, p. 5103, 1998.

[101] M. Hartmanova, F. Hanic, D. Tunega and K. Putyera, "Structural and Electro-Optical Properties of Co-Doped Yttria-Stabilized Zirconia," *Chemical papers,* vol. 52, p. 12, 1998.

[102] G. S. Lewsi, A. Atkinson and B. C. Steele, "Cobalt additive for lowering the sintering temperature of yttria-stabilized zirconia," *Journal of Materials Science Letters,* vol. 20, pp. 1155-1157, 2001.

[103] H. Zhou, J. Li, D. Yi and L. Xiao, "Effect of manganese oxide on the sintered properties of 8YSZ," *Physics Procedia,* Vols. 14-19, p. 22, 2011.

[104] H. Gao, J. Liu, H. Chen, S. Li, T. He, Y. Ji and J. Zhang, "The effect of Fe doping on the properties of SOFC

electrolyte YSZ," *Solid State Ionics,* vol. 179, pp. 1620-1624, 2008.

[105] F. Guo and P. Xiao, "Effect of Fe2O3 doping on sintering of yttria-stabilized Zirconia," *Journal of European Cramic Society,* vol. 32, pp. 4157-4164, 2012.

[106] Q. Dong, Z. H. Du, T. S. Zhang, J. Lu, X. C. Song and J. Ma, "Sintering and ionic conductivity of 8YSZ and CGO10 electrolytes with small addition of Fe2O3: A comparative study," *International Journal of Hydrogen Energy,* vol. 34, pp. 7903-7909, 2009.

[107] R. V. Wilhellm and D. S. Howarth, *Journal of American Ceramic Society Bulletin,* vol. 58, p. 228, 1979.

[108] A. Atkinson and T. Ramos, "Chemically-induced stresses in ceramic oxygen ion-conducting membranes," *Solid State Ionics,* vol. 129, pp. 259-269, 2000.

[109] S. P. Badwal and A. E. Hughes, "The effects of sintering atmosphere on impurity phase formation and grain boundary resistivity in Y2O3 fully stabilized ZrO2," *Journal of European Ceramic Society,* vol. 10, pp. 115-122, 1992.

Curriculum Vitae

Educational background:

PhD.

Department of Materials Science and Industrial Engineering,

University of Trento, Trento, Italy (2011-2014)

Master of Science

Department of Chemistry, Goa University, India (2008-2010)

Bachelor of Science

St. Xavier's College, Goa, India (2005-2008)

Publications and Proceedings:

Modification of sintering   behaviour of Ni based anode material by doping for Metal Supported-SOFC.
***Satardekar, P.**, Mortinaro, D. and Sglavo, V. M.* In Ceramic Engineering and Science Proceedings, Advances in Solid Oxide Fuel Cells IX*, (2013) 77*

Al doped Ni/YSZ anode material for fabrication of MS-SOFC by Co-sintering. ***Satardekar, P.**, Mortinaro, D. and Sglavo, V. M* .International Journal of Applied Ceramic Technology (***2014***), under review

Doping of YSZ for the fabrication of Metal Supported- SOFC by Co-sintering. ***Satardekar, P.**, Mortinaro, D. and Sglavo, V. M.* Under preparation

Patent

Patent filed at Italian Patent and Trademark Office (IPTO) in August 2013.
*Mortinaro, D., Bertoldi, M., Sglavo, V. M. and **Satardekar, P***.

Conferences

"Nickel Oxide doping for the production of defect-free Metal Supported-SOFC by co-sintering of tape cast multilayers"
Satardekar, P., *Mortinaro, D. and Sglavo, V. M. Oral presentation at 13th International Conference of the European Ceramic Society, June 23-27,* **2013,** *Limoges, France.*

"Doping of NiO and 8YSZ, and optimisation of tape cast multilayer design for production of metal supported solid oxide fuel cell by co-sintering"
Satardekar, P., *Mortinaro, D. and Sglavo, V. M. Oral presentation at 38th International Conference and Exposition on Advanced Ceramics and Composites, January 26-31,* **2014,** *Daytona Beach Florida, USA.*

Acknowledgements

I would like to begin by expressing my sincerest gratitude to my supervisor, Prof. Vincenzo Maria Sglavo, for giving me this opportunity to learn and explore. His encouragement and support throughout the period of my Ph.D. was enormous.

I am deeply grateful to Dr. Dario Montinaro for his guidance which enabled me to develop an understanding of the subject. It was an amazing experience working with him, and nice of him to clear my silliest doubts.

Many of my friends have helped me though these years: I specially thank Kiran, Anshu, Pradeep, Rajesh, Rahul, Piyush, Pushkar and Prasanta for always being there and making me feel like in home over here in Trento. I will always cherish the memories of our amazing trips in Europe, the stress relieving lunch and dinner parties, and of course the non-productive but still refreshing discussions during our tea breaks.

I am also thankful to all my friends and colleagues in the lab: John, Lam, Dawit, Andrea, Emanuelle, Francesca, Ali, Hamid, Mattia, Daniele and other for keeping the work environment friendly and so helpful.

My sincere thanks to all my professors and teachers in India without whose support I would not have made it till here. I also thank my MSc friends Sagar, Prajesh and Satu for encouraging me to do Ph.D and come so far.

Most important, none of this would have been possible without the love and patience of my family. I am thankful to my mom and dad for always letting me do what I loved to do. My thanks to my brother and sister for always being there for me as my good friends.